Project No. 10-876

Studies of Deteriorated Heat Transfer in Prismatic Cores Stemming from Irradiation-Induced Geometry Distortion

Reactor Concepts

Brian G. Williams
Idaho State University

In collaboration with:
Idaho National Laboratory
Independent Consultant

Steven Reeves, Federal POC
Piyush Sabharwal, Technical POC

NEUP Nuclear Energy University Programs
U.S. Department of Energy

Report

Studies of Deteriorated Heat Transfer in Prismatic Cores Stemming from Irradiation-Induced Geometry Distortion

10-876

Report Date

August 2015

For the Period

1 September 2010 through – 30 September 2014

Submitted to

The U. S. Department of Energy (DoE)
Nuclear Energy University Program (NEUP)

Contact/PI: Dr. Brian G. Williams
Dept. of Mechanical Engineering
Idaho State University
Pocatello, ID 83209
Phone: 208-282-4129
Email: willbria@isu.edu

Co-PIs: Dr. Richard R. Schultz
INL
Idaho Falls, ID 83415
Email: Richard.Schultz@inl.gov

Dr. Don M. McEligot
INL
Idaho Falls, ID 83415
Email: donaldm@uidaho.edu

Dr. Glenn E. McCreery
Consultant
Idaho Falls, ID 83404
Email: gem@srv.net

Introduction

A reference design for the Next Generation Nuclear Plant (NGNP) is to use General Atomic's Modular High Temperature Gas-cooled Reactor (MHTGR). For such a configuration in normal operation, the helium coolant flow proceeds from the upper plenum to the lower plenum principally through the core coolant channels and the interstitial gaps (bypass flow) that separate the prismatic blocks from one another (see Figure 1). Only the core prismatic blocks have coolant channels. The interstitial gaps are present throughout the core, the inner reflector region, and the outer reflector region.

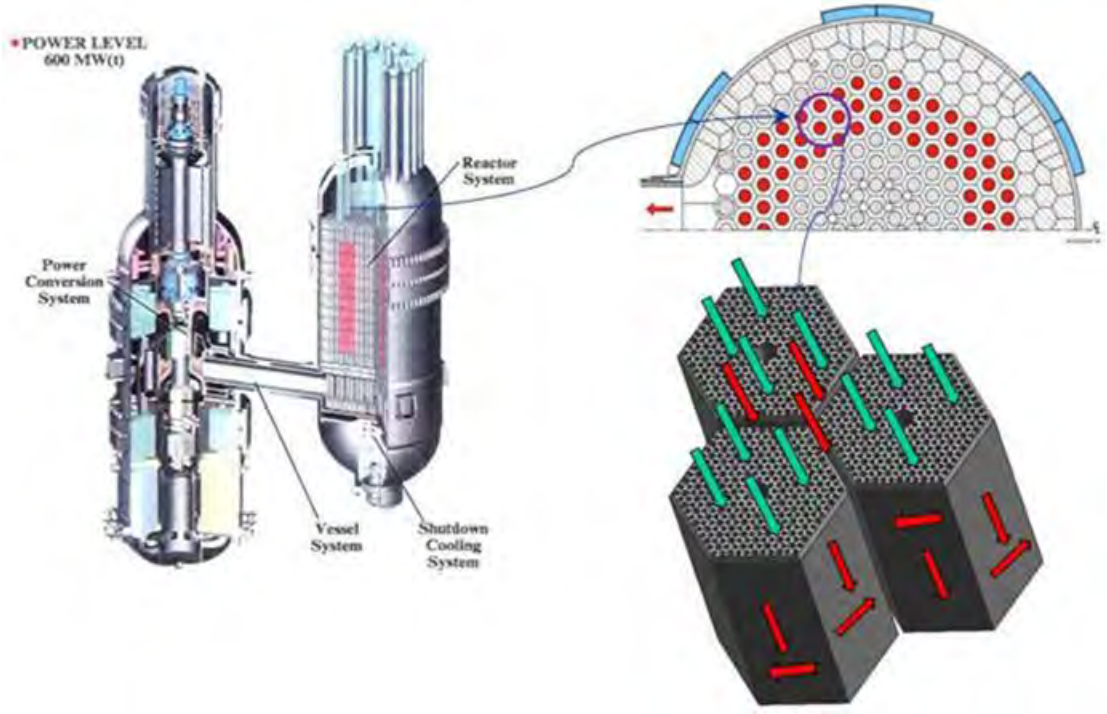

Figure 1. Conceptual images of the MHTGR, showing the prismatic block locations and the corresponding coolant flow paths.

Prior to irradiation[1], when a prismatic block is undistorted and the seals between blocks stacked one on top of another are intact such that horizontal leakage does not occur at the block tops and bottoms, the coolant channels are well defined and helium flow entering the coolant channels from the upper plenum will proceed to the lower plenum following the designed cooling passages. The interstitial gaps have a primarily average maximum width of approximately 4 mm prior to irradiation[2] for a typical design heated core.

---

[1] Irradiated graphite will become distorted as a function of exposure. The graphite distortion may lead to deteriorated heat

[2] R. R. Schultz, M. H. Kim, R. Vilim, G. Park, and Y. Hassan. 2009. *Experimental and Analytic Study on the Core Bypass Flow in a Very High Temperature Reactor,* First I-NERI Report, September, where the plans to quantify the flow behavior in a prismatic reactor bypass region are outlined in Schultz, R. et al, 2009, *Experimental and Analytical Studies on the Core Bypass Flows in a Very High Temperature Reactor*, INL/EXP-09-16745, September

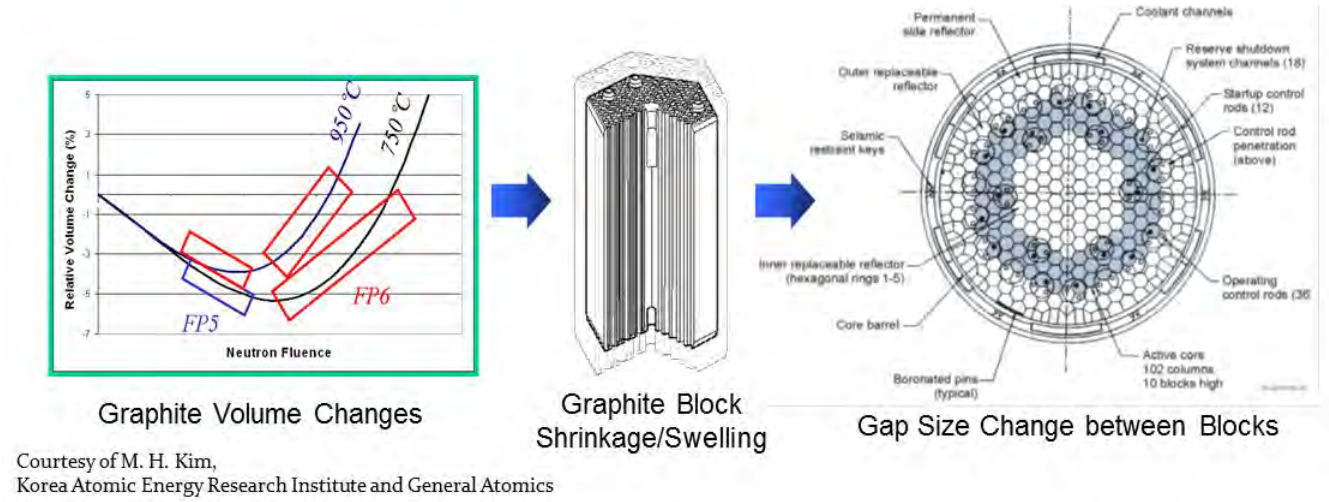

Figure 2. Graphite distortion due to irradiation by energetic neutrons as well as thermal expansion effects.

The bypass flows in a prismatic gas-cooled reactor (GCR) are of potential concern because they reduce the desired flow rates in the coolant channels and, thereby, can increase outlet gas temperatures and maximum fuel temperatures. In existing literature, bypass flows of *10 to 30 percent* of the total flow rate have been estimated. Consequently, it is appropriate to account for bypass flows in reactor thermal gas dynamic analyses.

Project Objectives

Accordingly, the ***objectives*** of this project include:

1. Fundamentally understand bypass flow and heat transfer at scaled, undistorted conditions and with geometry distortions scaled from the NEUP Project No. 09-453 data.
2. Develop improved estimates of associated loss coefficients, surface friction and heat transfer for systems and network codes.
3. Obtain related data for validation of CFD (computational fluid dynamic) or system (e.g., RELAP5) codes which can be employed in predictions for a GCR for normal power, reduced power and residual heat removal operations.

The improved estimates may come from existing literature, experiments and/or validated CFD predictions.

Most bypass studies have considered flows through and around groups of hexagonal blocks, including their coolant holes, so coolant flows, gap flows and others are all approximated simultaneously. In order to obtain better understanding and more accurate representations of the gap contributions, the proposed project will concentrate on the bypass flow and heat transfer in the gaps alone, essentially a "separate effects" study.

It is proposed that the following tasks be pursued in order to meet the project objectives:

1. Quantify to a better extent the pertinent geometries in both undistorted and distorted configurations.

2. Develop order-of-magnitude estimates of the flow conditions and, therefore, non-dimensional flow and heat transfer parameters over the ranges of expected operations.
3. Develop an effective liaison between CFD practitioners, systems/network analysts, vendors and laboratory scientists involved. From this effort, determine needs for systems/network codes.
4. Continue the examination of existing literature for flow and convective heat transfer in related geometries in order to improve quantitative descriptions of loss and heat transfer coefficients.
5. Develop a conceptual experiment design for measuring flow resistances, loss coefficients and convective heat transfer, in realistic gap configurations in order to provide improved assessment of CFD predictions for reasonable designs over an appropriate range of flow rates. Note that for this purpose a concentration on "individual" gap geometry is recommended instead of on overall core tests.
6. In conjunction with systems code and CFD analysts and vendors, design and conduct the appropriate experiments (essentially "separate effects" experiments rather than integral tests).

Parallel tasks, to be performed by the national laboratory collaborator, would be carried out concurrently but would not be considered within the cost-scope of this proposal. These tasks would include:

1. Assess CFD predictions for flow and heat transfer in comparable geometries by comparison to available measurements and analyses.
2. Employ experimental data from the proposed experiments to assess CFD capabilities in order to provide improved information (e.g., correlations) needed by systems safety codes to treat bypass flows.
3. Improve systems safety codes as needed.

Student Involvement

As a university, our primary goal is to educate and train students for their chosen professions. Therefore, the involvement of students with this project was strongly written into the proposal. Students play a critical role in the success of this endeavor. The following is a list of the students involved in this project and their primary area of responsibility.

Bradley Heath: At the time of Brad's involvement, he was an undergraduate student at Idaho State University (ISU), pursuing a Bachelors of Science (BS) degree in Nuclear Engineering (NE). His primary efforts towards this project included preliminary scaling analysis and efforts to transition the Skyline Thermal Fluids Laboratory (Skyline Lab)[3]. He graduated in December 2010 and currently works at the INL. Brad has recently completed a Masters of Science (MS) in Mechanical Engineering (ME) from ISU on an unrelated project.

Izzi Silver: Izzi is a MS graduate research assistant studying Mechanical Engineering at ISU. His primary efforts will focus on the instrumentation & measurement of the heated flow experiment's test section as well as the modeling and analysis of the deteriorated pressure drop data.

Logan Tew: While working on this project, Logan completed his BS degree in ME from ISU in December 2011. He then went on to complete a MS in ME from ISU in 2013 with his thesis title "Investigation of Plenum Flow Behavior with Different Entrance and Exit Geometries." His primary responsibilities have included the overall system performance measurement instrumentation, the flow

[3] The Skyline Lab has successfully moved from its Idaho Falls location to a new location housed within the Engineering Research Complex (ERC) in Pocatello, Idaho. The new lab is over 2,000 sqft of usable lab space, high ceilings (over 14 ft), as well as all the amenities of the old lab.

structure (piping/ducts and blowers) into and out of the test section, as well as flow conditioning (flow straighteners for instrumentation, inlet & outlet plenums for the test section).

Jari Safi: Jari completed his BS degree with a double major in Mechanical Engineering and Nuclear Engineering. His primary efforts have focused on a unique, inexpensive particle imaging velocimetry (PIV) system to measure flow velocities in our flow visualization experiment. Jari graduated in May 2011 and is currently at Penn State University, working towards his MS Degree.

Steven Heath: Steven is currently pursuing a BS degree in Civil Engineering. His primary efforts have included determining from the Skyline Lab existing equipment/instrumentation that could be used for this project as well as supporting all test efforts. Steve has been a mainstay and the "go to" guy for all hands-on aspects of this project.

Senior Design Group: For the 2011-2012 academic year, a Senior Design Team was formed and given the responsibility of the detailed mechanical design of the heated test loop. This group consists of ME students ***Jose Martinez*** and ***Randy Case*** as well as double major (ME & NE) ***Jari Safi***. This group's efforts focused on the design of a system to vary the geometry (gap spacing) of the heated plates in the test section as well as the structure & support for the overall flow loop. At the completion of their course in May 2012, a formal report, presentation, and drawing/design package was delivered. The support structure drawings have since been finalized and are currently in fabrication. The heated plate drawings are completed and are being given to vendors for bids.

Bric Balmforth: Bric completed an Honors BS degree in Mechanical Engineering at ISU. He is currently pursuing a MS in Biomedical Engineering at the University of Utah. His primary efforts have been focused on the design, implementation, and setup of the data acquisition system (DAQ), using National Instruments equipment.

Dane Sterbentz: Dane is currently working towards a MS in Measurement and Control Engineering (MCE) at ISU. He replaced Bric when Bric graduated and completed the DAQ system.

Konner Casanova: Konner graduate with a BS in Nuclear Engineering from ISU in 2014. He was brought on to this project primarily for testing, completing most of the pressure drop testing as well as preparing the system for the heated tests.

Ryan Loveland: Ryan is pursuing his MS in NE from ISU. He was also brought on to this project primarily for testing, completing most of the pressure drop and heated testing.

Michael Echevarria: Mike is currently working on a BS in ME at ISU. He was also brought on to this project primarily for completing the heated testing.

Larinda Nichols: Larinda is currently working on a BS in NE at ISU. She was also brought on to this project primarily for completing the heated testing.

Harishchandra Aryal: Harish is working on his MS in ME at ISU. He has been analyzing the heated flow data.

A. Papers Published and Conference Presentations

The following papers have been presented at conferences.

Silver, Isador, Brian Williams, Richard R. Schultz, Donald M. McEligot, and Glenn E. McCreery, 2012, "Scaling Analysis for the Use of Air in Place of Helium for a Heated Flow Experiment," Presented at the ASME 2012 Summer Heat Transfer Conference, July 8 – 12, Puerto Rico, USA.

Heath, Bradley, Jariullah Safi, Isadore Silver, Brian G. Williams, Richard R. Schultz, Donald M. McEligot, and Glenn E. McCreery, 2011, "Studies of Deteriorated Heat Transfer in Prismatic Cores Stemming from Irradiation-Induced Geometry Distortion," Presented at the American Nuclear Society: 2011 Annual Meeting, June 26-30, Hollywood, Florida.

McCreery, Glenn E., Logan Tew**,** Brian Williams, Donald M. McEligot, and Richard R. Schultz, 2013, "*MHTGR Prismatic Core Bypass Flow Patterns and Pressure Losses*," presented at the NURETH-15: 15th International Topical Meeting on Nuclear Reactor Thermohydraulics, May 12-16, Pisa, Italy.

As the data continues to be analyzed, we anticipate submitting addition papers, included refereed journals.

B. Scaling Analysis

Scaling analyses will be performed to quantify the effects of using air in place of helium as the working fluid. Using air would greatly decrease the complexity of the loop and allow for more parameter variations. The heated test loop will be configured to allow unheated (baseline) block testing as well as heated testing. The test section apparatus will be designed so as to allow for specified variations in gap spacing (both uniform and tapered) as well as misalignment between axially-located blocks; additionally, separate effects experiments may be used as needed.

The scaling analysis presented here addresses the physical parameters of air in an attempt to relate the conditions of helium in the VHTR core. This is accomplished through the use of the dimensionless parameters, Reynolds number (Re) and the dimensionless heat flux (q^+). The flow cross-sectional geometry used in this analysis was a simple rectangular channel of dimensions 375mm wide by 002 mm high (signifies the gap spacing). In addition, a channel length of 793 mm was used.

Analysis Using Dimensionless Heat Flux

The dimensionless heat flux is defined by the relationship[4]:

$$q^+ = \frac{q_s}{G \cdot C_P \cdot T_{Inlet}}$$

where q_s is the surface heat flux, G is the mass velocity, C_p is the specific heat of the fluid, and T_{Inlet} is the inlet temperature to the channel. Note that the inlet temperature must be in absolute values. The mass velocity is defined from the mass flow rate[5]:

[4] McEligot, D. M. and J. D. Jackson, 2004, "Deterioration criteria for convective heat transfer in gas flow through non-circular ducts," *Nuc. Engr. Design*, 232, pp. 327-333.

$$G = \frac{\dot{m}}{A_{cs}} = \rho \cdot V$$

where $\dot{m}$ is the mass flow rate, A_{cs} is the cross-sectional area of the flow channel, ρ is the density of the fluid, and V is the velocity of the flowing fluid. For internal forced convection, the rate of energy (Q) transferred to the fluid is known, hence, a relationship between the surface heat flux and the increase in fluid temperature (ΔT) can be found[6]:

$$Q = q_s A_s = \dot{m} C_P \Delta T$$

where A_s is the surface area in contact with the fluid. By substituting for the surface heat flux and the mass velocity into the dimensionless heat flux relation, it can be shown that

$$q^+ = \frac{A_{cs} \cdot \Delta T}{T_{Inlet} \cdot A_s}$$

Or, for a given temperature change, the relationship between ΔT and q^+ is

$$\Delta T = q^+ \cdot T_{Inlet} \cdot \frac{A_s}{A_{cs}}$$

Note, that for a fixed geometry and a given inlet temperature, the dimensionless heat flux is directly proportional to the temperature increase of the fluid. From this equation, it appears at first that the temperature increase is not dependent upon the flow rate of the fluid or on the type of fluid. However, it must be remembered that the definition of the dimensionless heat flux includes variations in flow rate and type of fluid; two different fluids at the same dimensionless heat flux does not imply the same surface heat flux or flow rate.

Also, from the ΔT equation above, it is evident that for two different conditions in which the only variation would be the inlet temperature, the condition with the large inlet temperature would experience the larger temperature increase. It should be noted, however, that the presence of T_{Inlet} in this equation is a result of the definition of the dimensionless heat flux. Therefore, for a given dimensionless heat flux, a larger inlet temperature would correlate to a larger actual surface heat flux. Obviously, the larger the actual surface heat flux the larger the expected temperature increase.

For the VHTR at operating conditions, the helium inlet temperature is a function of its location within the reactor. The expected inlet temperature in the bypass portion of the first block encountered in the reactor is 764 K; this will be designated as the maximum inlet temperature condition. For the heated laboratory experiment, which will be operating with air taken from the laboratory surroundings, the inlet temperature is anticipated to be 293 K. Figure B-1 contains a plot of the ΔT equation for these extreme inlet conditions.

---

[5] Melese, G., and R. Katz, 1984, "Thermal and Flow Design of Helium-Cooled Reactors," La Grange Park, Ill.: American Nuclear Society.

[6] Cengal, Yunas, 2002, *Heat Transfer: A Practical Approach*, 2nd. New York: McGraw-Hill.

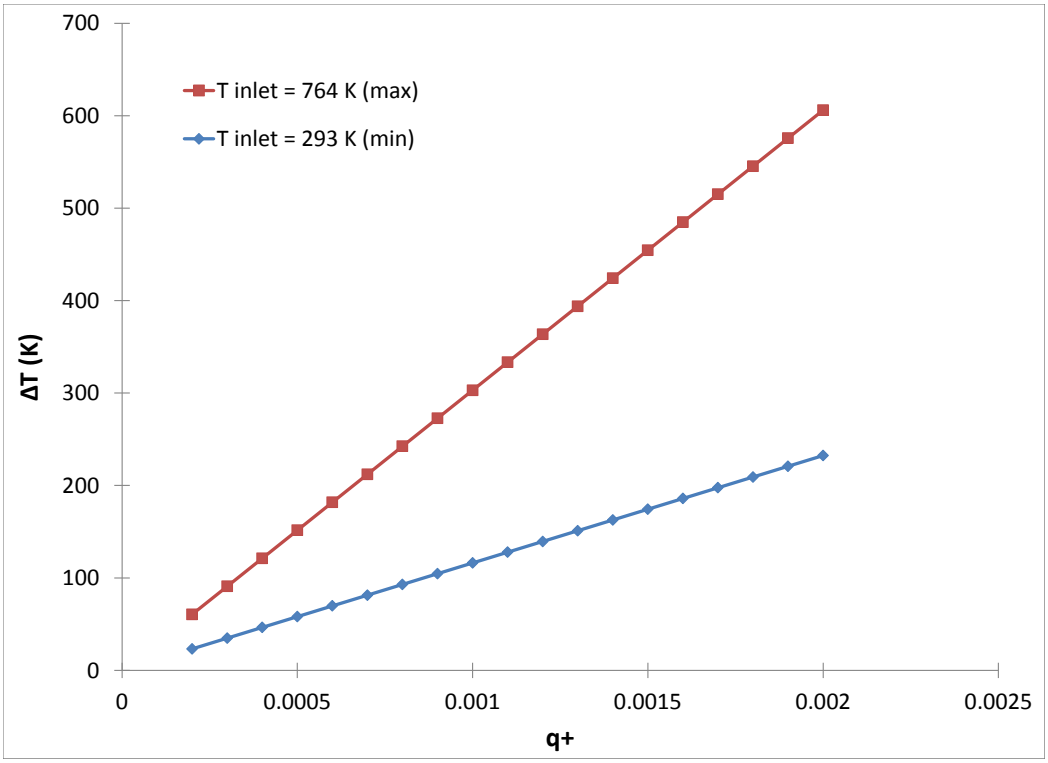

Figure B-1. Plot of expected gas temperature increase as a function of dimensionless heat flux, for the assumed flow geometry.

Analysis Using Actual Surface Heat Flux

It was also desired to examine the relationship between the fluid's temperature increase when subjected to an actual surface heat flux. The term actual surface heat flux implies a heat flux of units W/cm^2. As such, the temperature increase will also be a function of flow rate. In order to compare from the properties of one fluid to another, we use the Reynolds number, being defined as the ratio of inertial to viscous forces within a fluid. Starting with an energy balance, the expression for temperature change can be expressed in terms of flow and fluid properties:

$$\Delta T = \frac{q_s A_s}{\dot{m} C_P}$$

Next, from the definition of mass flow rate:

$$\dot{m} = \rho V A_{cs}$$

and the definition of Reynolds number:

$$\mathrm{Re} = \frac{\rho V D_h}{\mu}$$

where D_h is the hydraulic diameter and μ is the dynamic viscosity, an expression for the mass flow rate in terms of Reynolds number is given by:

$$\dot{m} = \frac{\mathrm{Re} \cdot P \cdot \mu}{4}$$

The hydraulic diameter is given according to the standard definition

$$D_h = \frac{4A_{cs}}{P}$$

where P is the wetted perimeter of the flow channel. Substituting produces an expression for the temperature increase as a function of fluid properties (μ and C_p), geometry (A_s and P), actual heat flux, and the dimensionless Reynolds number:

$$\Delta T = \frac{4q_s A_s}{\mathrm{Re} \cdot P \cdot \mu \cdot C_p}$$

This equation presents a relation to model temperature change as a function of fluid properties (μ and C_P), geometry (A_s and P), dimensionless flow rate (Re), and the actual surface heat flux. For a fixed flow channel geometry, A_s and P will be defined and assumed fixed. In a simple model, in which temperature-dependent changes in fluid properties are neglected, μ and C_P can be assumed constant. For a more complex model, these effects can be included; for this analysis, fluid properties are assumed constant over the heated flow channel. If a constant Reynolds number is assumed, this equation can then be used to calculate the temperature increase for varying surface heat fluxes. Figure B-2 shows a plot of this equation for both dry air and helium, at Reynolds numbers of 1000 (expected laminar) and 4000 (expected turbulent). The fluid properties used in these calculations are given in Table B-1 and are taken from Cengal and Boles[7].

Table B-1. Fluid Properties of Helium, Dry Air and Humid Air

	Inlet Temp (K)	Specific Heat (kJ/kg K)	μ (Pa•s)
Helium	764	5.2	2.0E-05
Dry Air	293	1.01	1.86E-05
20% Humid Air	293	1.7	1.82E-05
50% Humid Air	293	2.6	1.81E-05
70% Humid Air	293	2.8	1.81E-05

[7] Cengal, Yunus and Michael Boles, 2002, *Thermodynamics: An Engineering Approach*, 4th, New York: McGraw-Hill.

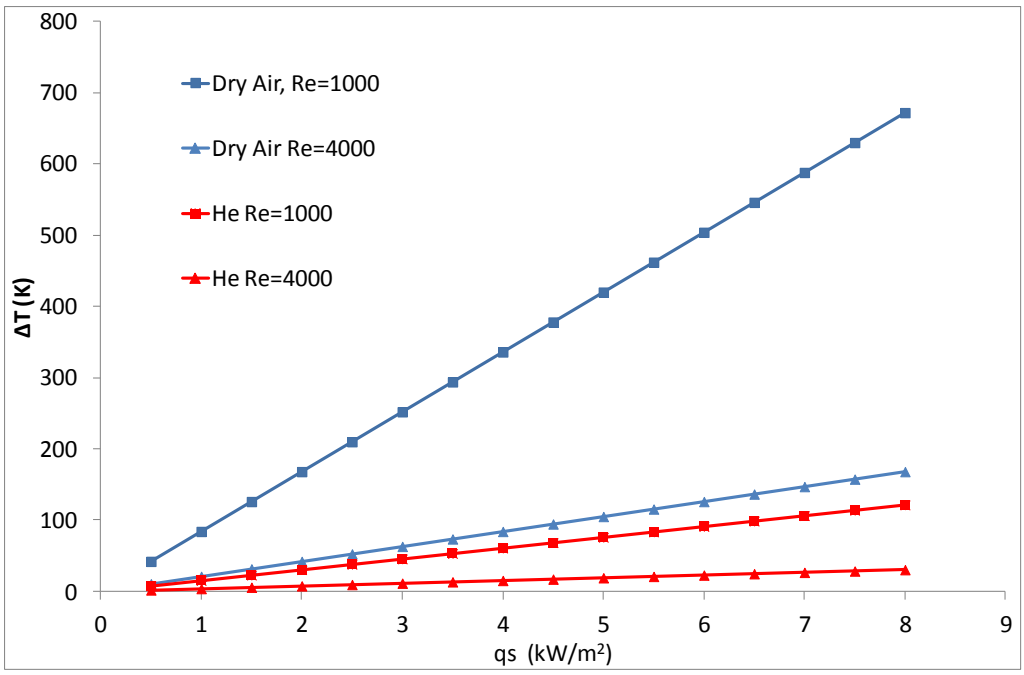

Figure B-2. Plot of ΔT for a given wall heat flux at a Reynolds numbers of 1000 and 4000.

As evident in Figure B-2, the temperature increase of dry air will be larger than that of helium, at the same surface heat flux and Reynolds number. This was expected because the specific heat for the helium is much greater than that of dry air; helium requires more energy per mass to change its temperature. Also from Figure B-2, at higher flow rates (i.e., greater Reynolds numbers), the temperature increase of a particular fluid will be less than with the lower flow rate. For a specified Reynolds number, the larger Re (4000) will result in more mass flowing through the heated channel, hence producing the lower temperature increase.

It was next determined that the impact with humid air would need to be investigated. More humid air will contain more water vapor, hence, an expected larger heat capacity. The first step in the process is to establish a relationship between specific heat and a thermodynamically determined property for the humid air. From basic thermodynamics, by assuming a strong temperature dependence on both specific heat and enthalpy, the relationship is expressed as:

$$C_p = \left(\frac{\partial h}{\partial T}\right)_p$$

where h is the specific enthalpy of a substance. To simplify, this in turn can be approximated as the slope of the h(T) line at constant pressure:

$$C_p = \left(\frac{\partial h}{\partial T}\right)_p \cong \left(\frac{\Delta h}{\Delta T}\right)_p$$

The data used to calculate the slope of h(T) was taken from the property calculator for moist air, available from Wolfram Mathematics[8]. Using the data found in Table 1, the ΔT equation can be plotted for the new

[8] "Calculator for Moist Air." *Wolfram Alpha*. Wolfram Aplha LLC, 2011. Web. 16 Jan 2012. <http://www.wolframalpha.com/entities/calculators/moist_air_calculator/yt/ul/ik/>.

values of specific heat, each corresponding to a particular relative humidity. Figure B-3 shows a plot of this equation for four relative humidity values (0% -- dry air, 20%, 50%, and 70%) as for a specified Reynolds number of 1000. The value for 20% relative humidity corresponds to the approximate average yearly values at the proposed laboratory (in Pocatello, Idaho). The value of 70% was assumed to be the maximum expected value in the event of a rare humid day. The 50% value was used as a further comparison. As evident in Figure B-3, the higher the relative humidity, the smaller the temperature increase. This was expected because more humid air will have a corresponding higher specific heat than dryer air. Also, it may be noted that there is a relatively large effect, for increasing humidity values, when the humidity is closest to dry air. However, for larger relative humidities (i.e., 50% and 70%), the relative change in temperature increase is much lower. For example, this can be demonstrated at a surface heat flux of 4 kW/m^2 in which dry air experiences a temperature change of approximately 325 K whereas 20% relative humidity air has a temperature increase of only about 175 K; the temperature increase values for the 50% and 70% relative humidity data points are almost indistinguishable.

Figure B-4 is a plot of the same relative humidity values with air at a greater flow rate (Re = 4000). From this figure, it is evident that the trends described for Figure B-3 also hold for Figure B-4, just that the values of the temperature increase are different; higher flow rates produce lower temperature increases for

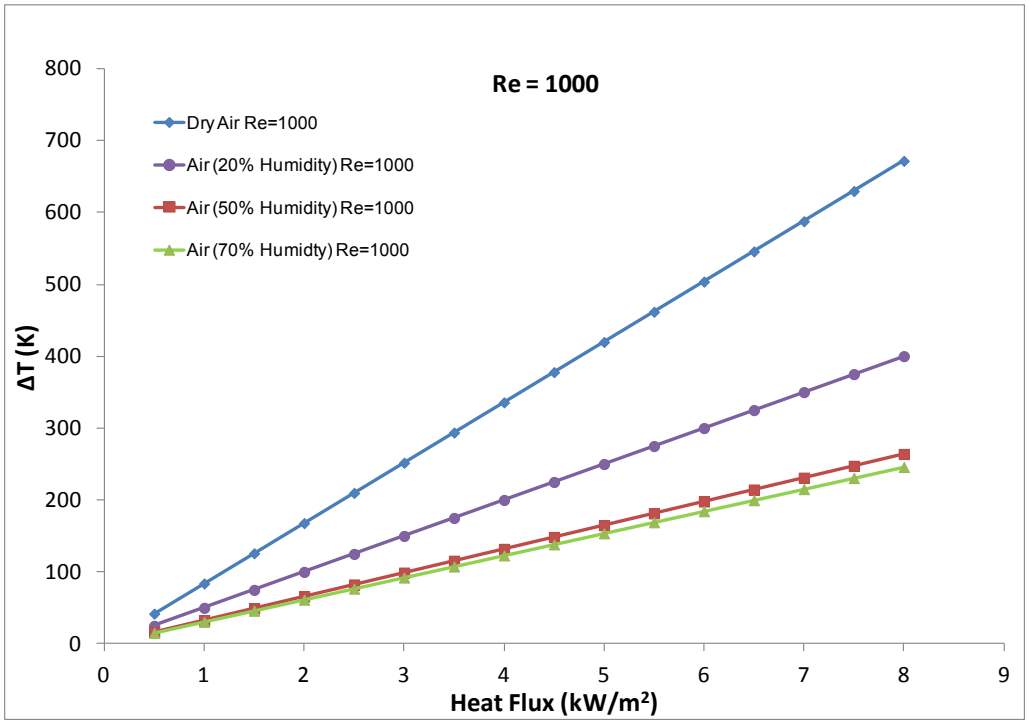

Figure B-3. Plot of ΔT of air for a Reynolds number value of 1000, at relative humidty levels of 0%, 20%, 50%, and 70%.

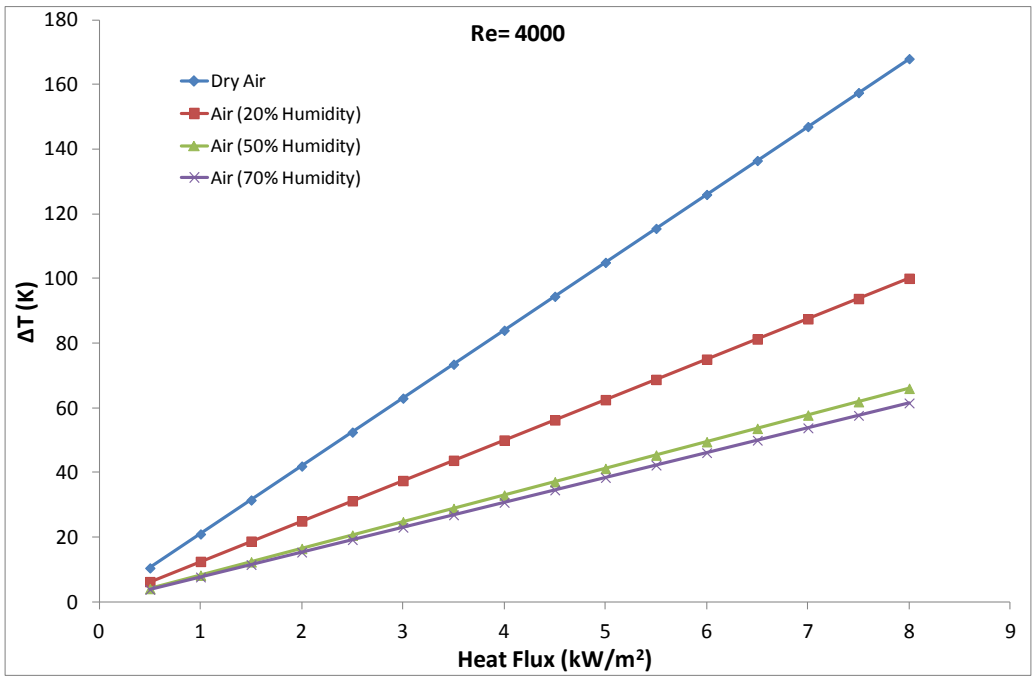

Figure B-4. Plot of ΔT of air for a Reynolds number value of 4000, at relative humidty levels of 0%, 20%, 50%, and 70%.

C. Particle Imaging Velocimeter (PIV)

Concurrent to the flow visualization efforts, work is progressing on the development of an inexpensive particle imaging velocimetry (PIV) system. Originally, we evaluated a particle tracking velocimetry (PTV) system prior to deciding upon using the PIV system. The PTV system requires complex algorithms to decipher the velocity vectors, high speed cameras, and typically has a low particle density. The PTV algorithms are not always reliable and the high speed cameras are usually expensive and error prone. For a PIV system, there are usually higher particle densities and only two successive images are needed to produce a velocity vector. Well established correlation algorithms from signal processing give statistical information about the flow's average heading; hence a flow field is obtained.

Our proposed PIV system will operate by using a camera running open shutter mode. Two flashes, mounted orthogonal to the camera, will be installed; once flash will operate with red light while the other will operate in blue. Within a darkened environment, the two flashes will fire at a known time lag (Δt). The camera shutter will then be closed. The image will then be analyzed, to separate out the red and blue channels, and then cross correlated.

Our novel PIV system has undergone its first set of testing. This testing was performed with a container of water in which the silver-coated hollow glass beads were inserted and then mixed. A simple explanation of the system is that a camera, with an open shutter, is in a dark environment. A flash system, first green and then red, is timed illuminate the glass beads at a specified spacing (Figure C-1). The simplicity of this system is due to elimination of an expensive high-speed camera; the timing between two frames is dictated by a simple, inexpensive timing circuit. The image is then separated into green (time zero) and red (delta time later) and then analyzed via PIV software to determine the velocity field (Figure C-2).

The next use of this PIV system will be with the bypass flow visualization experiment. The objective will be to acquire quantifiable data, in addition to the flow visualization. Velocity fields will help in

determining the regime of the flow (laminar versus turbulent, based on the shape of the velocity profile), the distance of the developing entrance length, as well as the flow patterns as the fluid transitions from one block through the beveled edges to the next block.

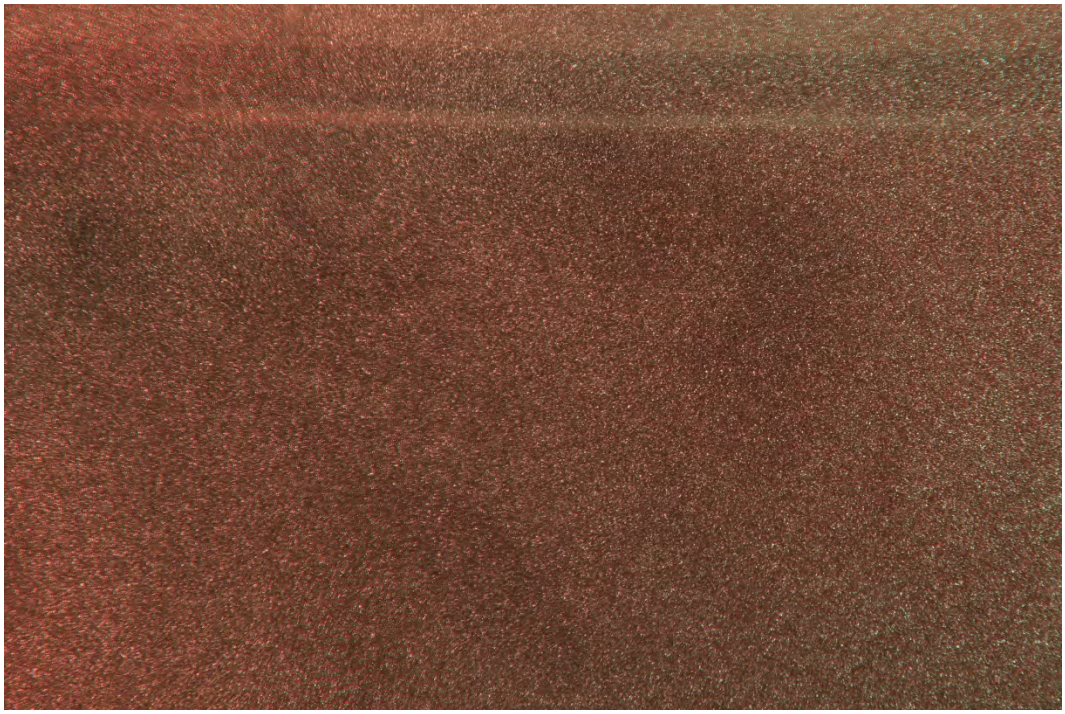

Figure C-1. Raw camera image from our PIV system. The green dots represent the images taken at the initial time when the green flash was excited, whereas the red dots represent the images taken after the set timing (via an open shutter) excited the red flash.

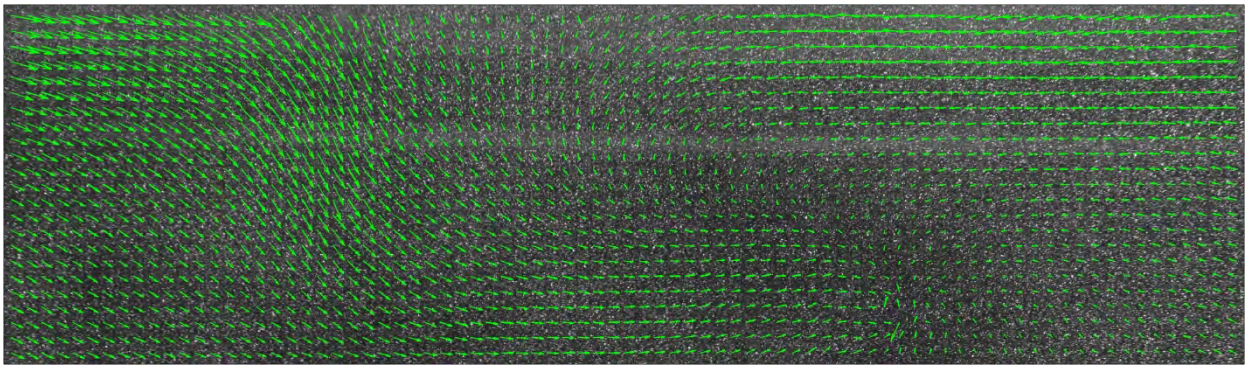

Figure C-2. Resolved velocity field, shown with the green arrows, for the raw PIV image shown in Figure C-1.

Appendix C contains a "how to" document on the operation of the PIV system. The PIV system is currently being integrated with the flow visualization experiment in order to obtain quantitative data of velocity profiles.

D. Flow Visualization Experiment

Dr. Glenn McCreery and Logan Tew have put together a draft report with regards to the flow visualization and pressure loss measurement efforts. Their draft report is presented below.

The Modular High Temperature Gas-Cooled Reactor (MHTGR) has been chosen as a reference design for the Next Generation Nuclear Plant (NGNP) project. This reactor consists of concentric stacks of graphite blocks containing embedded fuel elements. Helium will be used as the coolant and will flow through coolant channels within the graphite blocks as well as in the gaps separating the blocks (called the bypass flow). A key phenomenon that may lead to localized hot spots in the reactor is the degradation of heat transfer effects in the bypass flow due to geometry distortions. Geometry distortions are the result of the graphite blocks being irradiated with energetic neutrons as well as thermal expansion effects due to temperature changes. Idaho State University is studying heat transfer within the bypass flow and is developing a heated experiment to study the deterioration of heat transfer in the bypass flow stemming from these geometry distortions. Experimental data gathered from this project will be used to benchmark numerical codes used in the design and safety analysis of the MHTGR.

Flow visualization and preliminary pressure loss experiments were conducted prior to the final design of the heated experiment in order to characterize flow patterns approaching and within the bypass channel and to help quantify wall friction and pressure loss coefficients. A water-flow visualization apparatus was used to characterize bypass channel flow patterns using dye and particle tracers. The transparent acrylic plastic model consisted of an inlet plenum, a beveled entrance to the simulated rectangular bypass channel, a diamond shaped cut-out that simulated the junction between two fuel blocks, and an exit bevel. The cross-section dimensions of the bevels, cut-out, and (adjustable gap width) channel were full-scale. The results were recorded photographically and with high-definition video. A water flow apparatus similar to that used for flow visualization was used to measure pressure distribution within the channel. Flows in both the visualization and pressure loss experiments were varied from laminar to highly turbulent.

Flow visualization results and preliminary pressure loss measurements for one channel gap width (0.137 inch) are reported. The pressure loss data are related in this report to phenomena observed in the flow visualizations. The work to relate pressure loss measurements to existing correlations and to characterize pressure loss coefficients for the entrance, and bevel cut-out is ongoing. The channel outlet pressure loss coefficient has been has been identified as being close to 1.0.

The pressure loss apparatus has been relocated to the ISU Pocatello lab and has been re-plumbed. Pressure loss experiments will continue with series of measurements for other gap widths, both wider and narrower, than 0.137 inch. The apparatus is shown in its new home in the second appendix to this report.

Flow Visualization Apparatus

A water-flow visualization apparatus was machined from acrylic plastic using computer generated drawings. The transparent acrylic plastic model, as shown in Figures D-1 and D-2, consists of an inlet plenum, a beveled entrance to the simulated rectangular cross-section bypass channel, a diamond shaped cut-out that simulated the junction between two fuel blocks, and an offset diamond shaped cut-out (to simulate the junction between two misaligned fuel blocks) upstream of the exit. The cross-section dimensions of the bevel, diamond shaped cut-out, and (adjustable gap width) channel are full-scale. The channel length is 26.00 inch and width is 6.00 inch. Gap width is adjustable between 0.125 inch and 0.375 inch. Water flow is delivered to the inlet plenum, flows through the horizontally oriented channel, and is

then deposited in a large tub whose outlet flows to a floor drain. Flow rate is measured by a Rotameter located in the inlet line and confirmed by timing the filling of a 15 quart bucket with a stop-watch.

Flow was visualized by injecting dye or 10 micron diameter silver coated hollow glass spherical tracer particles. The dye or particles were injected either by hand-held syringes or by a Harvard Instruments model 33 syringe pump. Lighting for still photographs or high-definition video was provided by either a single quartz-halogen bulb or by a Sunpak 610 electronic flash oriented to provide side-scattered illumination through a narrow slit. The camera used for both still and video photography was a Canon 5D Mark II with a 24-105mm lens set to 105mm. The distance from the lens to the plane of focus and illumination was approximately 12 inch. Lighting and dye injection are shown in Figures D-3, D-4 and D-5.

Air bubbles accumulating within the channel, and especially within the diamond shaped cut-out, were a significant problem with early experiments. The air bubble problem was partially overcome by using a large, several hundred gallon, water storage tank for the water supply. Letting water sit in the tank overnight allowed dissolved air bubbles to nucleate, float to the surface, and be removed. Air bubbles that were entrained in the flow during filling of the apparatus were also a problem. These air bubbles were removed by using a long 1/16 in. I.D. wand with vacuum provided by air flow from a compressor flowing past the tee to the wand outlet (using the Bernoulli effect).

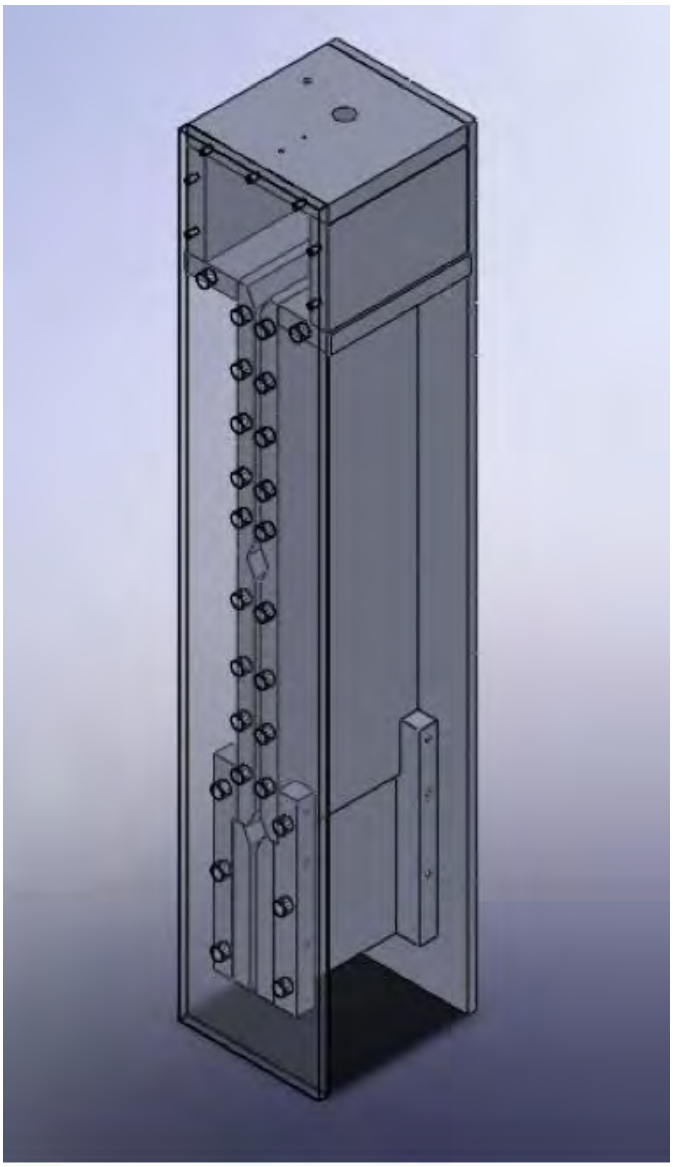

Figure D-1. Flow visualization apparatus assembly drawing.

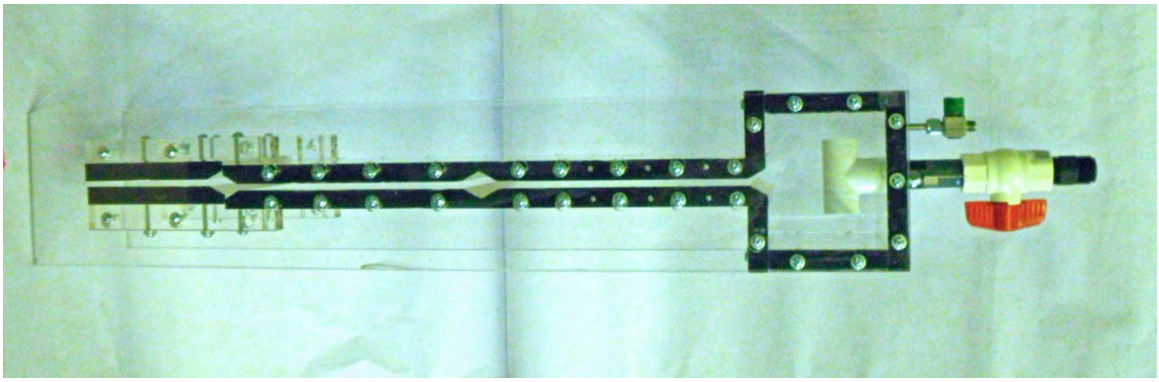

Figure D-2. Flow visualization apparatus side-view showing inlet plenum, flow channel with inlet bevel, diamond-shaped cut-out, offset cut-out and outlet.

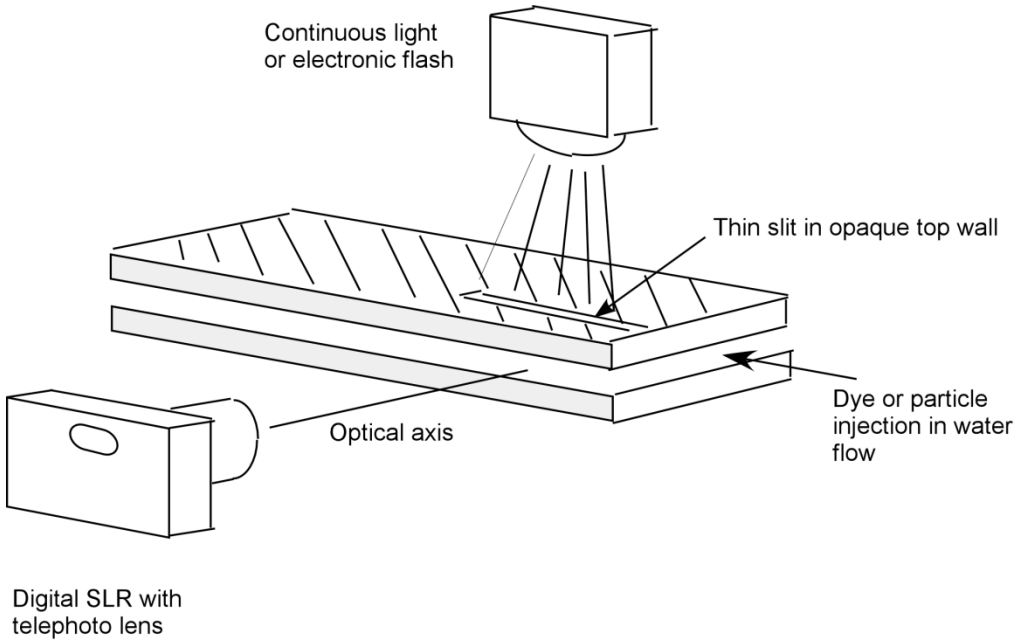

Figure D-3. Flow visualization side-scattered lighting schematic.

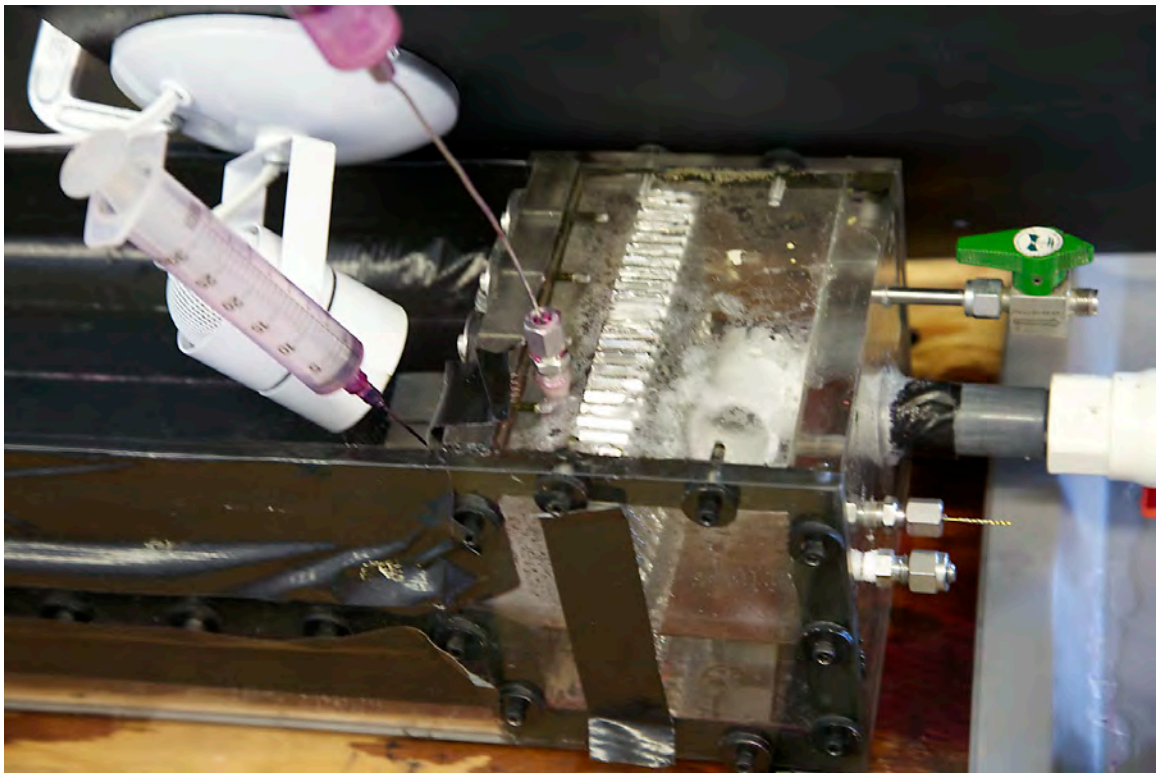

Figure D-4. Inlet region showing lighting, syringe injection of dye into inlet plenum, flow-straightening aluminum honeycomb, and inlet bevel region.

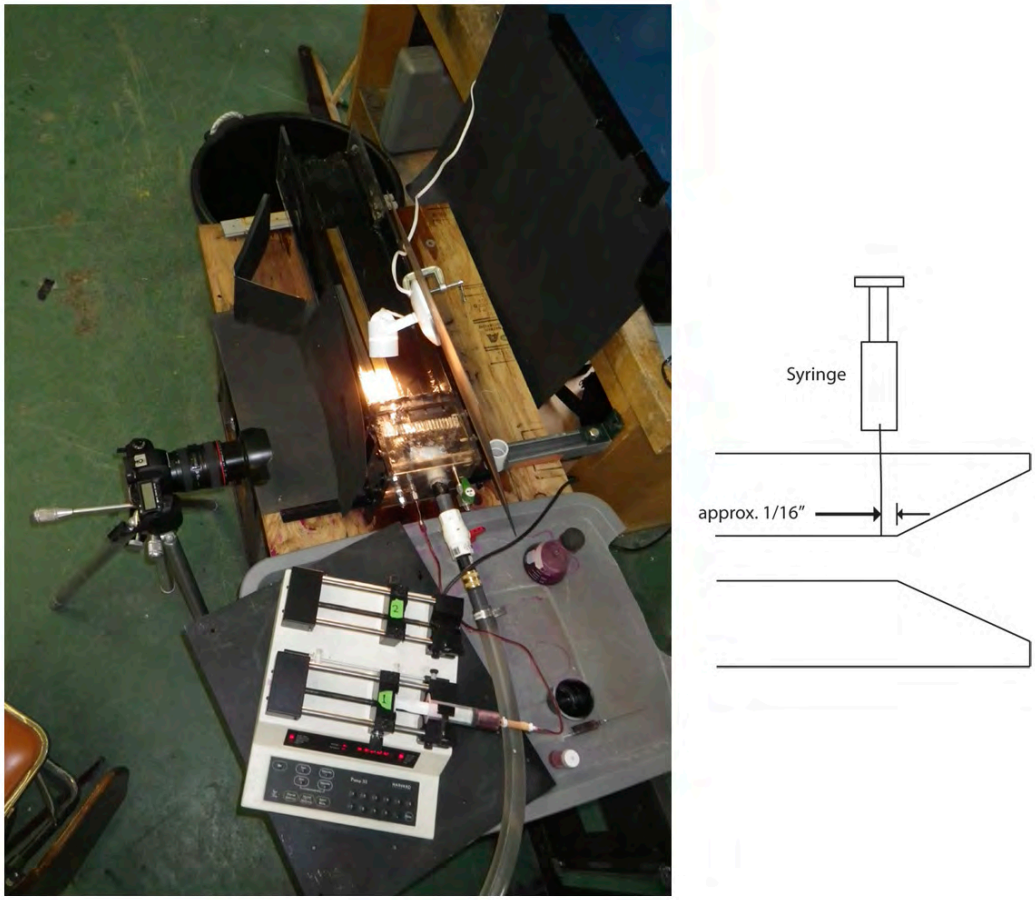

Figure D-5. Lighting and camera set-up for photographing inlet flow using a syringe pump for dye/particle injection 1/16" downstream of inlet bevel.

Sample Flow Visualization Photographs

A preliminary selection of photographs that illustrate laminar, transition and turbulent flow in the channel and components is presented below.

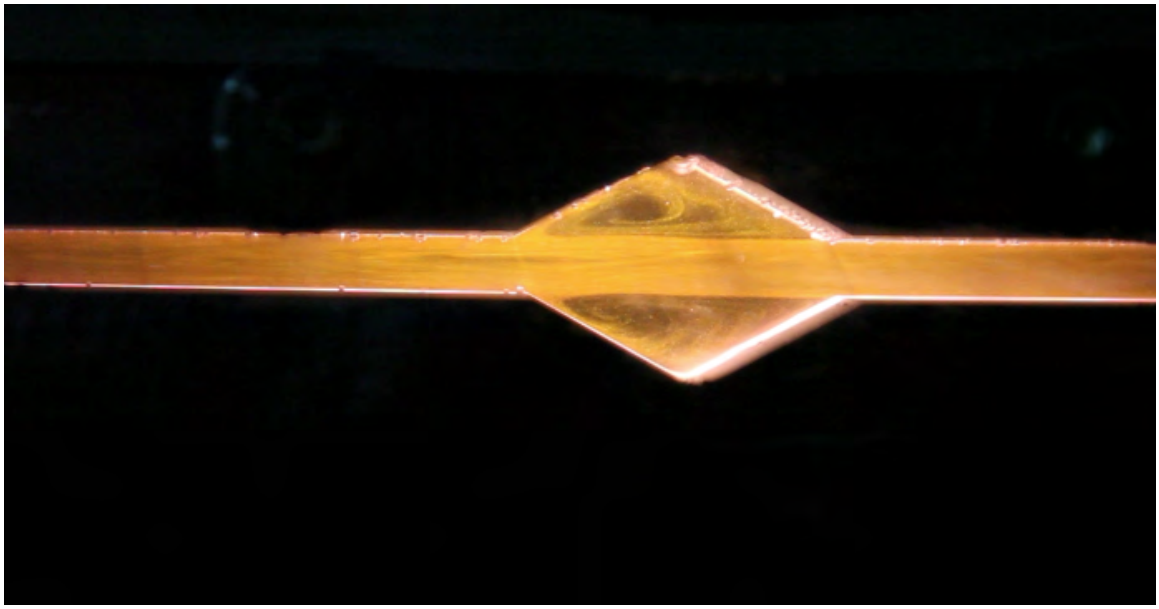

Figure D-6. Laminar bevel cut-out flow, Re = 780. The smooth inner flow core is surrounded by two slowly rotating vorticies.

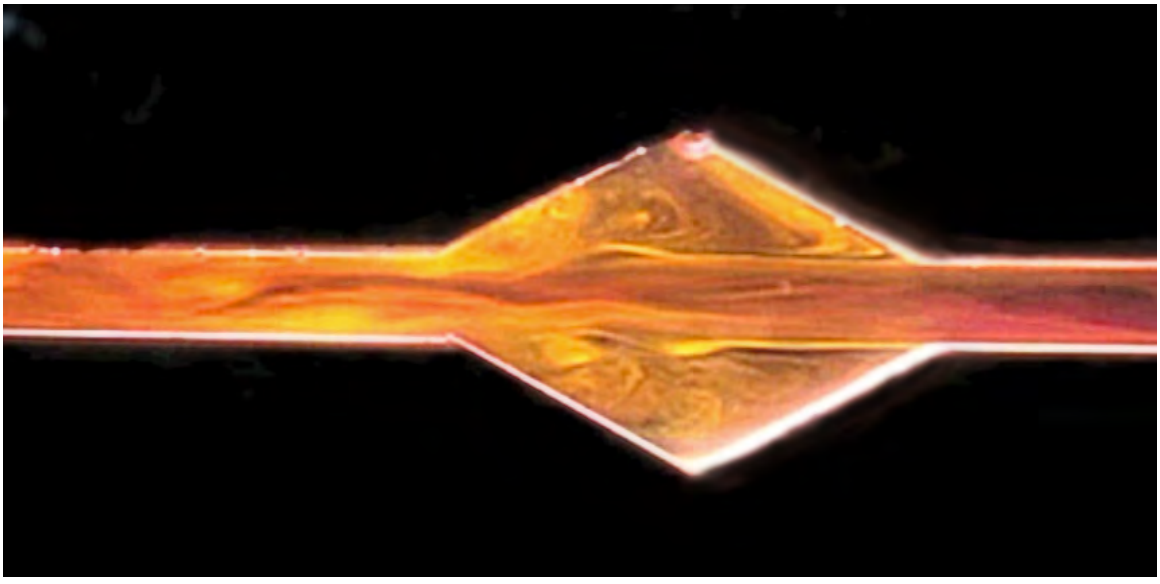

Figure D-7. Transition bevel cut-out flow, Re = 1,560.

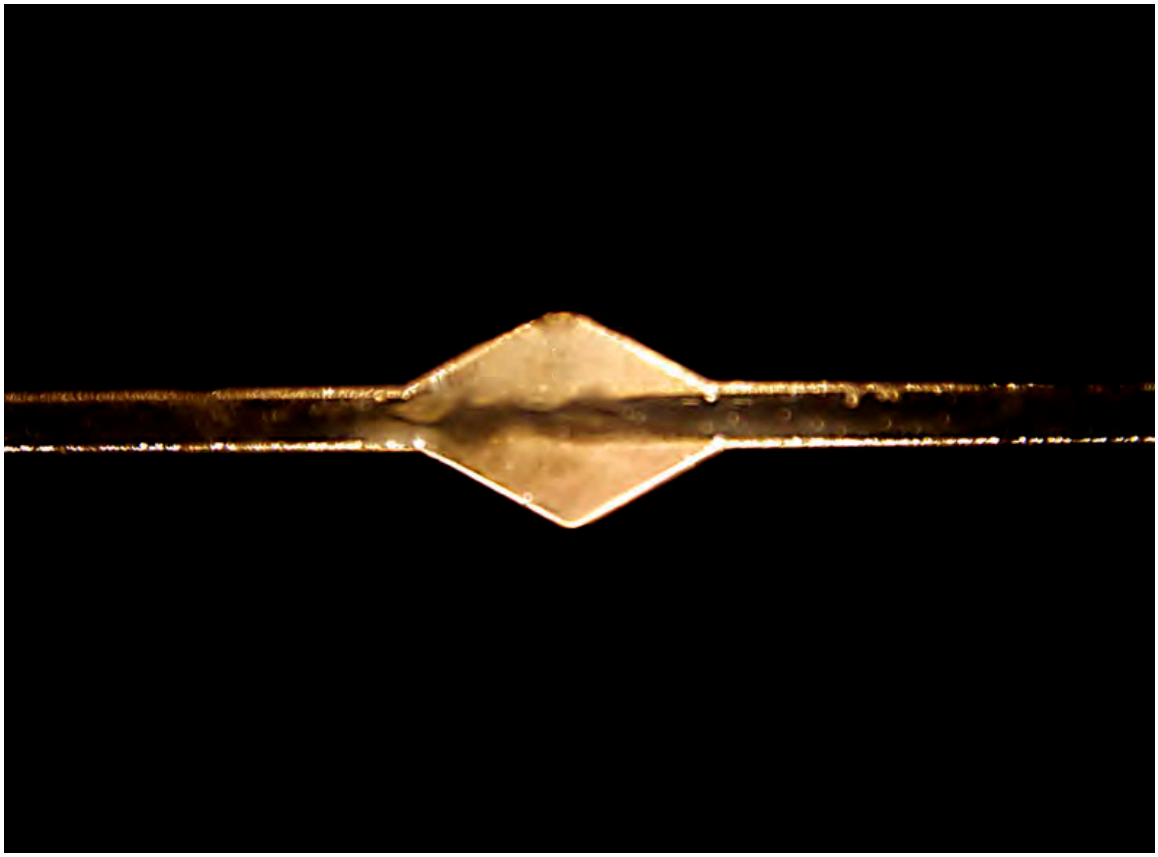

Figure D-8. Turbulent bevel cut-out flow, Re = 2,900.

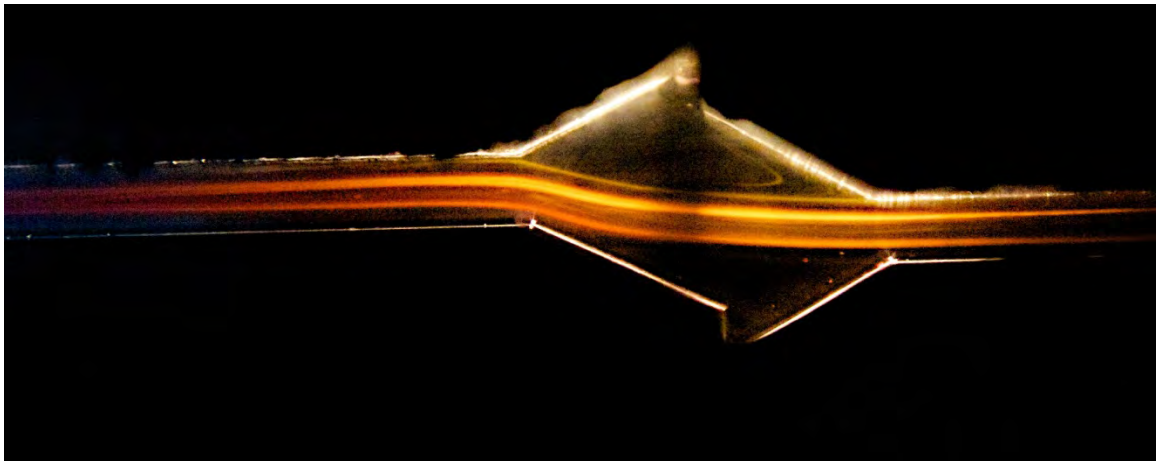

Figure D-9. Laminar offset bevel cut-out flow, Re =500.

Figure D-10. Transition offset bevel cut-out flow, Re = 1,560.

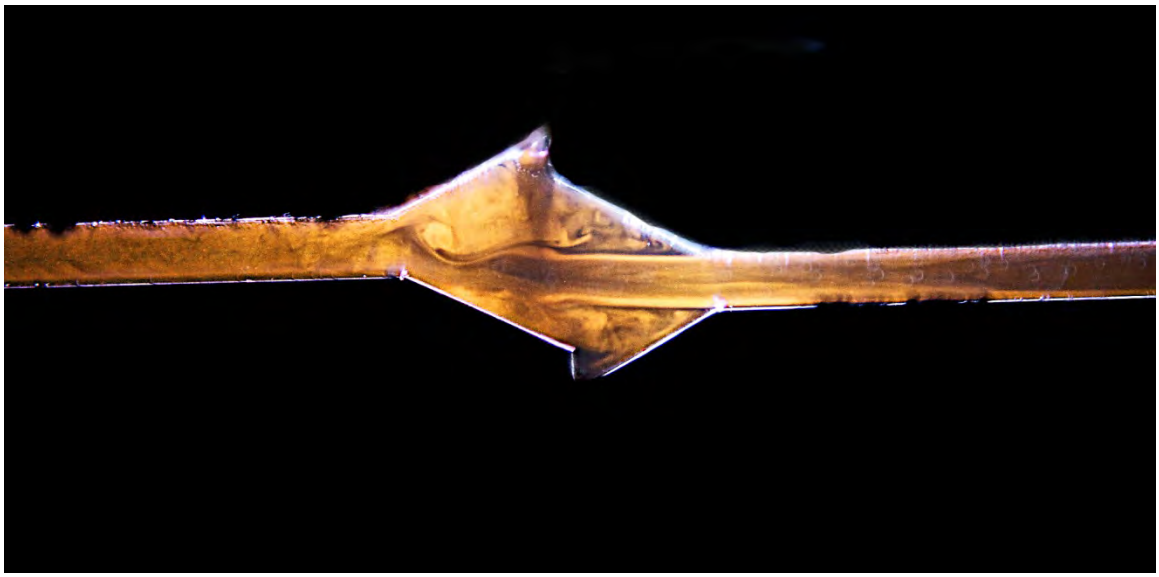

Figure D-11. Turbulent offset bevel cut-out flow, Re = 4,000.

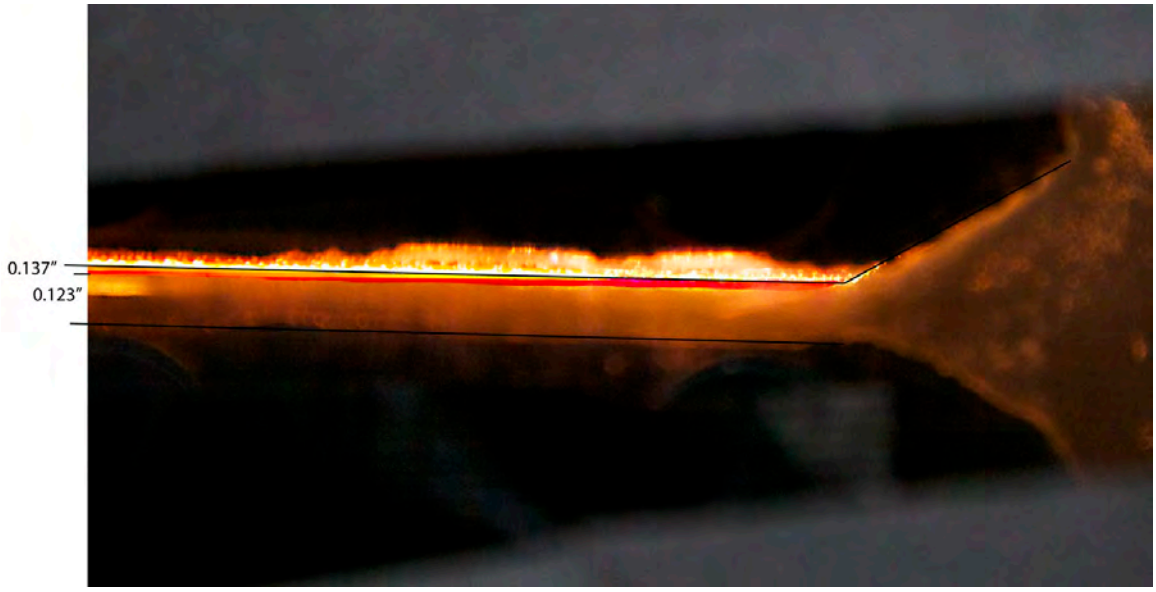

Figure D-12. Laminar entrance flow, Re = 780. Continuous red dye injection by syringe pump. The photograph shows that the vena-contracta downstream of the inlet bevel occupies approximately 80% of the gap width.

Pressure loss measurements

An apparatus similar to the flow visualization apparatus was constructed for plenum and channel pressure measurements. The channel length is 28.50 in. and the width is 6.00 in. The channel gap width is adjustable between 0.125 inch to .375 inch. The channel contains an inlet bevel, a diamond shaped cut-out, and an exit bevel. In addition to an inlet plenum, as was provided in the flow visualization apparatus, an outlet plenum with free-surface outlet flow was incorporated so that pressure loss across the outlet bevel could be measured. Flow rate is measured by a Rotameter located in the inlet line and confirmed with more accuracy by timing the filling of a 15 quart bucket with a stop-watch. Water temperature is measured with a finely graduated thermometer. The average gap width was measured after assembly by filling the channel with a carefully measured quantity of water. The procedure is described in Appendix D-1.

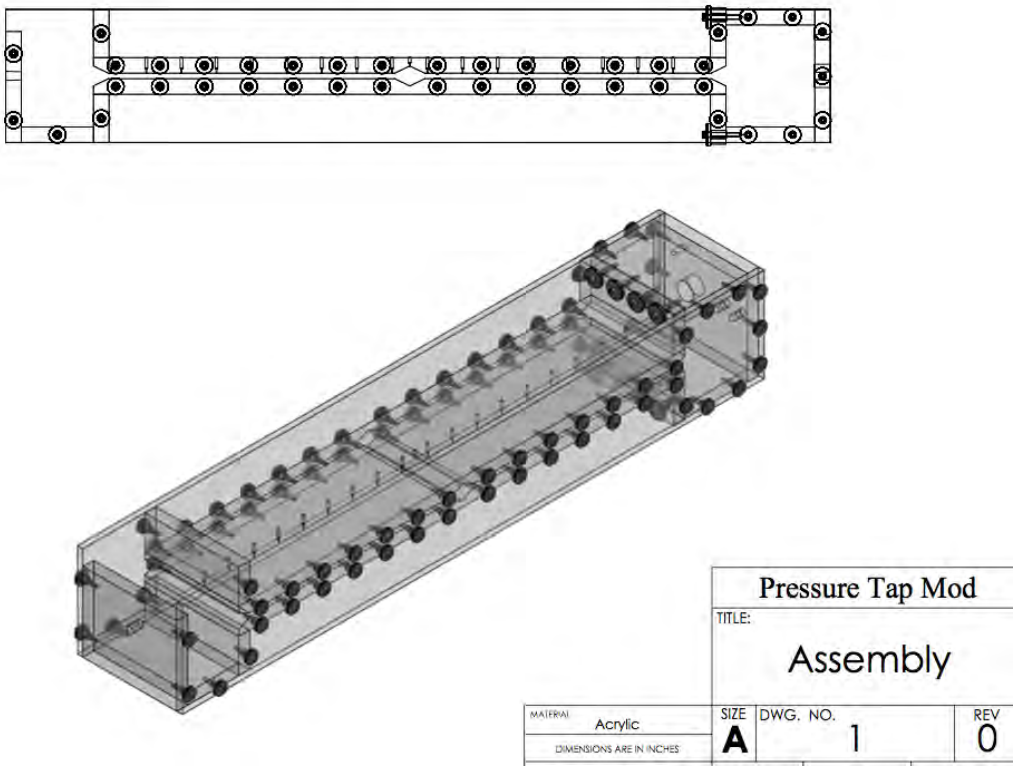

Figure D-13. Pressure loss measurements apparatus assembly drawing.

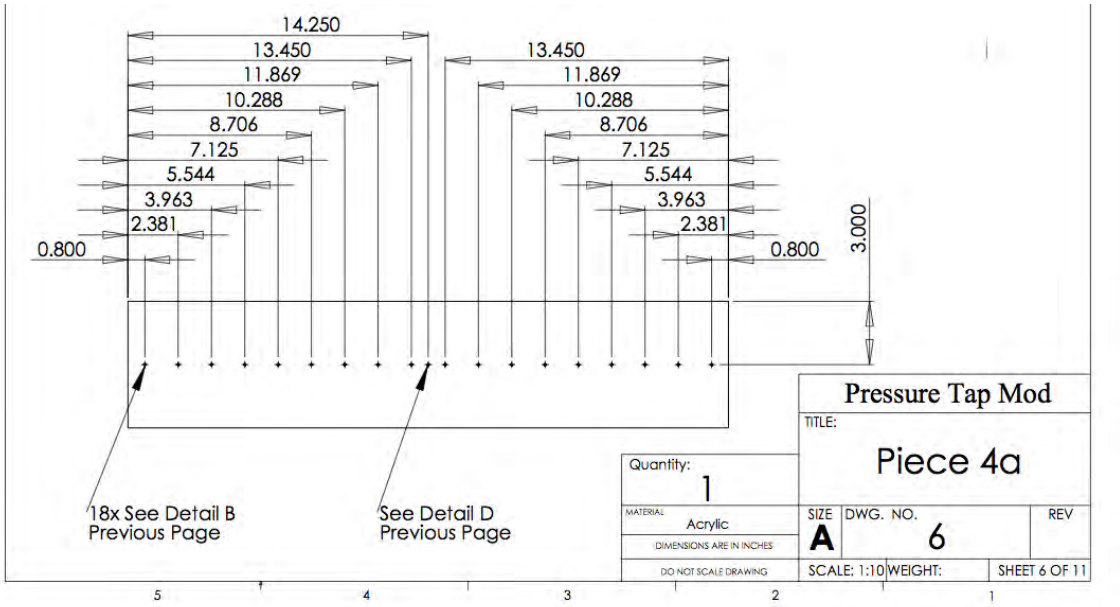

Figure D-14. Pressure tap locations in the top wall of the channel. Pressure taps are located at 21 positions, 19 in the top wall of the channel and one each on the channel center-line elevation in the inlet and outlet plenums.

Figure D-15. Apparatus set-up at the Skyline lab. Showing flow channel, inclined manometer connected to one pressure tap, and water flow from outlet plenum into the outlet tub.

Sample Pressure Measurements

A series of pressure measurements with the channel gap width set to 0.137 in. were obtained for flows varying from laminar to fully turbulent. Water temperature was held constant during any one experiment and varied from 13 ^{o}C to 14 ^{o}C over the range of experiments. Pressure measurements for all experiments are displayed in Figure D-16. Measurements are shown in more detail for Reynolds numbers of 1,500, 2,159, 3,940, and 6,495 in Figures D-17 through D-20.

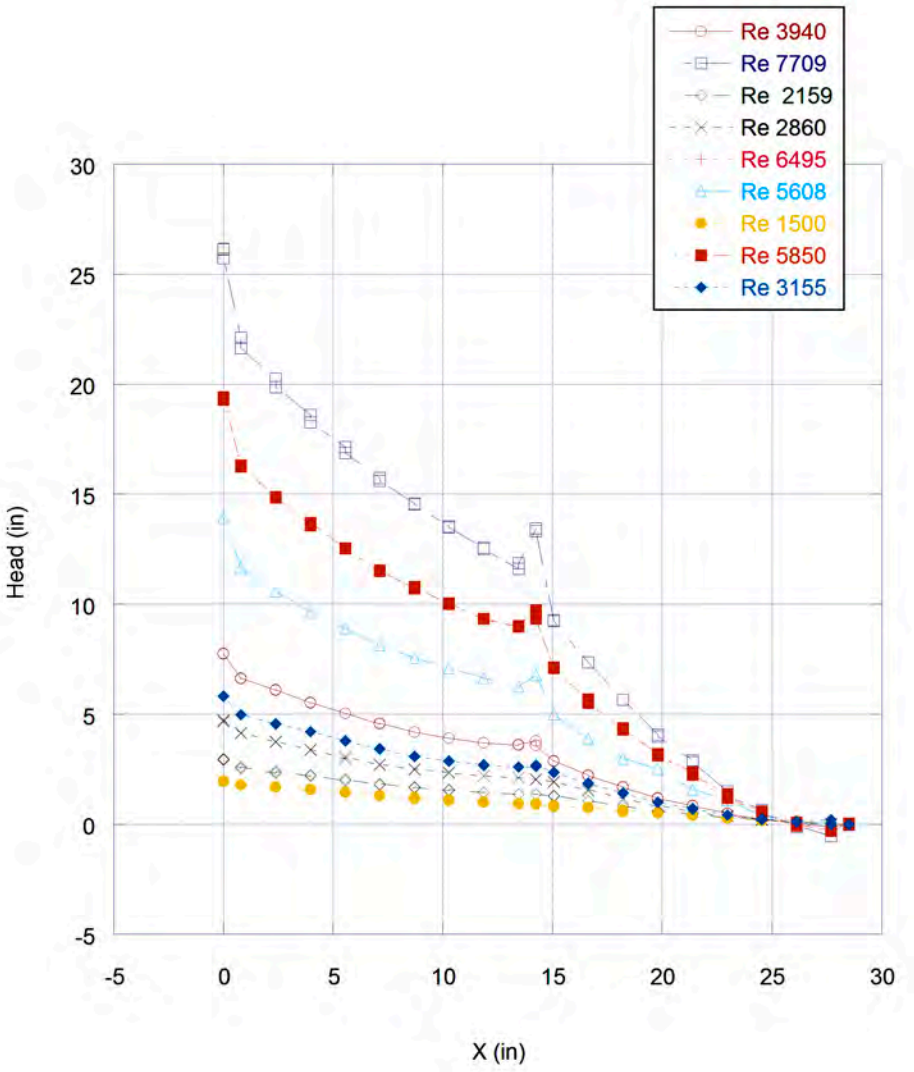

Figure D-16. Head versus distance from inlet for all data with channel gap width = 0.137". Head is relative to the channel center-line in the outlet plenum.

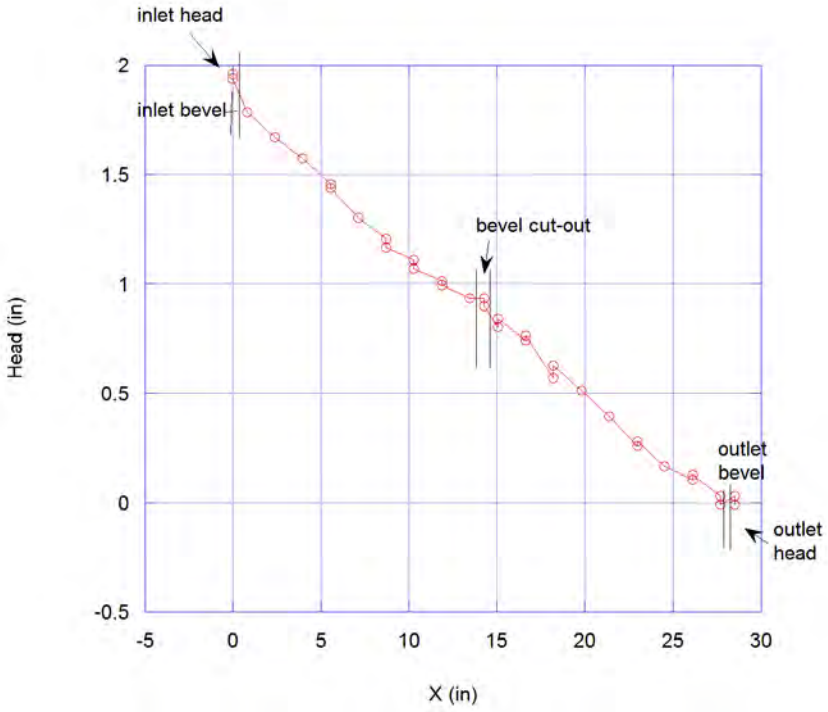

Figure D-17. Head versus distance for Re = 1,500 (laminar flow).

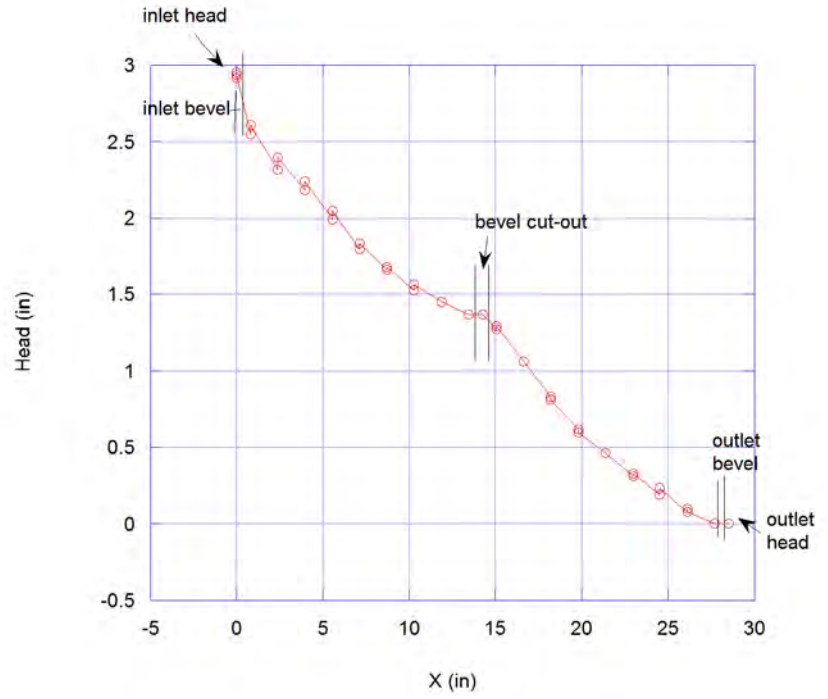

Figure D-18. Head versus distance for Re = 2,159 (transition or low turbulent flow).

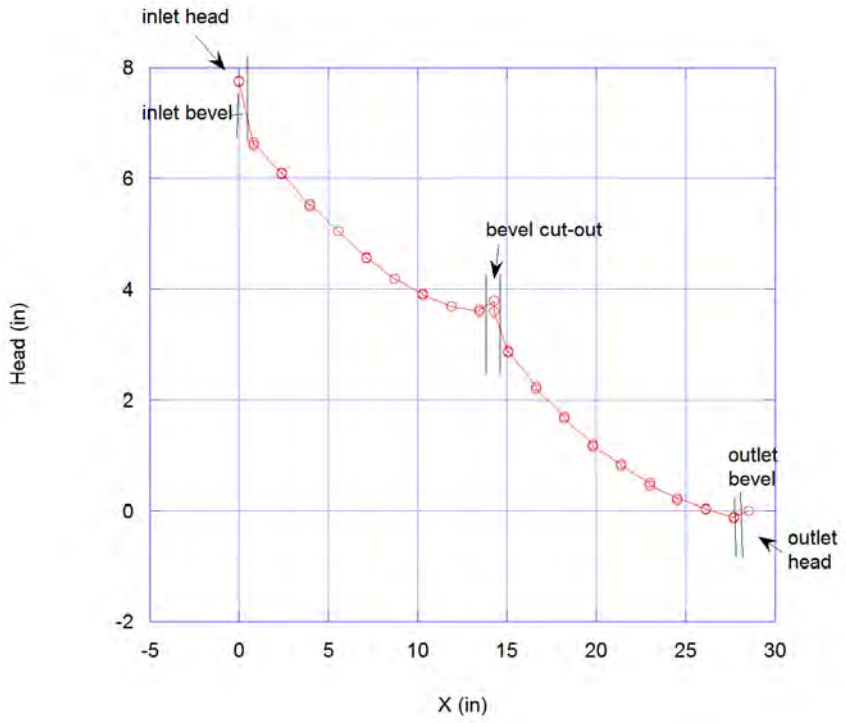

Figure D-19. Head versus distance for Re = 3,940 (turbulent flow).

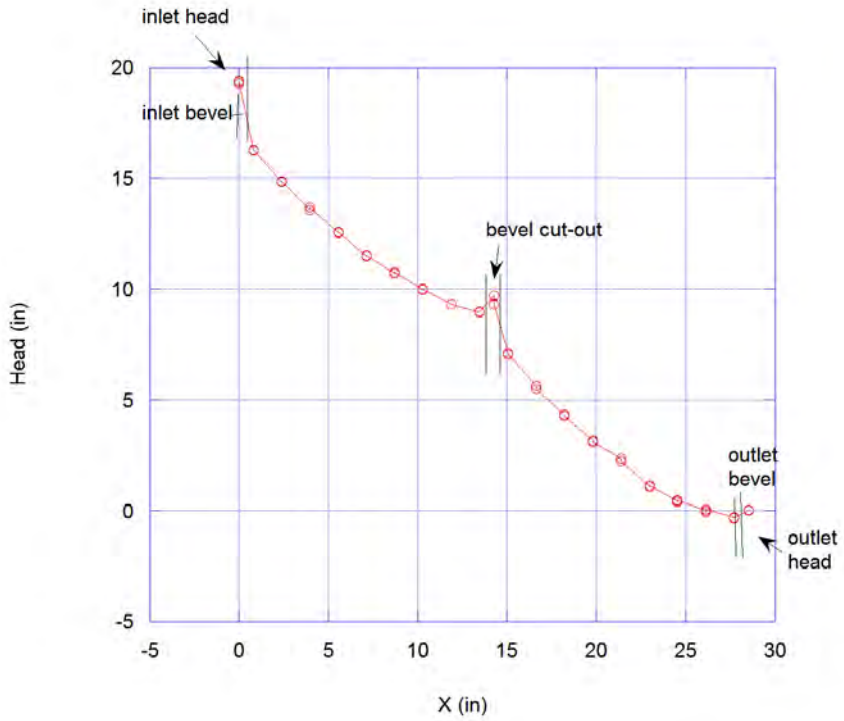

Figure D-20. Head versus distance for Re = 6,495 (fully turbulent flow).

The pressure measurements will be used to calculate loss coefficients and for comparison with friction loss correlations. This work is ongoing and will incorporate results from measurement series using other gap widths. A few preliminary observations are given:

1. The laminar flow visualization photographs for laminar flow through the diamond shaped bevel cut-out show that the main flow maintains its smooth profile as it transits the cut-out surrounded by two counter-rotating vortices. This implies that the pressure loss for laminar flow is small as the data confirms (Figure D-17).

2. There is little head change as the flow from the channel enters the outlet plenum. The change is essentially zero for laminar flow and only a very small amount of head recovery is shown for turbulent flow. This means that most or all kinetic energy is dissipated as channel flow mixes with low velocity flow in the outlet plenum. This exit loss coefficient is therefore equal to or close to 1.0.

3. The large vena-contracta observed at the inlet implies that the entrance loss coefficient is small. (If the geometry were circular rather than rectangular, results shown in Idelchik, "Handbook of hydraulic resistance and coefficients of local resistance and of friction", AEC-TR6630, 1960, the loss coefficient for the same dimensioned bevel at the entrance would be approximately 0.12).

4. A major effect of the bevel cut-out appears to be that the velocity profile relaxes from a laminar or turbulent profile to a square profile as flow transits the cut-out. The flow then appears to enter the downstream section of channel as entrance flow rather than well established flow because the pressure profile is very similar to that entering the channel from the inlet plenum. This presents a

quandary for calculating loss coefficient; does it represent pressure loss only across the cut-out or does it also reflect the additional pressure loss due to reestablishing entrance flow?

Measurement and Dimensional Uncertainties

Average gap width	± 0.002" (see Appendix D-1)
Channel wall flatness	± 0.001"
Head	± 0.04" (using inclined manometer at 29.4^{O} from horizontal)
Head	± 0.08" (using vertically oriented manometer)
Temperature	± 0.5 ^{o}C
Flow rate	± 1% (using bucket and stop-watch)
Flow rate	± 0.25 GPM (using Rotameter)
Machined dimensions	± 0.001"

Appendix D-2 contains information and pictures related to the relocation of the apparatus to the Pocatello laboratory.

Preliminary Comparison of Calculations with Turbulent Flow Pressure Loss Data

Calculations were performed with a Mathcad pressure loss program (developed by Dr. McCreery), and plotted with Kaleidagraph, using the explicit form of the Colebrook-Moody correlation for fully developed turbulent flow by Haaland[9]:

$$\frac{1}{f^{1/2}} = -1.8\ \log_{10}\left(\frac{6.9}{\mathrm{Re}_{DH}} + \left(\frac{k/D}{3.7}\right)^{1.11}\right) \qquad \text{(D1)}$$

where, k/D is the wall relative roughness ($5x10^{-6}$ for drawn tubing), Re_{DH} is the Reynolds number based on hydraulic diameter, and f is the Darcy friction factor.

White (p. 428) states that for non-circular turbulent duct flow "Best agreement between channel and pipe is predicted when one uses 0.64Dh as the "effective diameter" of the channel." So, instead of f*L/Dh, the value 0.64*f*L/Dh was used. It is unsure if "effective diameter" is being properly applied, since a similar statement was not evident in Schlichting[10]. However, it does give a much better agreement with the slope of the data.

The calculated head was matched to the data sufficiently downstream of the entrance as to avoid entrance effects (calculated development length = about 5 inches) and then again separately matched downstream of the diamond-shaped cut-out. Data and calculations for Re = 7,688 data are shown in Figure D-21 below. The difference between the two lines represents the loss due to the cut-out. The difference is approximately one velocity head (3.562 inches), or, in other words, $K_{cut\text{-}out}$ is approximately = 1.0. Similarly, at the entrance, the flow first accelerates, which represents a one velocity head decrease. The remained of the head change to the calculated line represents the head loss due to the entrance, $K_{entrance}$ of approximately 0.5.

[9] White, Frank M., 2006, **Viscous Fluid Flow**, 3rd edition, McGraw-Hill.

[10] Schlichting, H., 2000, **Boundary Layer Theory**, 8th edition, Springer.

At the exit, most data show that the head in the outlet plenum closely equals the head just upstream (although the data in the graph below shows a bit of head recovery). Therefore, $K_{exit} = 1.0$.

A preliminary look at our other turbulent data indicates that this calculation approach also provides a good fit.

For the Re = 7688 test, experiment conditions were: volumetric flow rate = 11.61 gpm, water average temperature = 12 °C, and the average gap width = 0.142 inches.

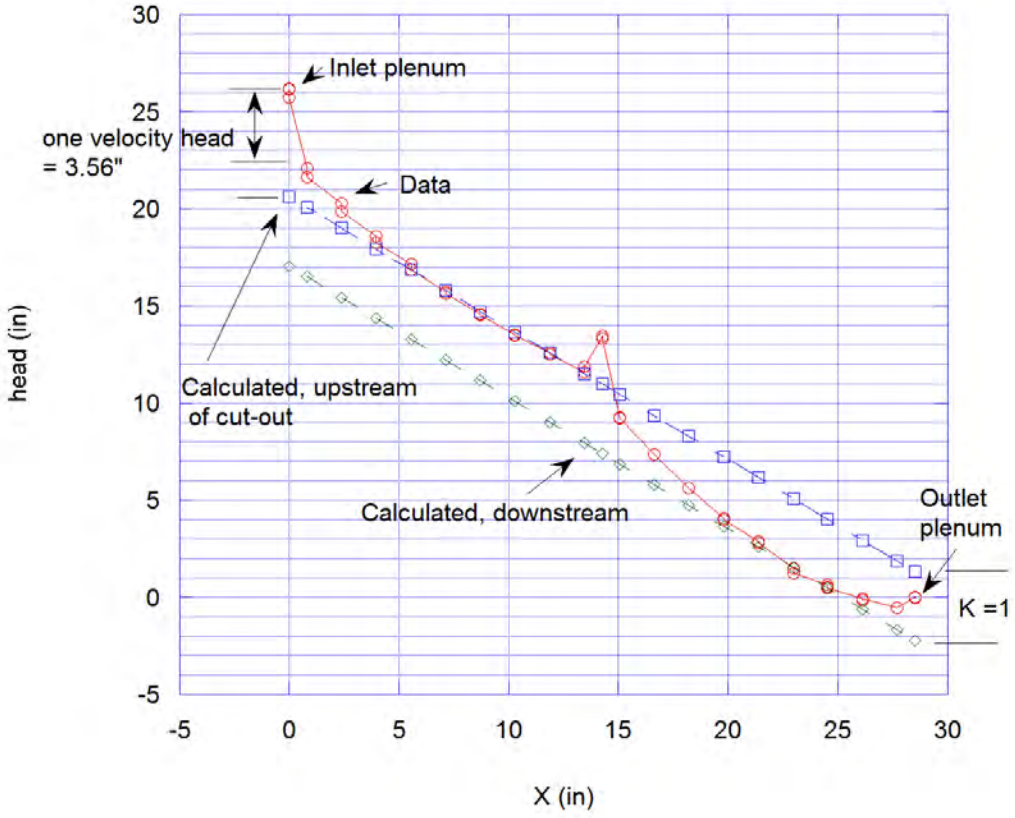

Figure D-21. Head versus distance, Re = 7688.

Calculations using the same method are compared with other turbulent flow data, shown below (Figures D-22 through D-26). The comparison looks good for the higher Reynolds number cases. The influence of developing flow on inlet loss coefficient is apparent for the three lower Reynolds number cases. Table D-1 gives the calculated K_{inlet} and $K_{cut\text{-}out}$ as a function of the test's Reynolds number.

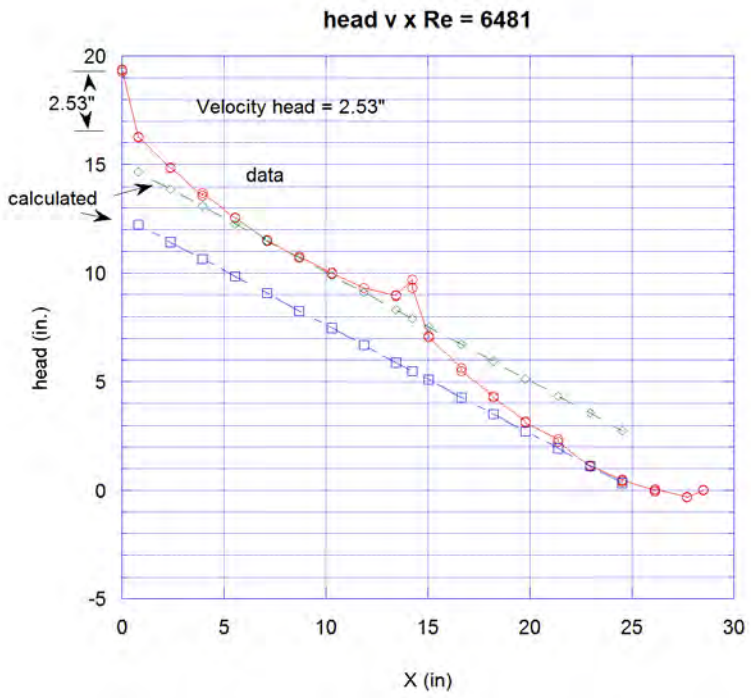

Figure D-22. Head versus distance, Re = 6481.

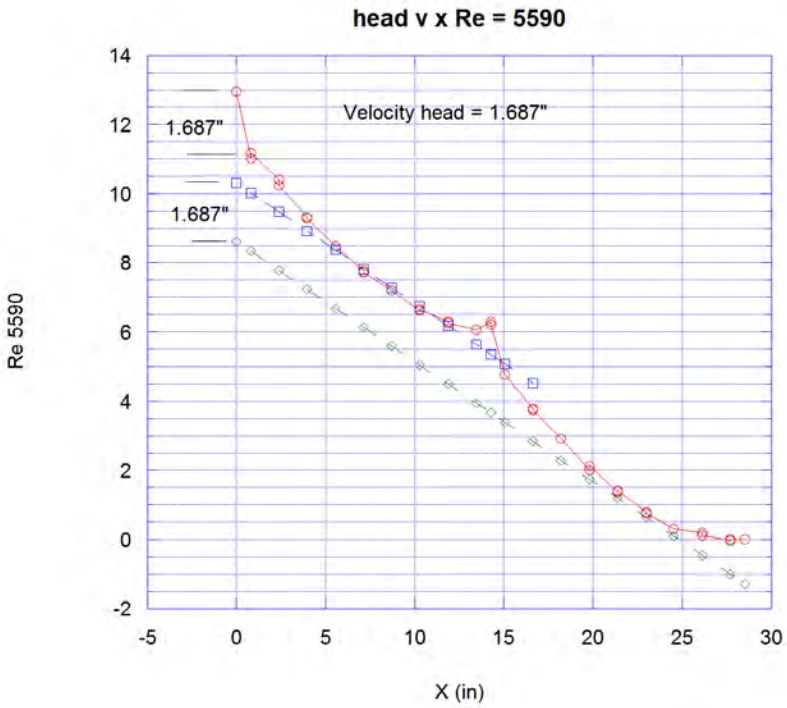

Figure D-23. Head versus distance, Re = 5590.

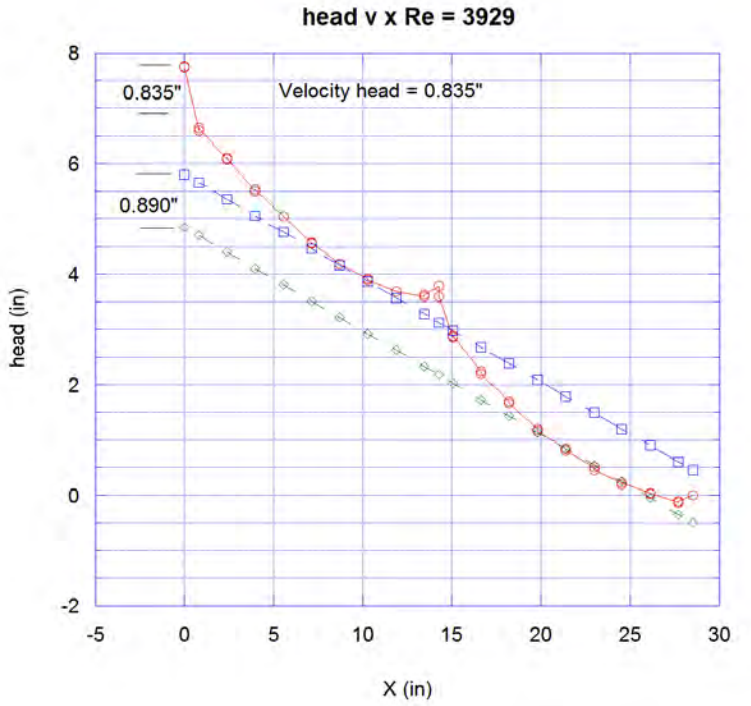

Figure D-24. Head versus distance, Re = 3929.

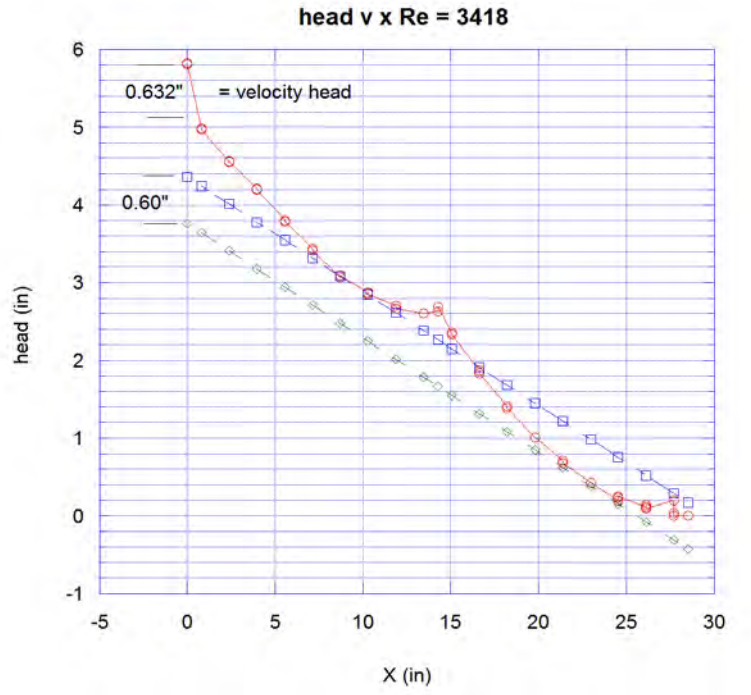

Figure D-25. Head versus distance, Re = 3418.

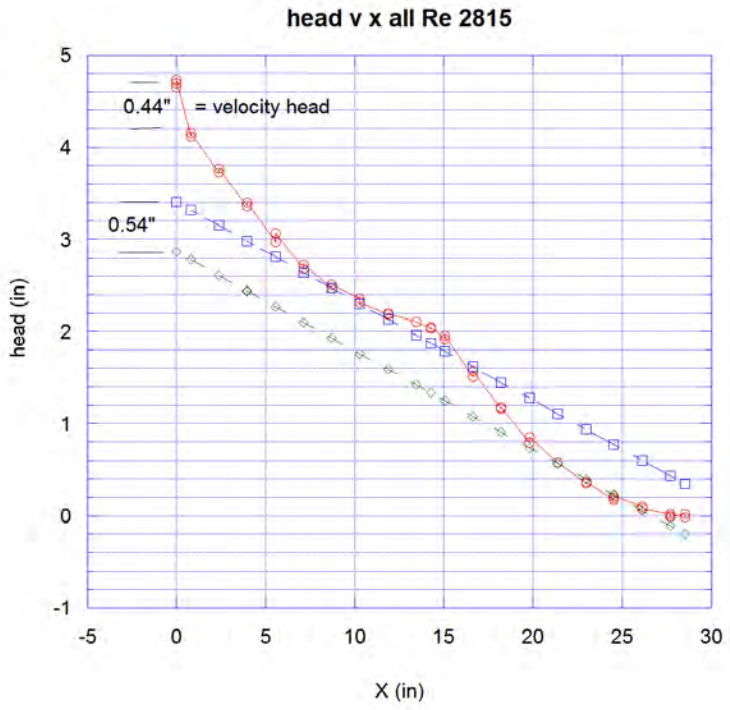

Figure D-26. Head versus distance, Re = 2815.

Table D-1. Calculated K-values for Tests.

Re	K_{inlet}	$K_{cut-out}$
6481	0.54	1.0
5590	0.57	1.0
3929	1.29	1.07
3418	1.32	0.95
2815	1.72	1.20

E. Plenum Flow Visualization Investigation

Within the experimental setup there are two plenums with different entrance and exit geometries. The plenum of most concern is the entrance plenum, directly proceeding the parallel-plate test section (see Figure E-1.) The issue is that a 3-in nominal pipe feed air into the top of the plenum whereas the test section flow geometry is essentially a wide, narrow slit. Of concern is the possibility of the flow from the circular pipe being biased towards an uneven flow profile when it enters the test section (see Figure E-2a.) The purpose being this testing was to determine flow conditioning that would take the circular-flow pattern exiting the pipe and convert it to a uniform flow into the test section (see Figure E-2b.)

Results indicate that a flow conditioning consisting of a 152 mm diameter circular plate located 32 mm from the pipe entrance would be adequate. A copy of the full flow visualization report can be found in Appendix E.

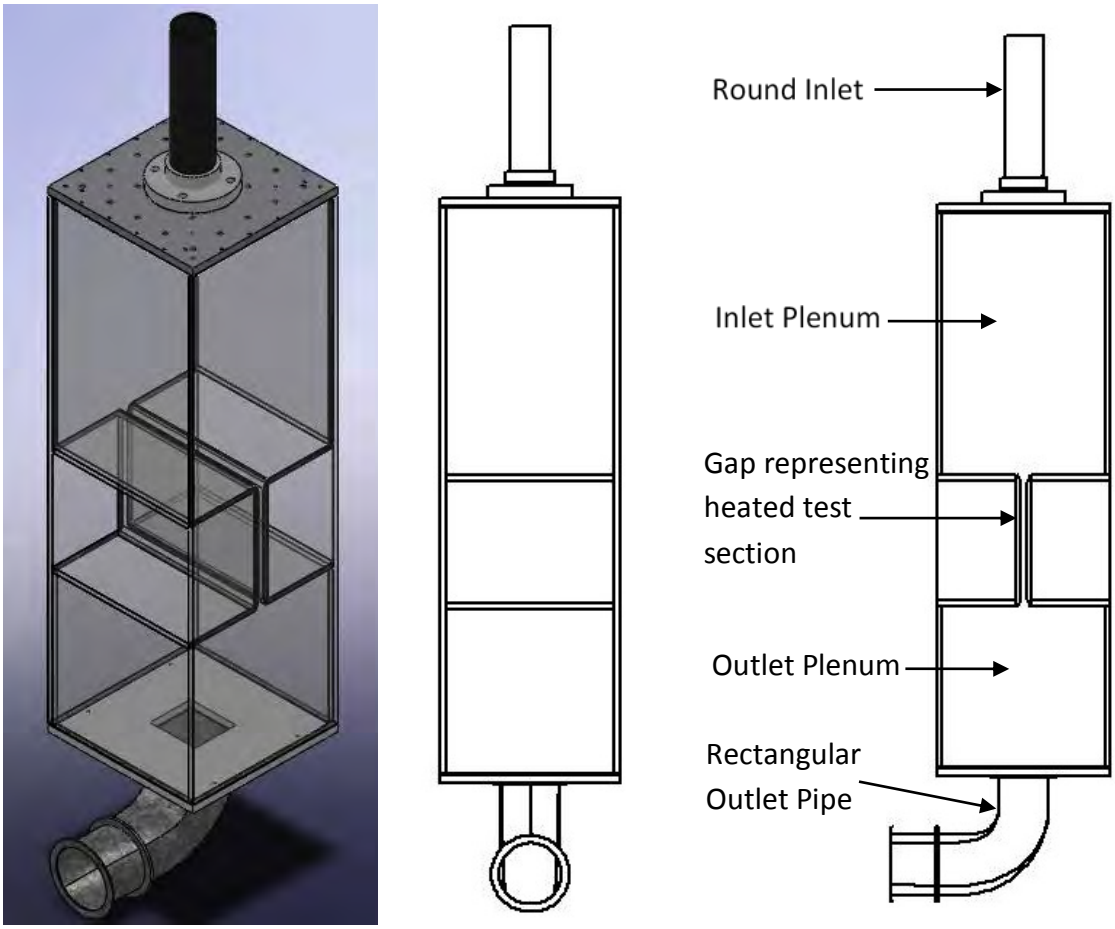

Figure E-1. Drawings showing (a) an orthographic, (b) front, and (c) side view of the flow visualization experimental setup.

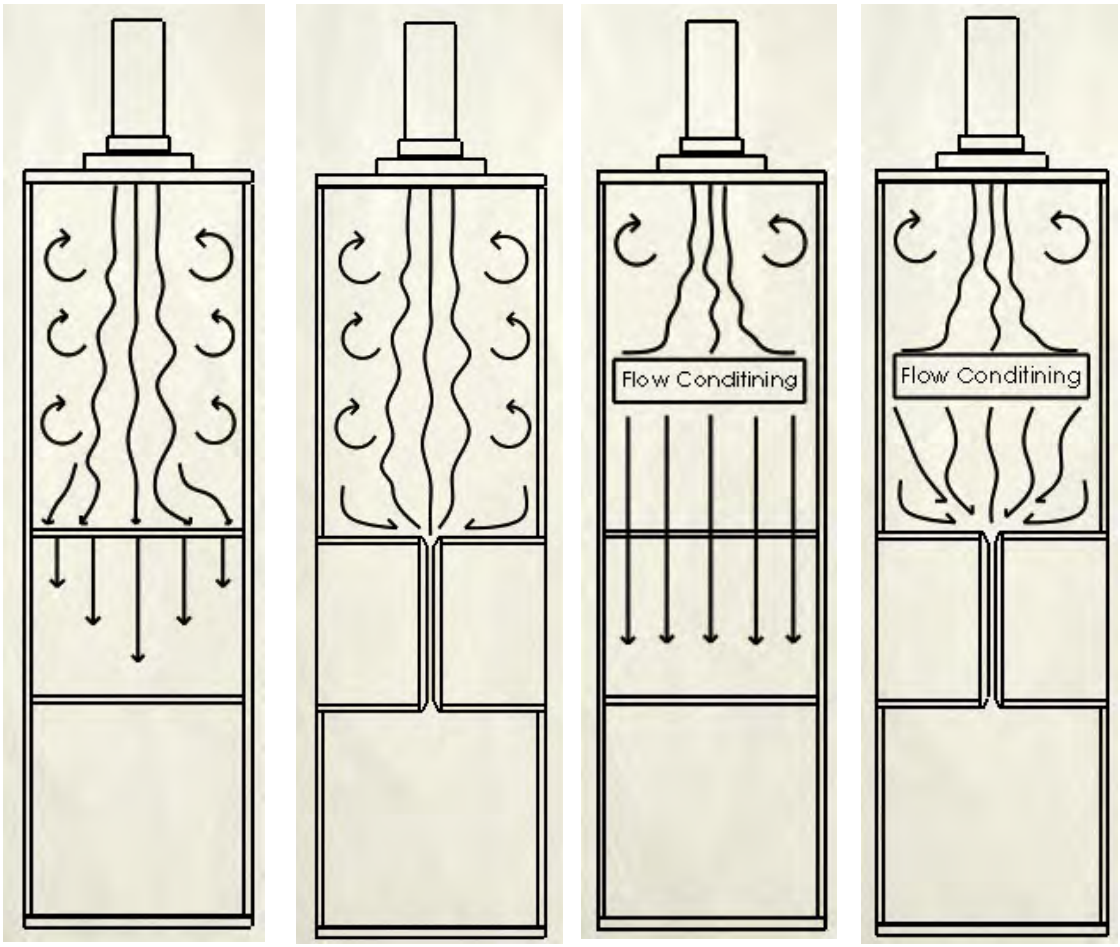

(a) (b)

Figure E-2. (a) Anticipated and (b) desired flow patterns within the inlet plenum and gap spacing; front and side views.

F. Heated Flow Loop

The heated flow experiment will use air in place of helium. This will allow for the system to be "open" as opposed to closed (i.e., there will be no need for a complex sealing of the loop to eliminate helium leaks as well as a heat rejection system – the heated air can be exhausted safely to the surroundings). Operational parameters, such as mass flow rate, temperature, and pressure, will be varied with air in order to match non-dimensional parameter values expected with a helium-flow system. These averaged non-dimensional parameters are:

Reynolds number (Re_{Dh}):

$$Re_{Dh} = \frac{\rho \cdot V \cdot D_h}{\mu}$$

Heat flux (q^+):

$$q^+ = \frac{q_w^{"}}{G \cdot C_{p \cdot T_{ave}}}$$

Acceleration (K_v):

$$K_V = \left(\frac{\nu}{V_b^2}\right) \cdot \left(\frac{dV_b}{dx}\right)$$

Buoyancy (Bo^*):

$$Bo^* = \frac{g \cdot \beta \cdot q_w^{"} \cdot D_h^4}{k \cdot \nu^2 \cdot Re_{Dh}^{3.425} \cdot Pr^{0.8}}$$

For normal MHTGR operating conditions and gaps ranging from 1 mm to 8 mm, the parameters are

$$1800 < Re_{Dh} < 70{,}000$$

$$0.00002 < q^+ < 0.0002$$

$$1 \times 10^{-8} < K_v < 5 \times 10^{-8}$$

$$8 \times 10^{-11} < Bo^* < 9 \times 10^{-11}$$

For pressurized cooldown (LOFA), Re_{Dh} is expected to decrease below 2000 within about sixty seconds and then to remain below 500, indicating that laminar flow would be likely. Some order-of-magnitude estimates of the appropriate *laminar* non-dimensional parameters during residual heat removal in a pressurized cooldown scenario (again for 1 to 8 mm gaps) are

$$8 < Re_{Dh} < 300$$

$$0.0003 < q^+ < 0.08$$

$$5 \times 10^{-6} < K_v < 3 \times 10^{-5}$$

$$8 \times 10^{-4} < |G_{avg}/R_{ave}| < 0.4$$

Where is $|G_{ave}/R_{ave}|$ is evaluated at the average gas temperature and is defined by:

$$\left|\frac{G_{ave}}{R_{ave}}\right| = \left|\frac{g \cdot \beta \cdot \rho^2 \cdot q_w^{"} \cdot s^3}{8 \cdot k \cdot \mu \cdot G}\right|$$

The air delivery system must be capable of providing air at a flow rate that produces Reynolds numbers, as measured in the test section, in the range of 500 to 10,000. The exact transition value for laminar to turbulent flow will be deduced from the flow visualization experiment. The gap spacing was originally going to be variable between 1 mm up to 15 mm, independently controlled at each end of the plate (for taper control). Due to fabrication limitations, the plate geometry was increased by a factor of two in order to be capable of providing the desired gap spacing to the flatness of the aluminum surface. Therefore, the test section consisted of 1.25 prismatic block lengths with a nominal gap spacing of 4 mm. The width of the test section was 375 mm; this produces a width-to-gap ratio of approximately 93, which in turn minimizes edge effects and allows the system to be considered an "infinitely wide" parallel plate. The transition from the entrance plenum to the first plate will provide a different entrance effect (i.e., development of both the momentum and thermal boundary layers) than from the first plate into the second plate, across the diamond-shaped transition region. Surface-mounted heaters provided a minimum of a 40 °C temperature increase per block at Reynolds number of 10,000 and the gap spacing of 4 mm.

The Senior Design performed a mechanical design of the heated loop during the 2011-2012 academic year. Specifically, they were responsible for the mechanical mechanisms associated with the test section (how to support the flow channel; how to vary the geometry; the heater sizing, plate designs, and insulation) and the overall support structure. A preliminary design review (PDR) for the Senior Design team was held on 13 March 2012 and was attended by the members of this project, including students and INL collaborates. A final report was submitted 17 April 2012. Figure F-1 shows the solid model of their final system design.

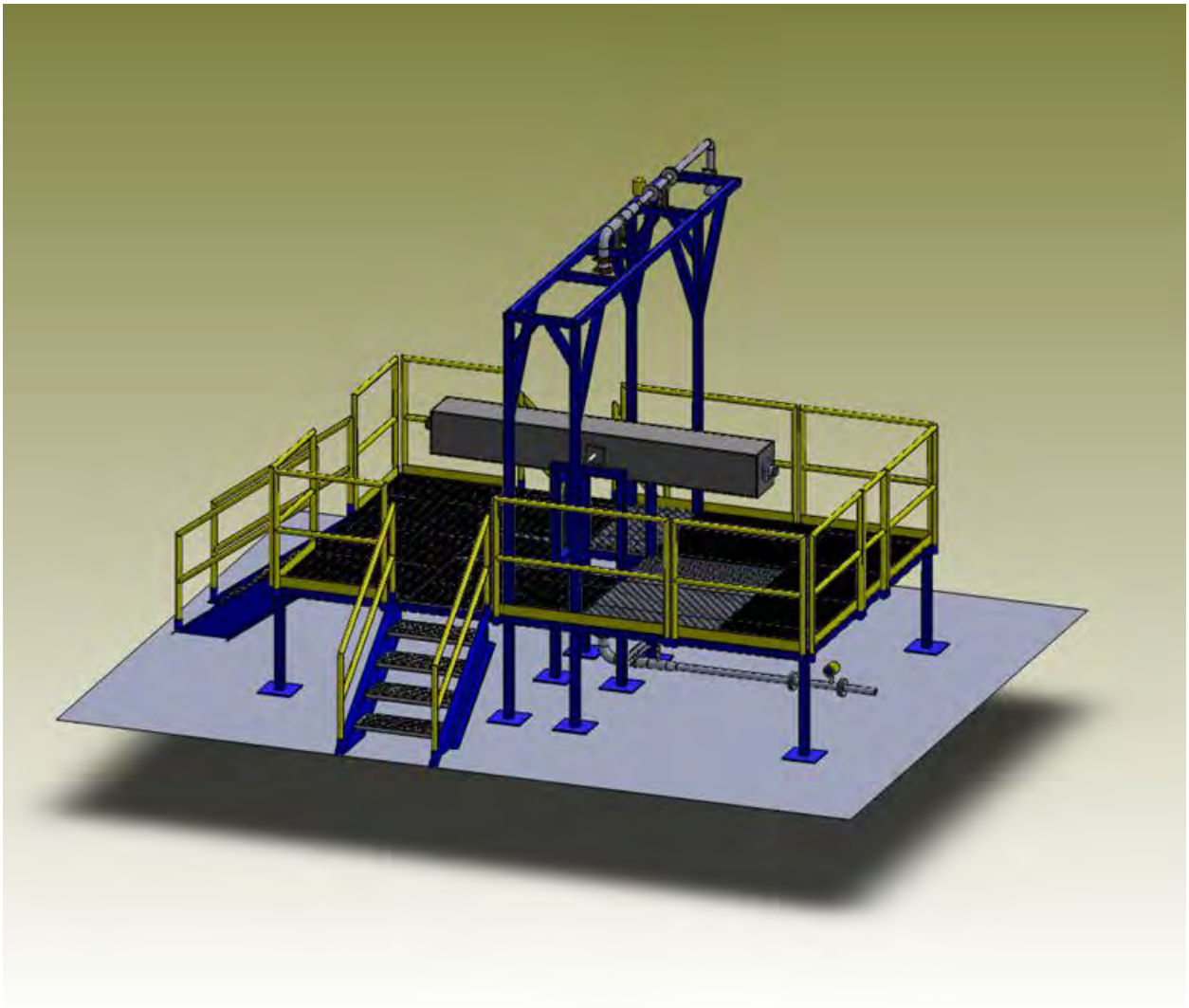

Figure F-1. Solid model of the heated loop design, including the support structure, test section (shown in its horizontal access position), and the associated inlet/outlet piping.

A design of the heated aluminum plates was given to local precision machine shops for evaluation. Shops were selected on their usage of CNC mills of sufficient size to machine the plates from a solid block of aluminum. The overall plate dimensions are 1980 mm long by 360 mm wide. For the designed 2-mm gap spacing, it was discovered that the needed flatness tolerance (0.1 mm or 5% of the gap spacing) would only be possible at considerable expense; it was not possible to guarantee that the plates could meet the flatness requirements even after going through the expensive post-machining grinding process. As a result, the scaling of the heated plates was increased to a factor of 2. This scaling involved doubling the gap spacing (from a minimum of 2 mm to 4 mm), increasing the bevel size by a factor of 2, and moving the diamond-shaped cut-out to a single location (approximately 1586 mm down the plate). In addition, the material Alumax Mic-6 was recommended to be used in place of standard Al 6061-T6. Alumax Mic-6 is a cast aluminum that has better flatness tolerance capability and "moves" less when machined (by approximately ½, as compared to the 6061). This cast aluminum has almost the same thermal conductivity and specific heat and an adequate yield strength to meet the design requirements. Figure F-3 shows a picture (taken from the solid modeling design software) of one plate and Figure F-4 shows a drawing of the same plate with the thermocouple locations identified.

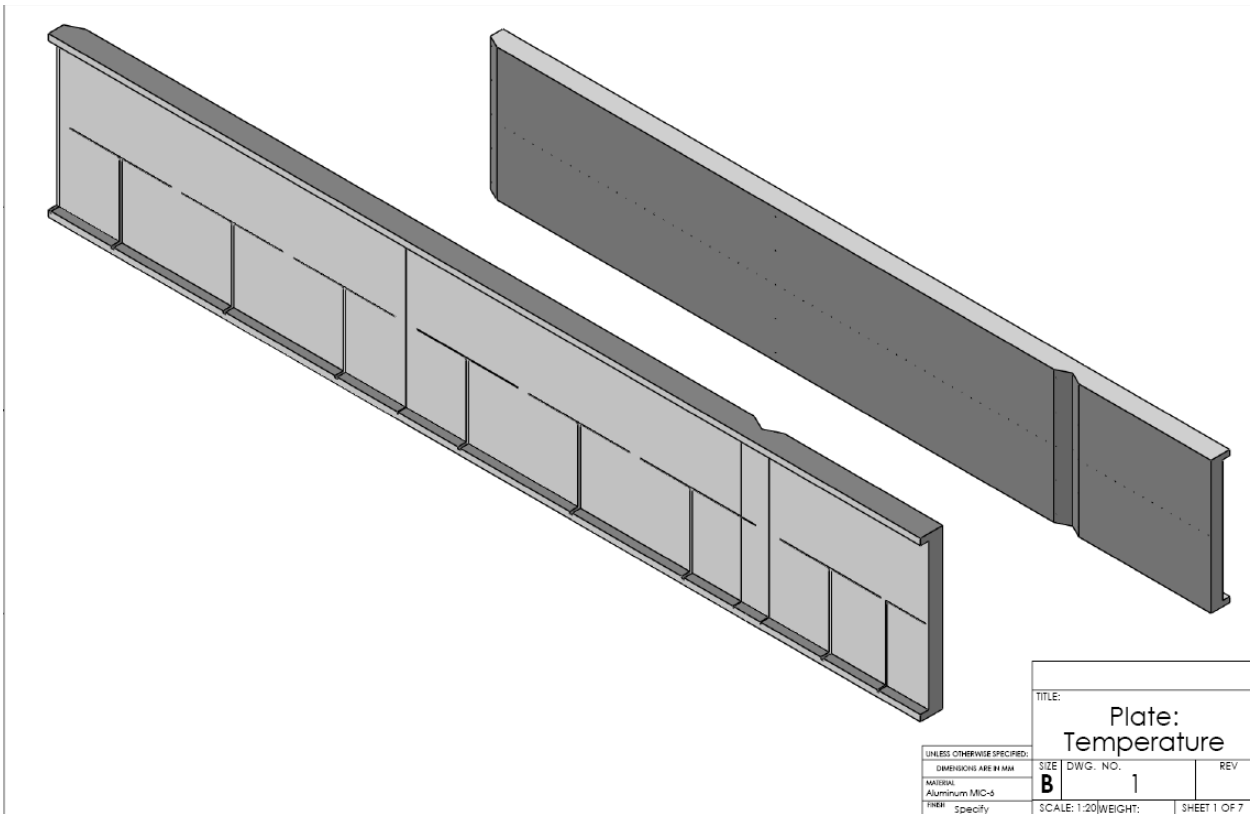

Figure F-3. Solid modeling picture of the most current design of the heated plates.

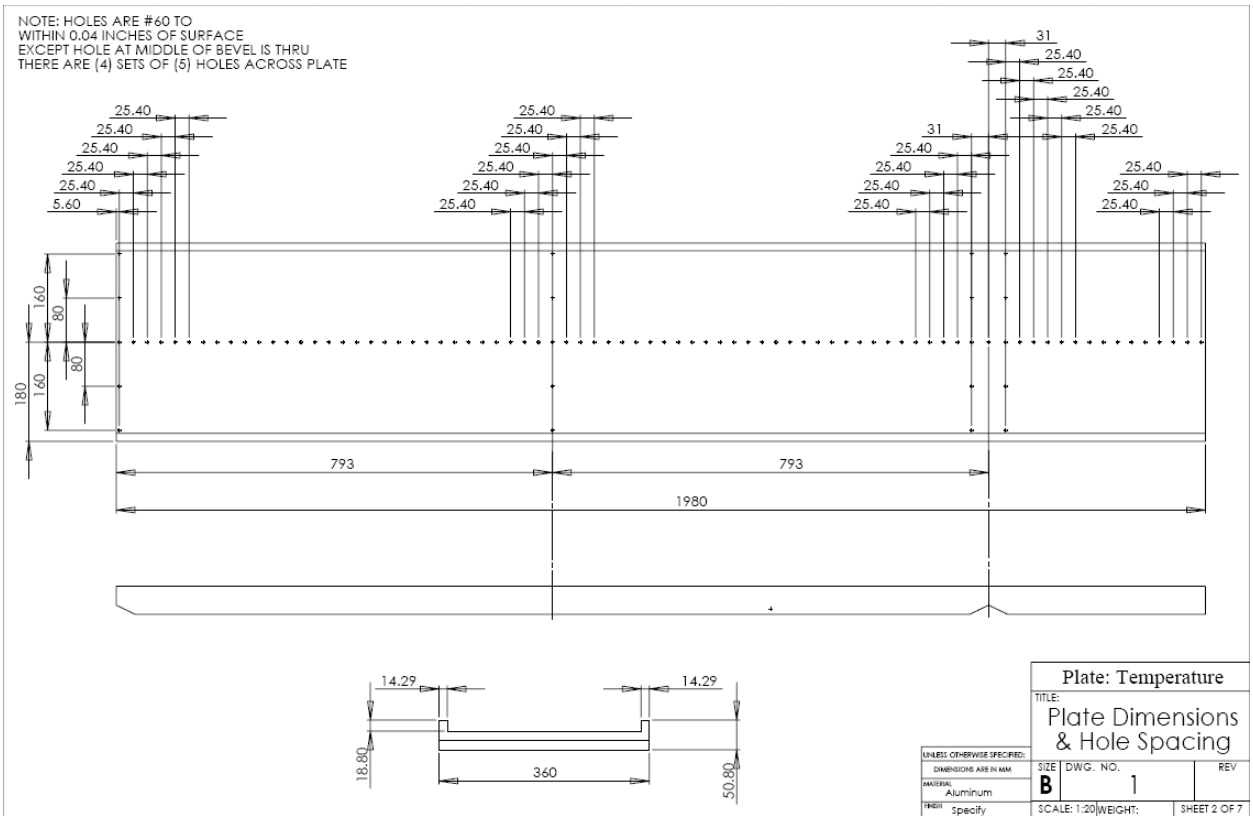

Figure F-4. Heated plate drawing showing thermocouple locations.

One issue we are having with the design of the heated plates is the dimensions of the bevels. The bevel dimensions are critical to the flow profile between the hated plates for two primary reasons. First, the transition from laminar to turbulent flow (i.e., corresponding Re_{DH}) is heavily influenced by the entrance configuration; the geometry of the bevels essentially dictates this configuration. Second, the scaling of our system (e.g., the proposed factor-of-two scaling in the most recent design, shown in Figures F-3 and F-4) is really based on the scale as applied to the bevels. The bevel dimensions are based upon information that was received through Hugh McIlroy (retired from the INL's MIR facility) which he presumably received from General Atomics (see Figure F-5 for these bevel dimensions). We are currently in the process of tracking down through documented sources the actual dimensions for the prismatic block designs.

Bric Balmforth is continuing to integrate the instrumentation to the National Instrument's (NI) LabView DAQ system. This is being accomplished in the lab by individually testing out each instrument type with the SCXI chassis and 1103 cards. To date, temperature sensors have been verified and the humidity/temperature/barometric pressure device is being integrated. The final DAQ computer has been setup and is currently being used for these integration check-outs.

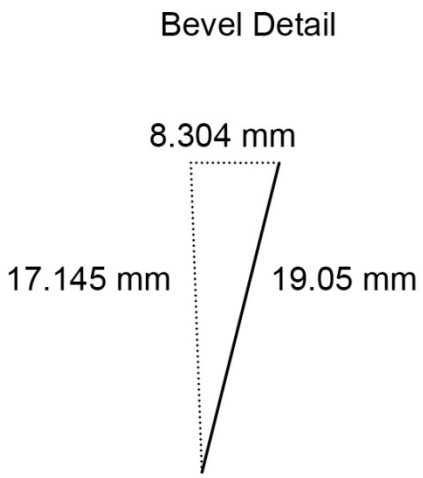

Figure F-5. Current full-scaled bevel dimensions being incorporated into the heated plate designs.

G. Quality Assurance (QA)

From November 15 – 17, 2011, our group met with Mr. Darren Jensen and Ms. Val Seeley, at the ISU campus, for a NEUP QA assist visit. As a result of this visit, our NEUP team met on November 30, 2011 to develop strategies for complying with DoE NEUP QA requirements. The minutes from this meeting are given in Appendix G.

H. Analysis of Pressure Drop Data

(Glenn McCreery 9-22-14) Air flow pressure loss experiments were conducted to quantify wall friction and pressure loss coefficients in a model bypass channel. The model channel is scaled to twice the dimensions of the Modular High Temperature Gas-Cooled Reactor (MHTGR) prototype gap, entrance bevel, and diamond-shaped cut out (which represents the junction of two fuel blocks). The length and width of the model are foreshortened from the prototype. Flows in the experiments were varied from laminar to fully turbulent regimes. Turbulent flow loss coefficients for the entrance, exit, and bevel cut-out are estimated. Pressure measurements are compared with predictions in this document.
Two series of experiments were conducted. The first series examines well-developed laminar and turbulent flow in a region downstream of the entrance and compares the data with predictions using pressure loss correlations. The second series compares individual pressure measurements along the length of the channel with loss coefficients that were obtained previously in our water flow patterns and pressure loss experiments (McCreery, et al., 2013[11]), and with pressure loss correlations. Two channel gap widths of 4.077mm average and 3.03mm average were employed in the experiments. Pressure change was calculated using a Mathcad computer program that employs an iterative marching solution to solve for pressure versus distance from the entrance of the apparatus.

I. Comparison of well-developed laminar and turbulent flow data with pressure loss correlations

Measurements of pressures (P) at each individual pressure tap indicate that flow in the region between 24.441 inch from the channel inlet to 60.441 inches is well developed, with approximately constant dP/dx, for both laminar and turbulent flow conditions. The data for differential pressure across this span for the air flow channel with an average gap width set to 4.077mm indicate that the laminar to turbulent flow transition begins at approximately Reynolds number (Re) = 3,000, and is complete before Re = 3,700. Additional data obtained for the channel with gap width adjusted to 3.03mm average gap width indicates approximately the same transition Reynolds number range.

The laminar flow data closely follows a linear curve fit for dP/dx versus Re, as it should for well developed laminar flow with Darcy friction factor f = 96/Re,

where,
V = bulk velocity
D_h = hydraulic diameter
ρ = density
For fully-developed low-Reynolds number turbulent flow, the correlation of Beavers et al. [1971], was employed. The correlation for Darcy friction factor, f, is,

and,

[11] G.E. McCreery, L.J. Tew, B.G. Williams, R.R. Schultz, and D.M. McEligot, "MHTGR core bypass flow patterns and pressure losses", 15th International Meeting on Nuclear Reactor Thermal Hydraulics, NURETH15-146, Pisa, Italy, May, 2013.

The range of applicability is stated as Re = 5,000 to 24,000.

In addition, for well-developed turbulent flow, the "modified Reynolds number" first proposed by Jones [1976][12], and recommended by White [2006][13] for turbulent flow in rectangular ducts friction factor was employed in the calculations. The modification is applied to the explicit form of the Colebrook-Moody correlation by Haaland [1983][14], and is a function of channel aspect ratio. For the large aspect ratio rectangular duct employed in these experiments, the modification is to multiply the Reynolds number used in the Haaland correlation by a factor of 2/3. This modification has the effect of increasing the friction factor by approximately 5% to 10% for the Reynolds number range of these experiments. The data are also compared with calculations using a constant friction factor.

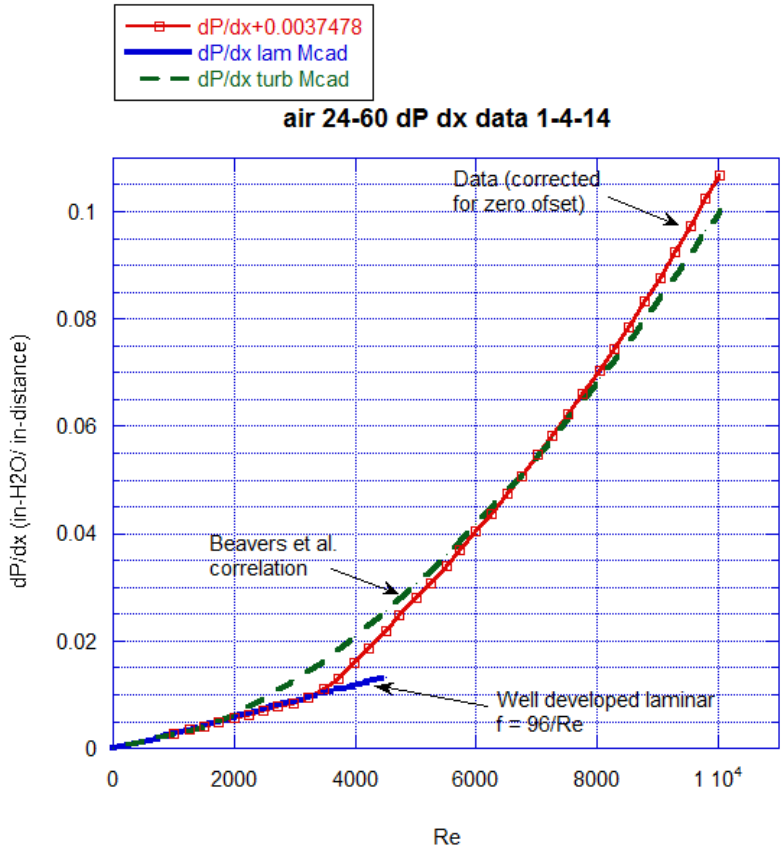

Figure H-1. Data compared with well developed laminar model and Beavers, et al. (1971) turbulent correlation. (dP/dx = $DP_{24.4\text{-}60.4}$/36). Data y uncertainty is 0.015 in-H2O/36 = 0.0004 in/in.

[12] Jones, O.C., "An improvement in the calculation of turbulent friction in rectangular ducts",*Trans. ASME*, vol. 98, 1976, pp. 173-181.

[13] White, F.M., "*Viscous fluid flow*", third edition, McGraw-Hill, New York, 2006.

[14] Haaland, S.E., ""Simple and explicit formulas for the friction factor in turbulent pipe flow", *J, Fluids Eng.*, vol. 105, 1983, pp. 89-90.

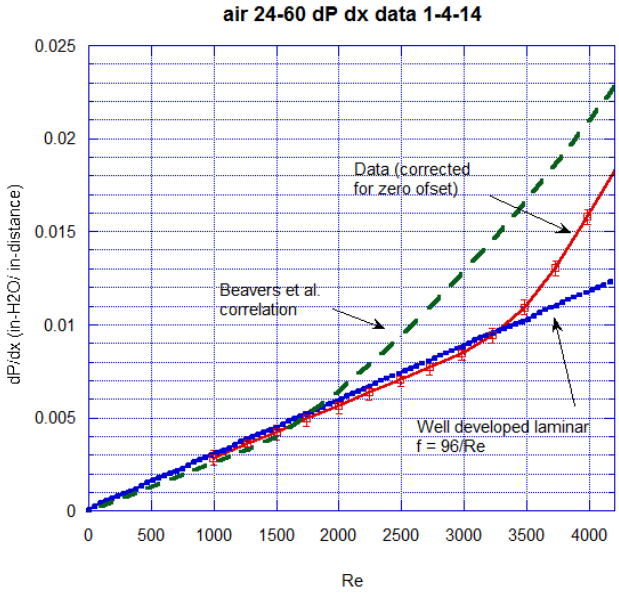

Figure H-2. Data compared with well developed laminar model and Beavers, et al. (1971)[15] turbulent correlation for Re < 4,300. Transition from laminar flow starts at approximately Re = 3,200.

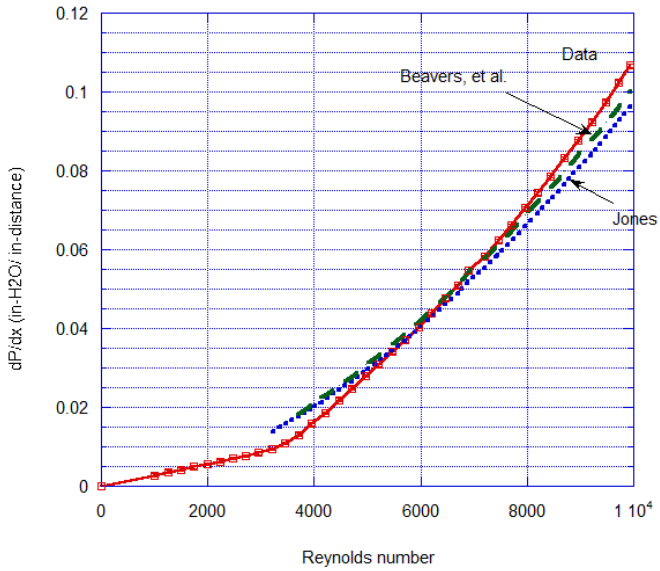

Figure H-3. Data compared with well developed turbulent flow correlations of Beavers, et al. and Jones, 1976. for Re > 3,500. The Beavers, et al. (1971) correlation does better, although both overpredict the data near the transition region and underpredict the data for higher Reynolds numbers.

[15] G.S. Beavers, E.M. Sparrow and J.R. Lloyd, "Low Reynolds number turbulent flow in large aspect ratio rectangular ducts", *Trans. ASME Basic Eng.*, Vol 6, pp. 296-299, June 1971.

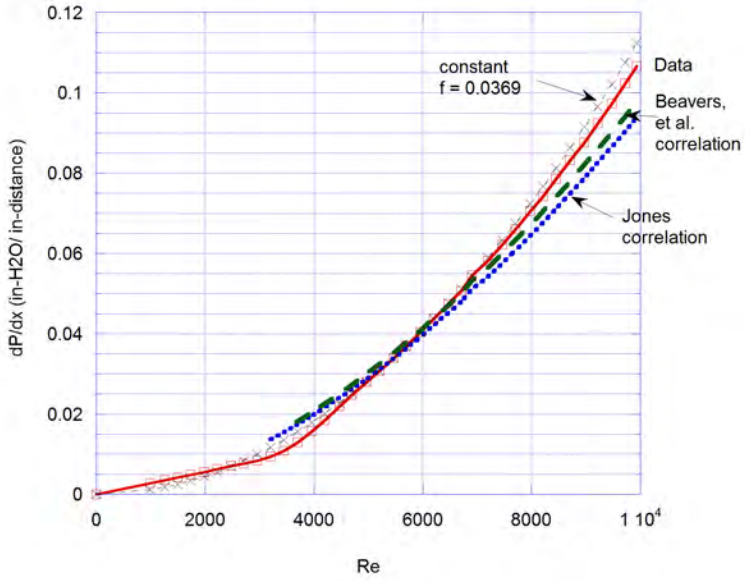

Figure H-4. Turbulent flow data (Re > 4,000) compared with Beavers, et al. (1971) correlation, f = constant = 0.0369., and a power law curve fit to the data. If f = constant, then, dP/dx = constant*$Re^{2.00}$. (The curve fit to the turbulent flow data shows dP/dx = constant* $Re^{2.0028,}$ quite close to dP/dx = constant*$Re^{2.00}$) The Beavers, et al., 1971, correlation matches the data at Re approx. = 7,000, at which point f-Beavers = 0.0369, the value chosen for the constant f comparisons.

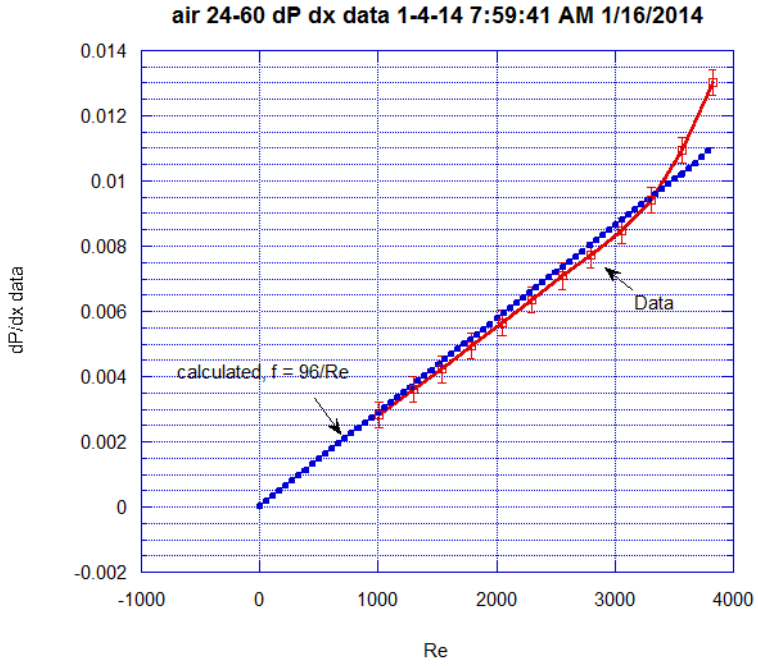

Fig H-5. Comparison of calculated dP/dx with data for laminar flow. Friction factor f = 96/Re. Data y uncertainty is 0.015 in-H2O/36 = 0.0004 in/in.

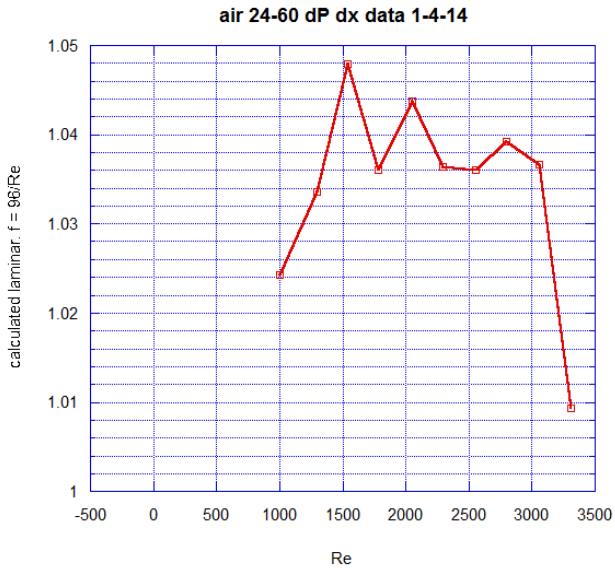

Figure H-6. Ratio of calculated dP/dx divided by data for laminar flow.

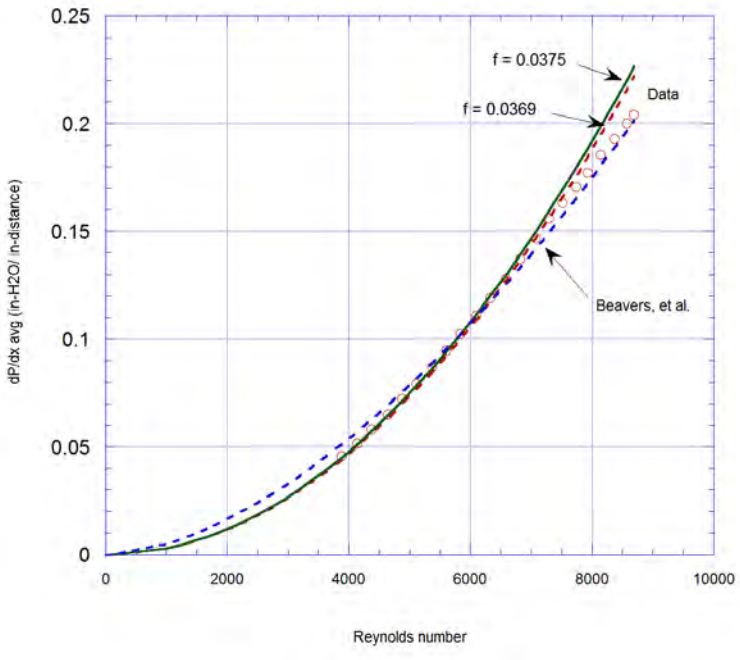

Figure H-7. Turbulent flow data (Re > 3,700) for 3.03mm gap width compared with Beavers, et al. (1971) correlation, f = constant = 0.0369., and best fit, f = constant = 0.0375. The Beavers, et al., 1971, correlation matches the data at Re approx. = 6,500, at which point f-Beavers = 0.0375, the value chosen.

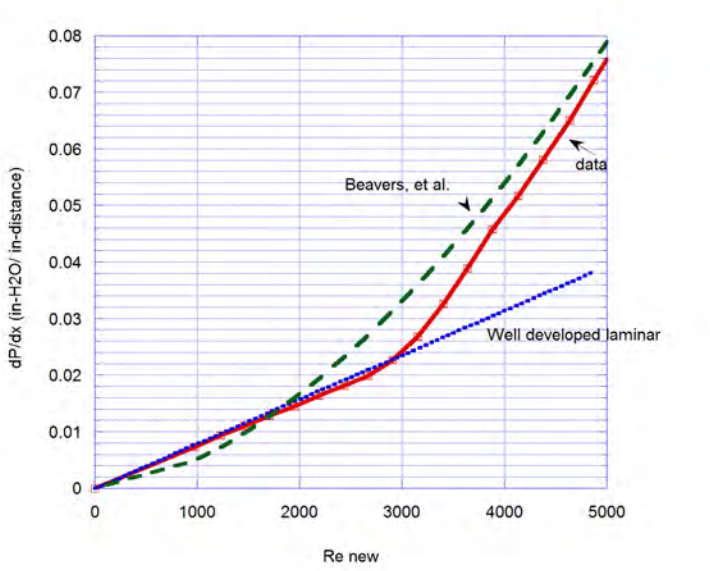

Figure H-8. Pressure gradient data (Re < 5,000) for 3.03mm gap width compared with Beavers, et al. (1971) correlation and well=developed laminar flow (f = 96/Re). Transition from laminar flow starts at approximately Re = 3,000.

II. **Comparison of full channel length data with calculations**

Calculations were performed using a Mathcad program for pressure loss along the complete length of the air flow apparatus, including the inlet region. The program incorporates a choice of either Shah (1978)[16] or Schade and McEligot (1971)[17] for laminar entry flow pressure loss and the choice of either Beavers, et al. (1971) or a constant friction factor for turbulent flow. Schade and McEligot (1971) is used for the present calculations.

For transition flow, the larger value of either the entry flow friction factor or turbulent flow friction factor was used in the original program. However, this approach needed to be modified due to the Beavers et al. (1971) correlation significantly overpredicting pressure loss in the transition flow region, as discussed in the conclusions.

Data and calculations for the channel employing a 4.077mm gap width are presented in this section.

[16] R.K. Shah, "A correlation for laminar hydrodynamic entry length solutions for circular and non-circular ducts", *ASME J. Fluids Eng*., Vol. 100, pp. 177-179, 1978.

[17] K.W. Schade, and D. M. McEligot, "Cartesian Graetz problems with air property variation". *Int. J. Heat Mass Transfer*, Vol. 14, pp. 653-666, 1971.

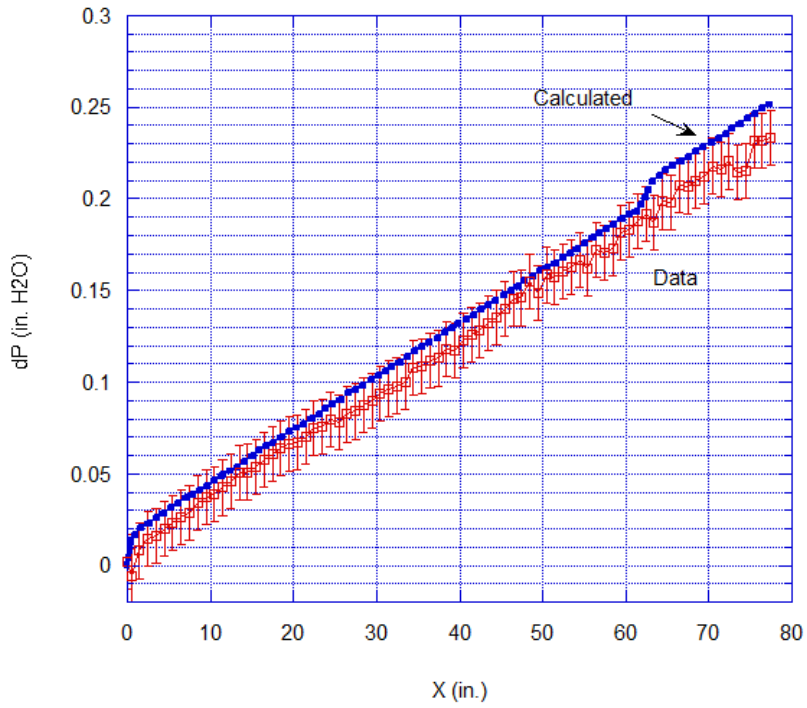

Figure H-9. Comparison of calculations with data for Re = 1,011 (labeled as 1,000 in 12-23-13 data). The choice of a loss coefficient of 0.5 for the diamond-shaped cut-out appears to be too large for this Reynolds number (but looks good for higher Reynolds numbers, even laminar). The pressure change at the inlet is due primarily to acceleration pressure change ( ), and secondarily to inlet pressure friction loss.

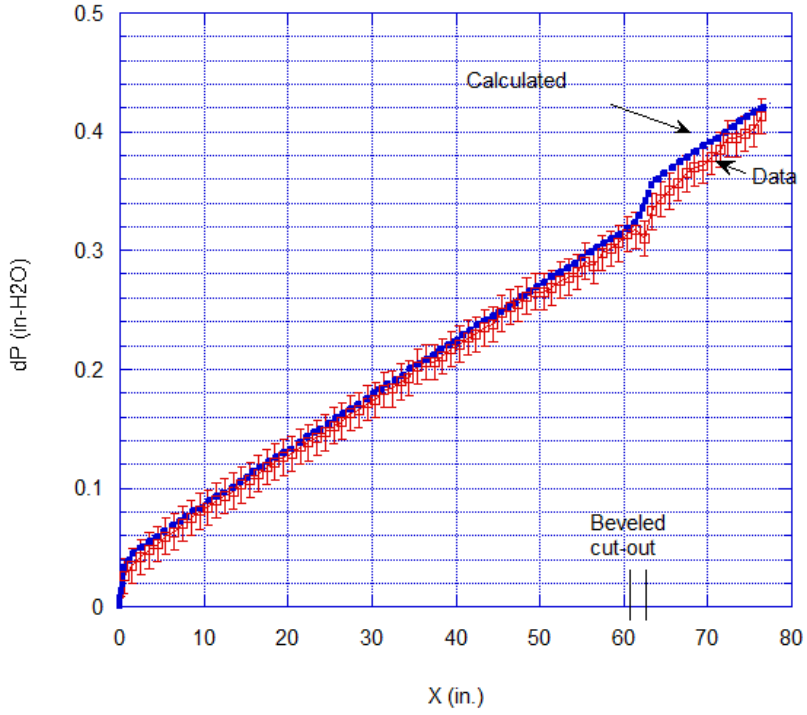

Figure H-10. Comparison of calculations with data for Re = 1,606 (labeled as 1,600 in 12-23-13 data).

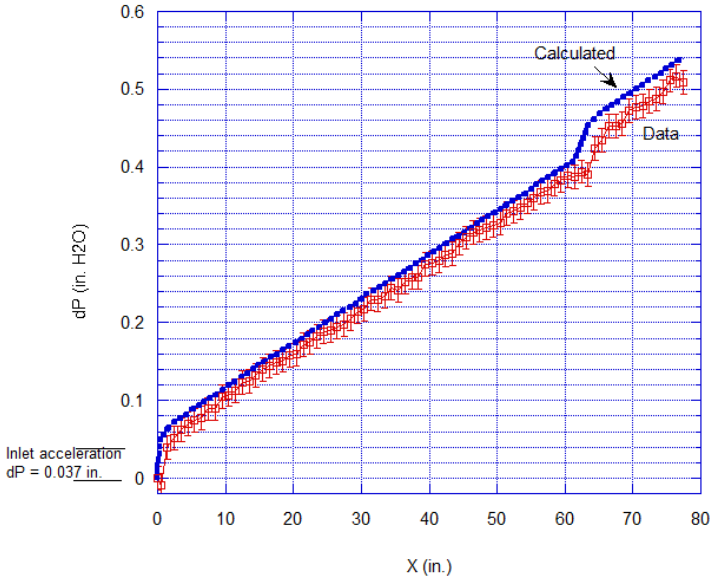

Figure H-11. Comparison of calculations with data for Re = 1,973 (labeled as 2,000 in 12-23-13 data).

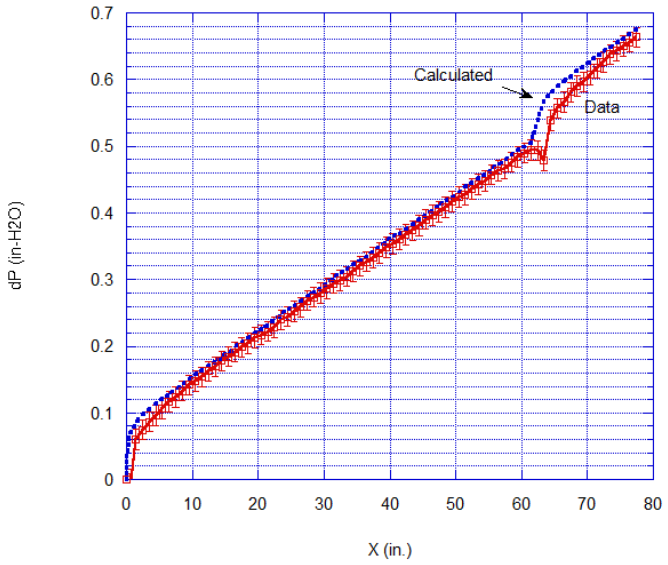

Figure H-12. Comparison of calculations with data for Re = 2,368 (labeled as 2,400 in 12-23-13 data).

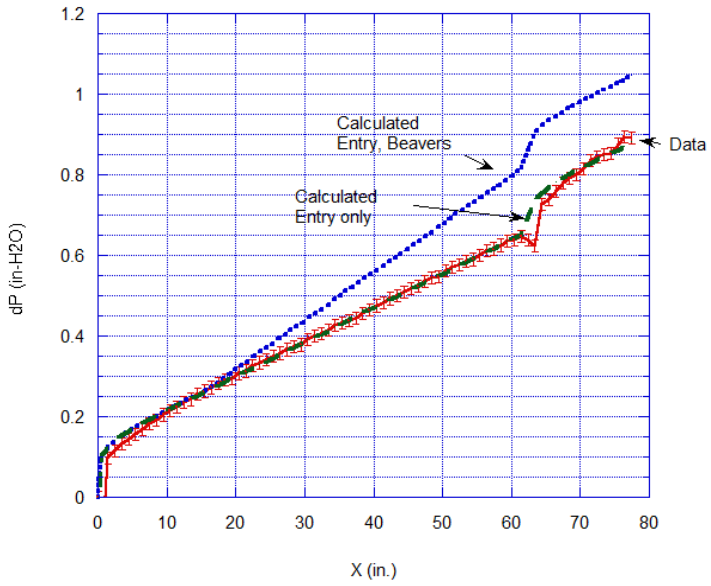

Figure H-13. Comparison of calculations with data for Re = 2,945 (labeled as 3,000 in 12-23-13 data). Obviously, the laminar entry flow solution produces a better comparison than using the greater of the entry flow solution or that calculated by the Beavers correlation.

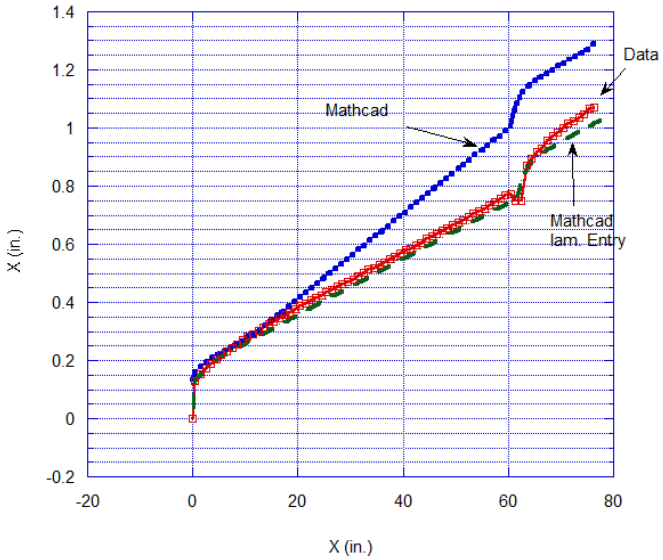

Figure H-14. Comparison of calculations with data for Re = 3,294 (labeled as 3,281 in 1-21-14 data). The Mathcad calculation initially used the higher of the entry flow solution or the Beavers et al. correlation. The strictly entry flow solution is more accurate.

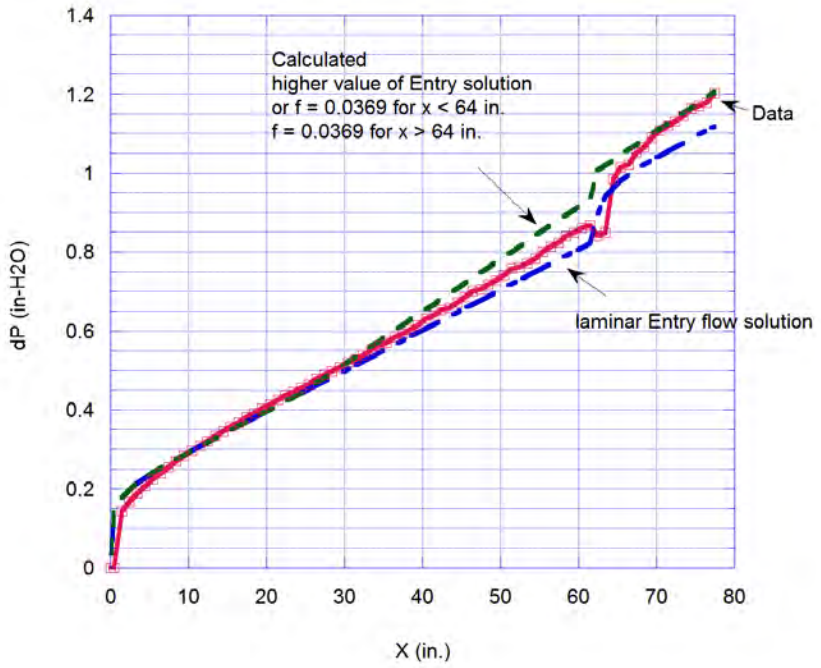

Figure H-15. Comparison of calculations with data for Re = 3,510 (labeled as 3,494 in 1-21-14 data). Flow is in the middle of transition.

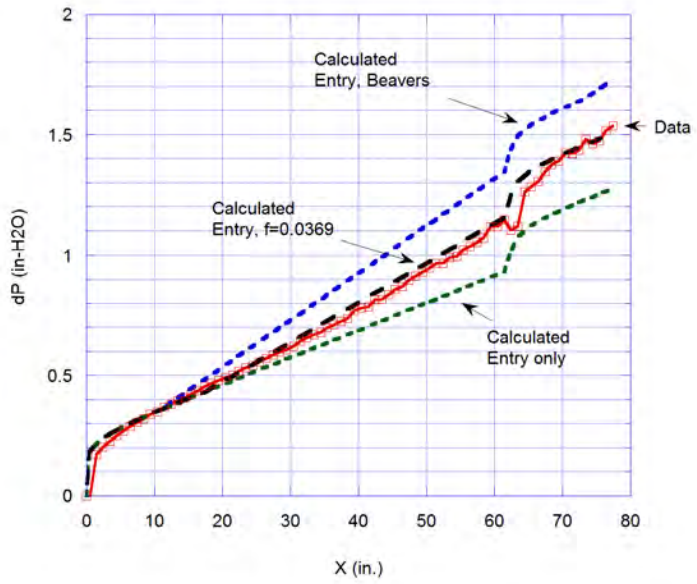

Figure H-16. Comparison of calculations with data for Re = 3,927 (labeled as 4,000 in 12-23-13 data). Transition to turbulent flow appears to be complete.

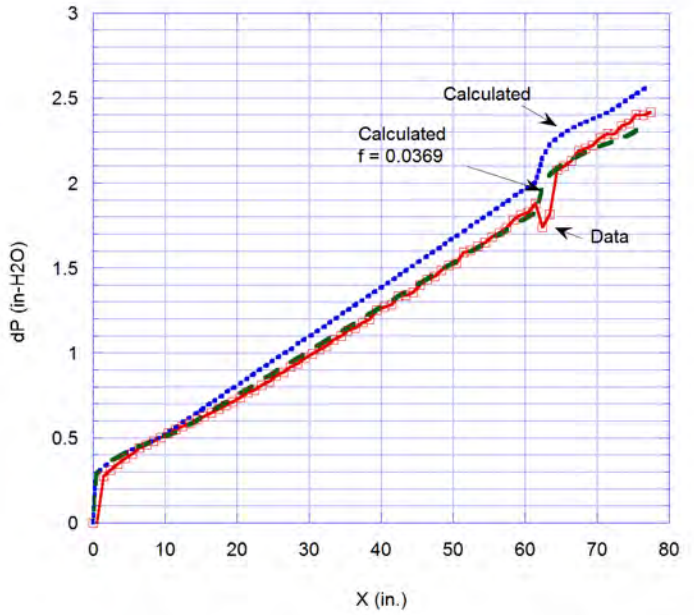

Figure H-17. Comparison of calculations with data for Re = 4,985 (labeled as 5,000 in 12-23-13 data).

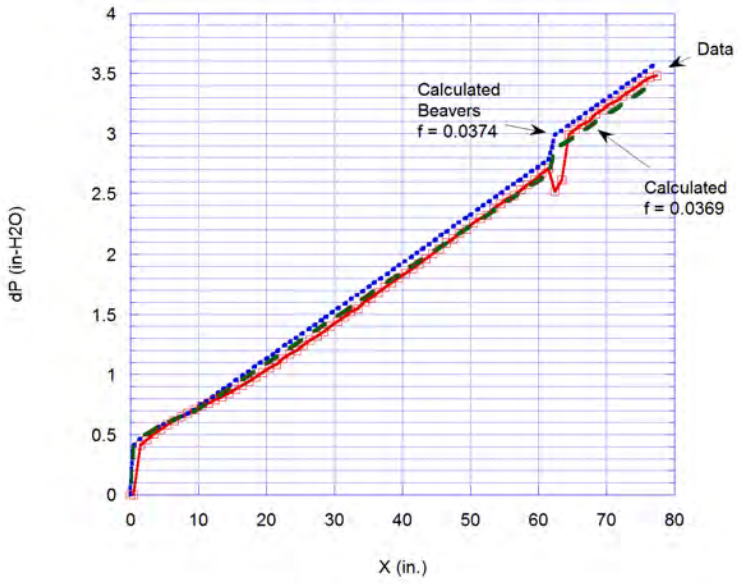

Figure H-18. Comparison of calculations with data for Re = 5,955 (labeled as 6,000 in 12-23-13 data).

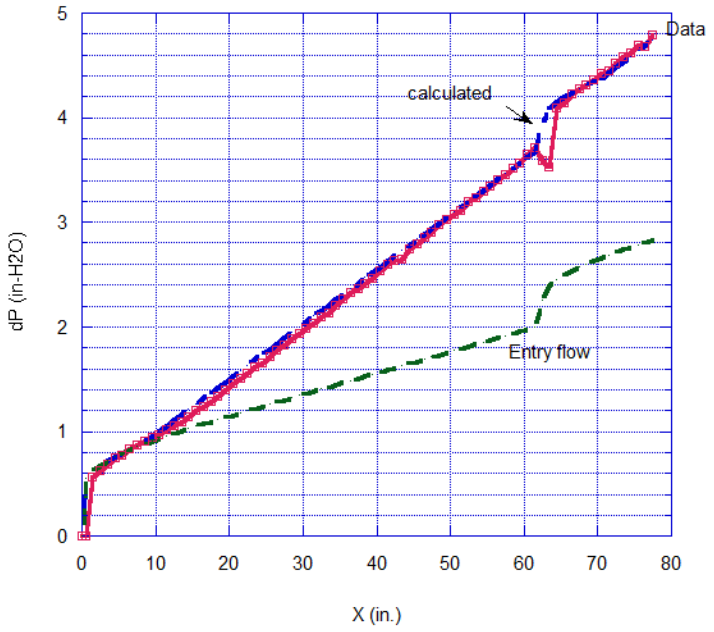

Figure H-19. Comparison of calculations with data for Re = 6,985 (labeled as 7,000 in 12-23-13 data).

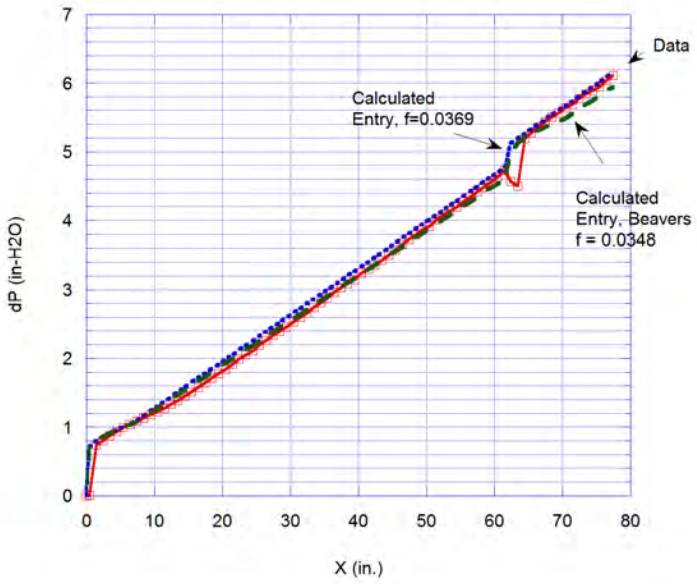

Figure H-20. Comparison of calculations with data for Re = 7,948 (labeled as 8,000 in 12-23-13 data).

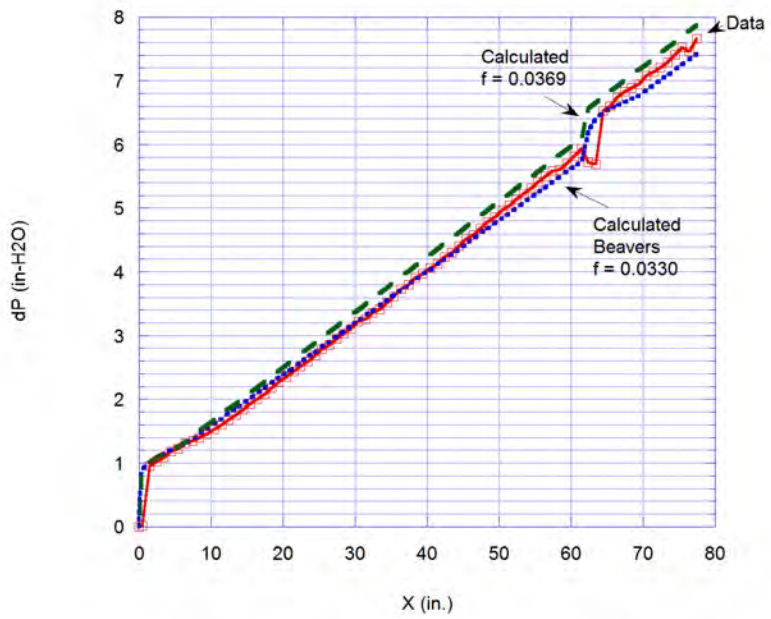

Figure H-21. Comparison of calculations with data for Re = 8,983 (labeled as 9,000 in 12-23-13 data).

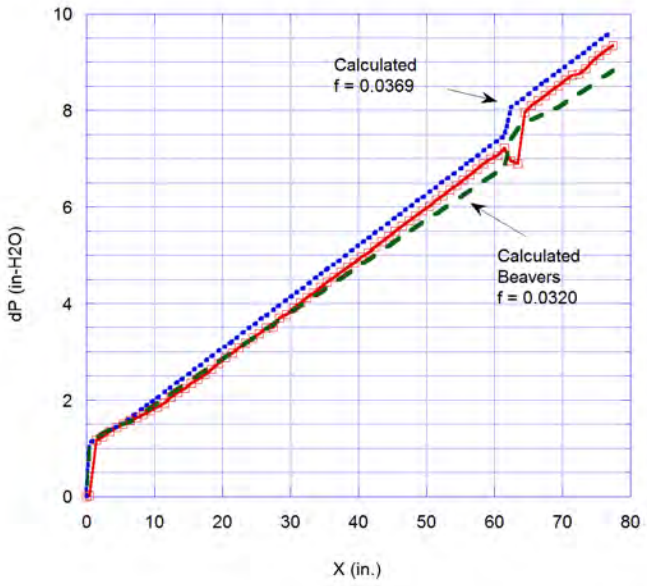

Figure H-22. Comparison of calculations with data for Re = 9,954 (labeled as 10,000 in 12-23-13 data).

Additional comparisons for 3.03mm gap width channel data

The experiments using a 3.03mm average gap width show very similar comparisons with calculations as the preceding experiments employing a 4.077mm average gap width. Three comparisons are shown for the 3.03mm gap width data. Loss coefficients for both the entry and beveled cut-out appear to be the same as for the 4.077mm gap width to within experimental uncertainty (Kinlet = 0.15 0.05, Kcut-out = 0.5 0.05).

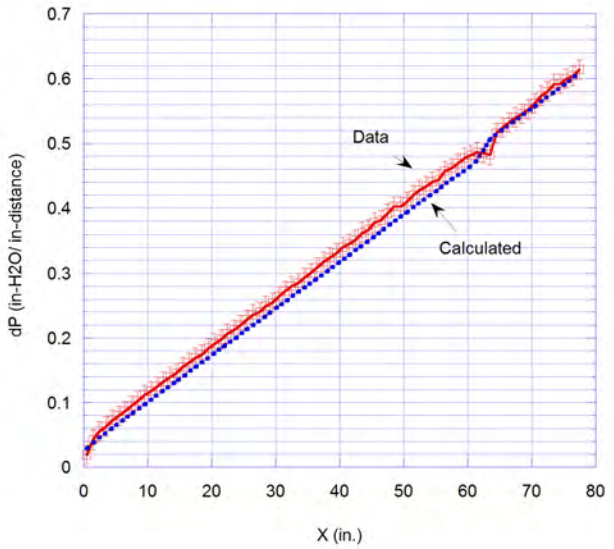

Figure H-23. Comparison of calculations with data for Re = 981 (labeled as 1,000 in 6-13-14 data).

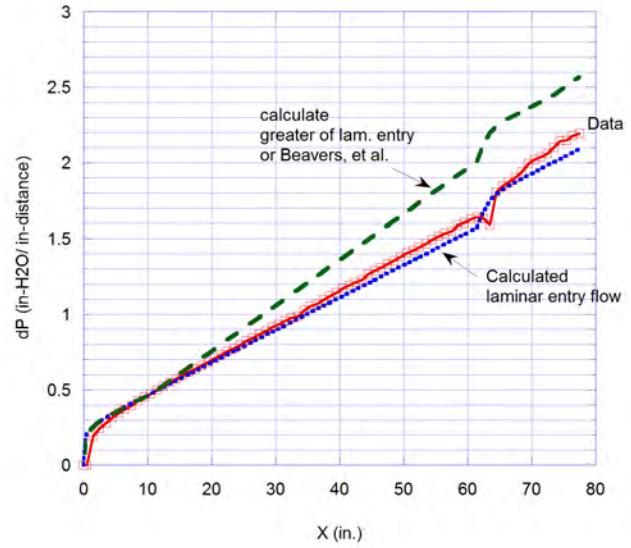

Figure H-24. Comparison of calculations with data for Re = 2,918 (labeled as 3,000 in 6-13-14 data).

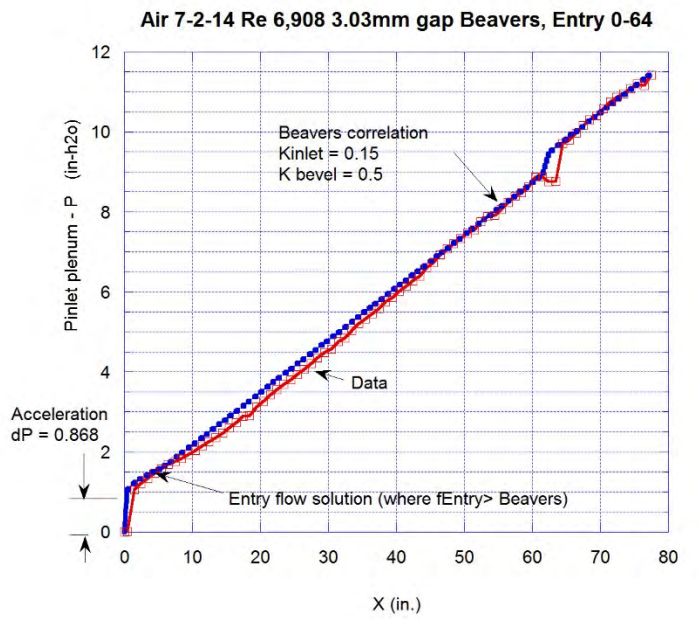

Figure H-25. Comparison of calculations with data for Re = 6,908 (labeled as 7,000 in 6-19-14 data).

Conclusions related to well-developed flow

The data deviates from a linear dependence on Re at Re = approximately 3,000 to 3,200. This Re is then the lower limit of the laminar-turbulent transition.

The transition to turbulent flow, based upon the pressure loss curve, appears to be complete at a Reynolds number between approximately 3,500 and 3,700.

The Beavers, et al. (1971) correlation compares reasonably well with the data (within 5%) for Re > 5,000, but not so well at lower turbulent Reynolds numbers, which is below the stated range of applicability.

The Jones (1976) correlation compares similarly to the Beavers et al. correlation at lower turbulent Reynolds numbers, but less favorably at higher Reynolds numbers (within approximately 10%), where it underpredicts the data.

Using a constant friction factor of 0.0369 for the 4.077mm gap width data, and 0.0375 for the 3.03mm data provide a better fit to the data for Re > 3,700 than does either the Beavers, et al. correlation or the Jones correlation! (The difference in predicted pressure loss between using a constant f of 0.0369 and 0.0375 is approximately 2%). However, our data range extends to only 10,000 and it would be expected from other studies that friction factor would gradually decrease with increasing Reynolds numbers. The start of this decrease may be seen in Figure H-4, where the pressure loss data is slightly lower at higher Reynolds numbers than calculated with the assumption of constant friction factor.

Conclusions related to individual pressure measurements

The laminar entrance flow comparisons predict the data fairly well. Most (but not all) calculations are within the error band of the dP data (0.015 in. H2O).

The choice of loss coefficient for the diamond-shaped cut-out for both laminar and turbulent flow was set at K = 0.5; the same value determined from the water flow experiments (0.5 0.05). This value remains valid for the air flow experiments. The exception appears to be for the lowest laminar flow cases of Re = 1,011, for the 4.077mm gap width, and Re = 981, for the 3.03mm gap width, where the loss coefficient appears to be lower. The water flow visualization experiment show smooth flow through the cut-out surrounded by counter-rotating vortices at these low Reynolds numbers (McCreery, et al., 2013), so a lower loss coefficient than for higher flow is to be expected.

The value of the inlet loss coefficient was determined to be 0.15 0.05 from the water flow experiments. This is probably still at least approximately correct, but it is difficult to determine accurately since the inlet pressure loss is a small fraction of the acceleration pressure change for air flow at the inlet and it is hard to distinguish the two. In any case, the inlet pressure loss is a very small fraction of the total pressure loss for all cases examined.

The friction factor was assumed to be the larger of either the entry flow solution or the turbulent flow solution (from either the Beavers, et al. (1971) correlation or the assumption of constant friction factor). For the turbulent flow cases presented, the approach looks good at the entrance, where the shape of the dP curve has a hump characteristic of the laminar flow entry solution. The same approach was initially employed downstream of the cut-out, but the dP curve for turbulent flow looks flatter and without the hump. Apparently (and not surprisingly), the flow remains turbulent as it flows through the cut-out, which is consistent with the flow visualization results of the water flow experiments (McCreery, et al., 2013). This appears to be the case for Reynolds numbers extending down to at least 6,000.

The most accurate calculation approach for calculating the pressure loss curve is to:

(1) Use the laminar entry flow solution for Re < approx. 3,500. Downstream of the diamond-shaped cut-out, use the entry flow solution with entry starting at the cut-out.

(2) At Reynolds number greater than 3,500 and upstream of the diamond-shaped cut-out, use the higher value of either the laminar entry flow solution or a constant friction factor (f= 0.0369 for the 4.077mm gap width or f= 0.0375 for the 3.03mm gap width). Use this constant friction factor downstream of the cut-out (since flow appears to remain turbulent).

It would be desirable to obtain data at Reynolds numbers higher than 10,000 to test this approach or to develop a new one. It is expected from other studies that friction factor would eventually decrease at higher Reynolds numbers.

Our data is sufficiently accurate to permit the development and publication of an improved turbulent friction factor correlation for flow in a high aspect ratio rectangular channel provided that we obtain additional data for higher Reynolds numbers and for a variety of gap widths.

I. Preliminary Analysis of Heated Flow Data

A preliminary analysis of the heated flow data was performed (Glenn McCreery, 10-30-14) and follows. A Mathcad (Mathsoft, 2001)[18] computer program was written to calculate wall to fluid heat transfer in the air flow apparatus. The program uses a marching solution, starting at the entrance, to calculate physical properties of air (density, specific heat, conductivity, and viscosity) at each node as a function of local calculated temperature and pressure. Input mass flow rate and heater power are used along with the fluid physical properties at each node to calculate wall to fluid heat transfer rate. Uniformly distributed and steady-state power input are assumed. The calculation procedure is outlined in the flow diagram in Figure I-1.

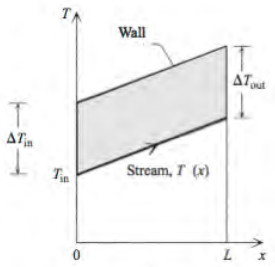

Figure I-1. Mathcad Heat transfer program simplified flow diagram.

[18] Mathsoft Inc, *Mathcad 2001*, Cambridge, MA, 2001.

Heat transfer correlations employed in the computer program include, for turbulent flow, a choice of Dittus-Boelter (1930)[19], or Campbell-Perkins (1968)[20], which was developed for gas flow in a square channel, and is the preferred choice. The Campbell-Perkins correlation is

where,

Nu = Nusselt number = h D_h/K
h = convection coefficient W/m2/K
K = thermal conductivity W/m/K
D_h = hydraulic diameter m
Re = Reynolds number
Pr = Prandtl number
T_w = wall temperature K
T_B = fluid bulk temperature K

For laminar flow the entry flow heat transfer correlation of Bejan (1995)[21], based on data of Shaw and London (1978)[22], is employed, as described below, in Figure I-2.

[19] Dittus, F. W., and Boelter, L. M. K., "Heat Transfer in Automobile Radiators of the Tubular Type", *Univ. Calif. Publ. Eng.,* 2(13), 443–461; *Int. Commun. Heat Mass Transfer,* 12, 3–22, 1930.

[20] Campbell, D.A., Perkins, H.C., "Variable property turbulent heat and momentum transfer for air in a vertical rounded corner triangular duct", *Int. J. Heat Mass Transfer* ,11, 1003- 1012, 1968.

[21] Bejan, A., *Convection Heat Transfer,* 2nd ed., Wiley, New York, 1996.

[22] Shah, R. K., and London, A. L. (1978). "Laminar Flow Forced Convection in Ducts", Suppl. 1 to *Advances in Heat Transfer,* Academic Press, New York.

The thermal entrance region of the parallel-plate channel with uniform heat flux and Hagen–Poiseuille flow is characterized by (Shah and London, 1978)

$$\mathrm{Nu}_x = \begin{cases} 1.490x_*^{-1/3} & x_* \le 0.0002 \\ 1.490x_*^{-1/3} - 0.40 & 0.0002 < x_* \le 0.001 \\ 8.235 + 8.68(10^3 x_*)^{0.506} e^{-164x_*} & x_* > 0.001 \end{cases} \quad (5.39)$$

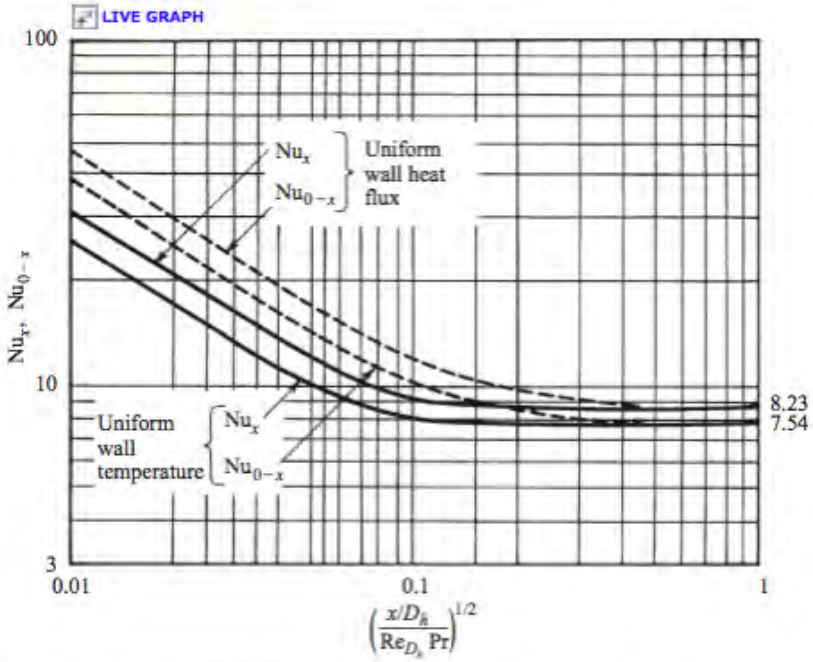

Figure 5.9 Heat transfer in the thermal entrance region of a parallel-plate channel with Hagen–Poiseuille flow. (From Bejan, 1995; drawn based on data from Shah and London, 1978.)

Where,

Figure I-2. Thermal entrance laminar flow heat transfer correlation of Bejan (1995).
Pressure as a function of distance from the entrance is calculated in the same manner as for our pressure loss experiments, as explained previously in this report (Section H). The laminar entry flow solution of Schade and McEligot (1971) for frictional pressure loss is used for Reynolds numbers of less than 3,700, and the turbulent flow correlation of Beavers, et al. (1971) is used for higher Reynolds numbers.

Sample calculations

The results of three sample calculations are presented. The calculations were performed prior to data being available for comparison. The three are chosen to illustrate typical results for laminar, transition, and turbulent flow. Heater power for all three cases is 0.60 kW, and inlet temperature is set at 26 ^{o}C. Air mass flow rates are respectively, 22.8 kg/hr, 45.6 kg/hr, and 101 kg/hr.

Laminar flow, case #1:. Inlet Reynolds number is approximately 2,060. The increase in air viscosity with temperature accounts for the decrease of Reynolds number with distance. hc (kW/m^2-K) is the turbulent convection coefficient from Campbell and Perkins, and hlam is the laminar flow entry coefficient from Bejan. All temperatures are ^{o}C.

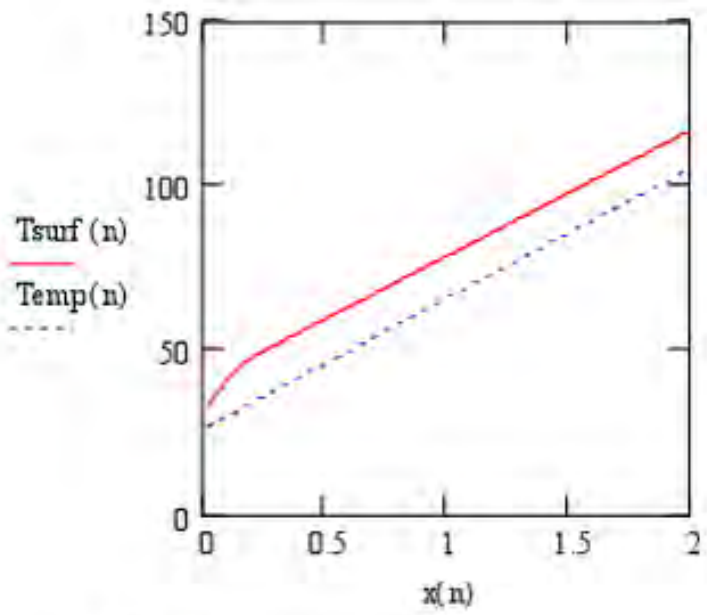
150
100
50
0
Tsurf (n)
Temp(n)
0
0.5
1
1.5
2
x(n)

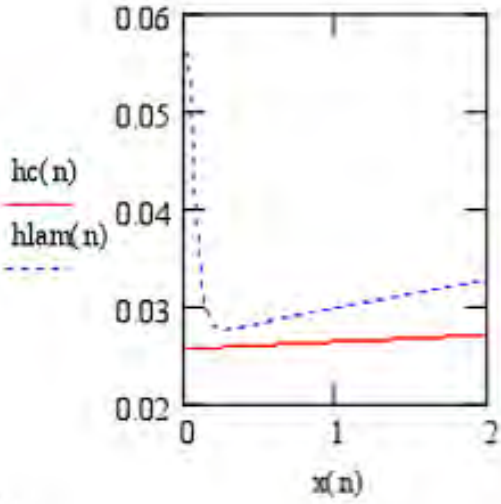
0.06
0.05
0.04
0.03
0.02
hc(n)
hlam(n)
0
1
2
x(n)

O_c
kW/m2-K

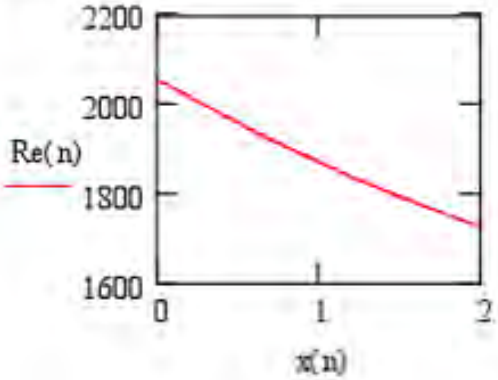
2200
2000
1800
1600
Re(n)
0
1
2
x(n)

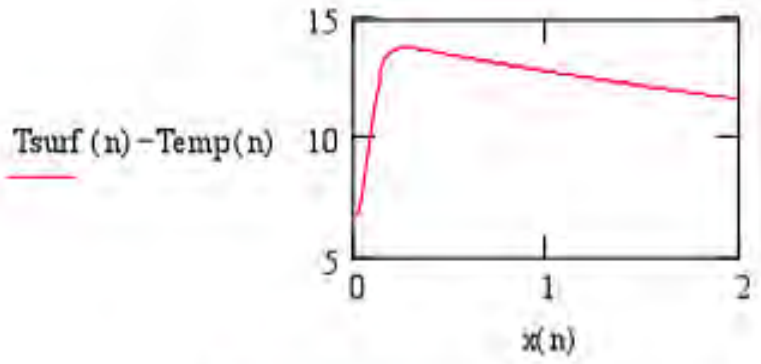
15
10
5
Tsurf (n) – Temp(n)
0
1
2
x(n)

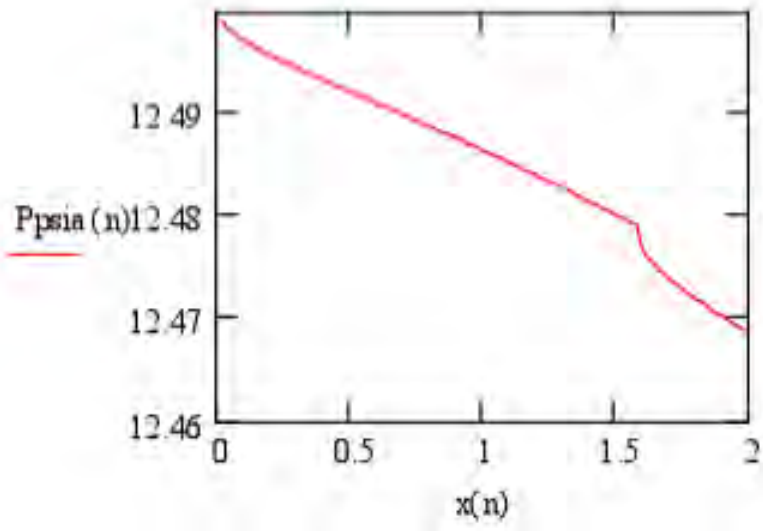
12.49
12.48
12.47
12.46
Ppsia (n)
0
0.5
1
1.5
2
x(n)

Transition flow, case #2: or close to transition case. Inlet Reynolds number is approximately 4,100, and decreases to approximately 3,700 at the exit.

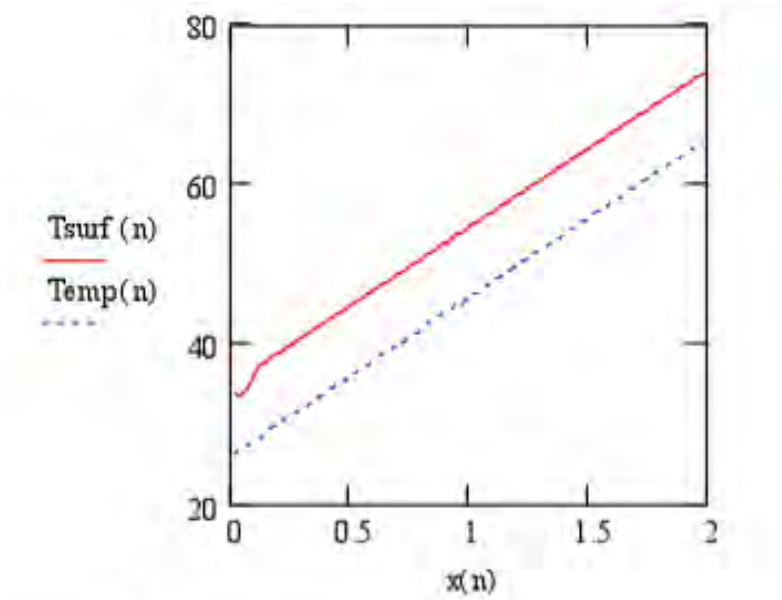

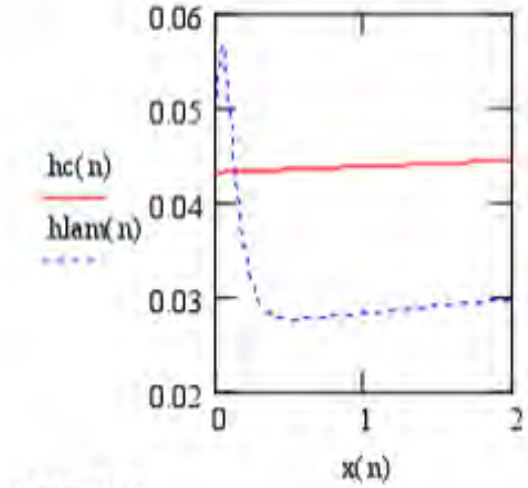

kW/m2-K

O_c

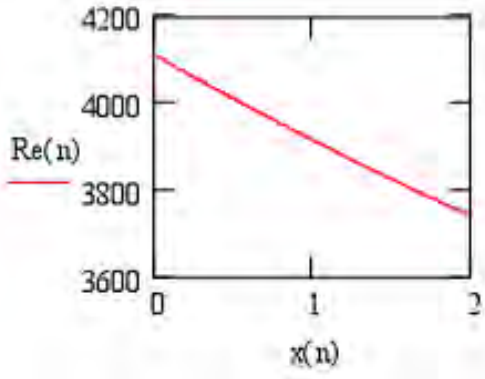

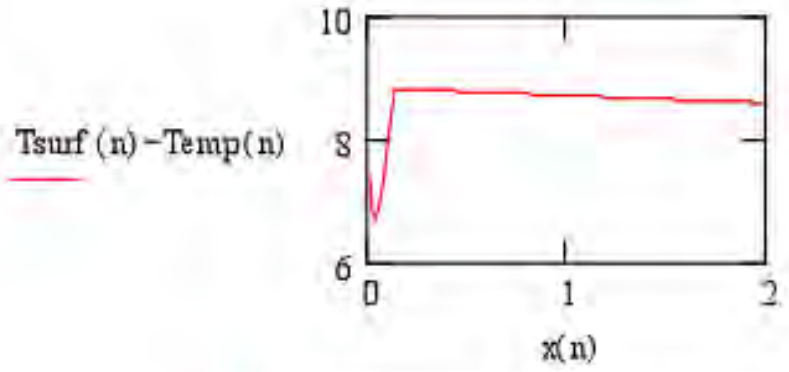
Tsurf (n) − Temp(n)
10
8
6
0
1
2
x(n)

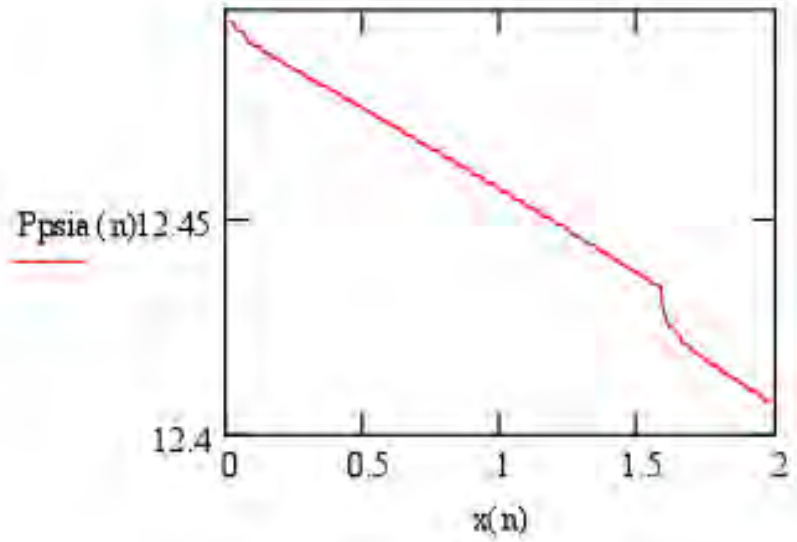
Ppsia (n)12.45
12.4
0
0.5
1
1.5
2
x(n)

Turbulent flow, case #3: Inlet Reynolds number is approximately 9,100.

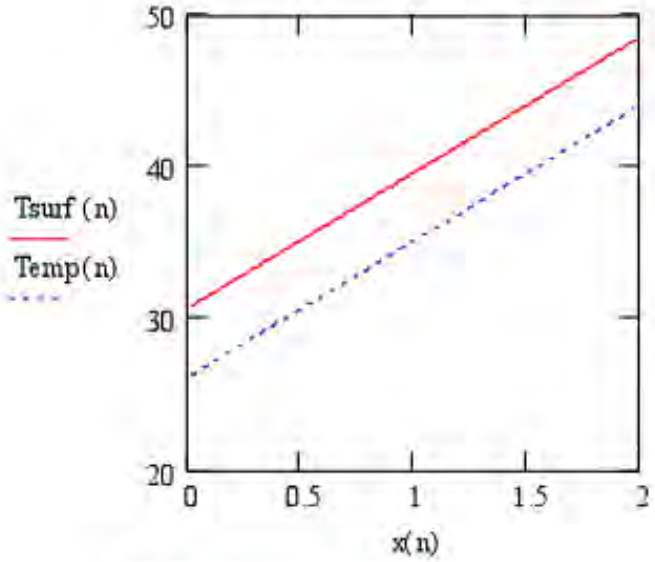

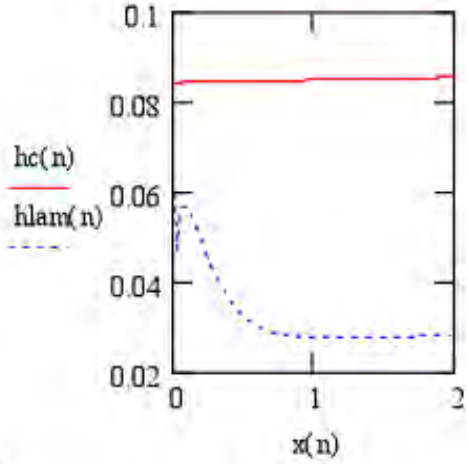

O_c
kW/m2-K

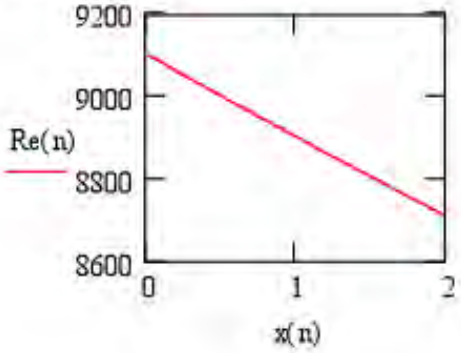

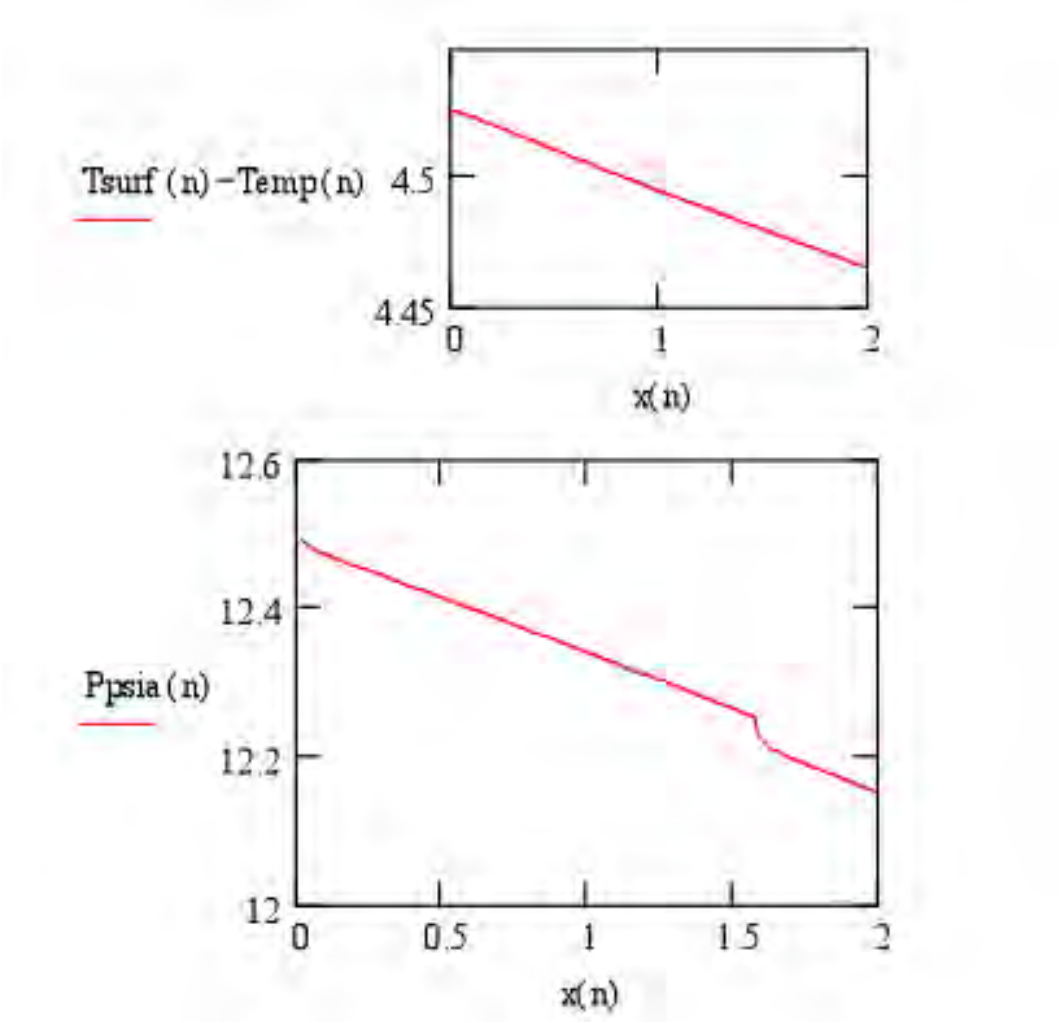

Further analysis is currently in process, being performed by Harish Aryal, as part of his MS degree in ME. An addendum to this report will be attached once the work is completed.

J. Collaboratve Meetings

The P.I. and students have scheduled weekly meetings to discuss the project and its progress.

Graphite Block Discussion

On 22 February 2011, team members (Brian Williams, Richard Schultz, Don McEligot, and Izzi Silver) met with William Wines (INL) at the CAES building to discuss graphite block geometry distortions. We discussed the issues effecting geometry distortions (irradiation and coefficient in thermal expansion) as well as the surface roughness characterization of the graphite blocks. Several emails and further contact has ensued.

I-NERI Project

On 16 March 2011, Brian Williams and Richard Schultz met with team members of the I-NERI Project "Experimental and Analytical Study on the Core Bypass Flow in a Very High Temperature Reactor" at their 5th progress review meeting in Honolulu, Hawaii. This meeting was held in conjunction with the 8th ASME-JSME Thermal Engineering Joint Conference (Williams attended this conference as well).

INL MIR Facility Tour

On June 6, 2011, the P.I. (Brian Williams) and two students (Jari Safi and Izzi Silver) were given a tour of the INL's Matched Index of Refraction (MIR) facility. This facility involves flow testing that includes optical measurement techniques as well as the insertion/use of the silver-coated spheres. Dr. Hugh McIlroy, the director/P.I of the MIR facility hosted the tour. Overall, a very good visit for everyone who attended from our NEUP team.

Appendix C

PIV System “How To” Guide

The PIV System How-to Document

Note to reader:

The following is an informal document detailing how the PIV system works and the work that still needs to be finished. The document assumes basic understanding of the PIV technique (refer to my presentation about the system for more detail).

Background/Basic Idea:

The PIV system is built using two camera flashes, each tinted a different color (red and green in this case). The idea is to take two successive pictures of the silver coated glass beads flowing with the working fluid, and then put them through a cross correlation algorithm to find the average displacement. Since typical video cameras can only take successive pictures at about 33 ms intervals (16 ms for really good ones), and have really low image qualities (the maximum resolution currently available is 1290 x 1080, which dwarfs compared to the rather inexpensive still cameras), we will instead be storing the two pictures on a single frame in a DSLR still camera. I plan to accomplish that by keeping the camera's shutter open and using two different flashes to capture just one frame. The flash timing is handled by the complicated looking circuit which can be attached to two flashes. When these pictures are taken in two of the three basic colors (R, G, or B), they can be easily separated out (a digital image is stored as a 2D array that stores 3 bytes for each pixel, where each byte consists of a value between 0 and 255 defining the redness, blue-ness, or green-ness of the pixel). Since the flashes are effectively the "shutter mechanism" of the setup, the whole operation needs to take place in complete (or as much as possible) darkness. The separated pictures can be put through PIV-Lab to find the velocity field.

The diagram below shows a top view of the system.

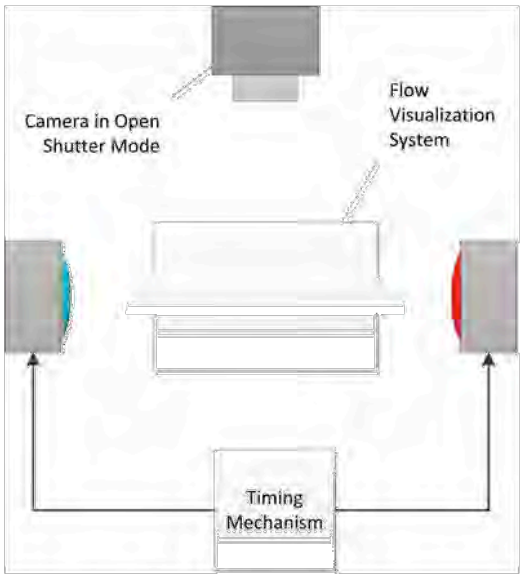

How the circuit works:

I don't know, but here is how to operate it (more information can be found here http://hiviz.com/kits/instructions/du-manual.htm):

- Attach each of the flash connectors to one of the flashes. Orient the flashes the "correct way" (more on that later), and turn them on (and remember to turn them off at the end of the day).
- Attach a 9V low amperage power source to the connectors which are already connected to a 9V battery holder (alternatively, use a 9V battery). Currently, a power source set to 9 volts is already attached (connection shown in the figure below).

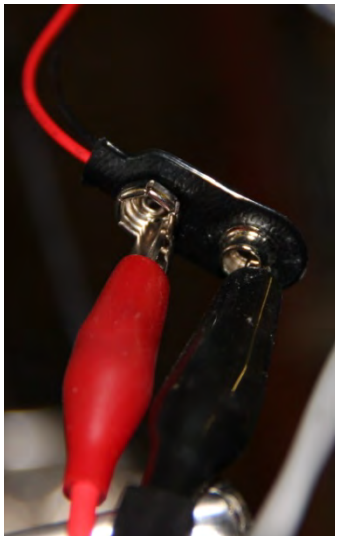

- Find the pots connected between the Red bar closest to J and the Blue bar closest to J. If you orient the device so that they are on top, the left one is for fine adjustment (grey pot in the figure

below) and the right one is for coarse adjustment (blue pot in the figure below).

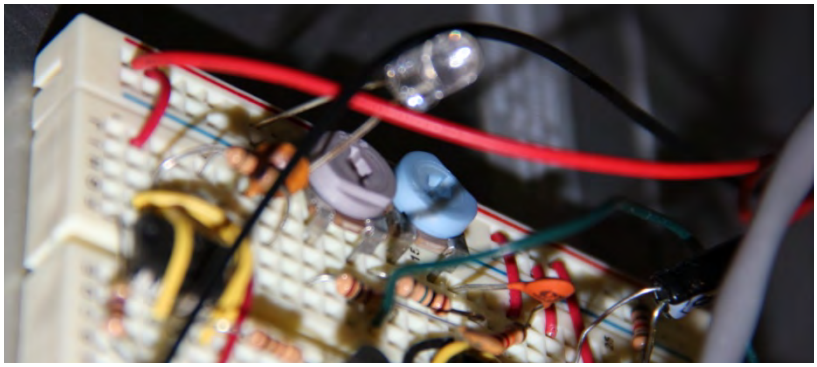

- If you attach a DMM here to find the resistance (make sure the power is off), you can find the time delay between flash fires using the calibration curve (the Excel file should have been turned in with this document, in the Timer Calibration folder). A plot of the calibration is given below:

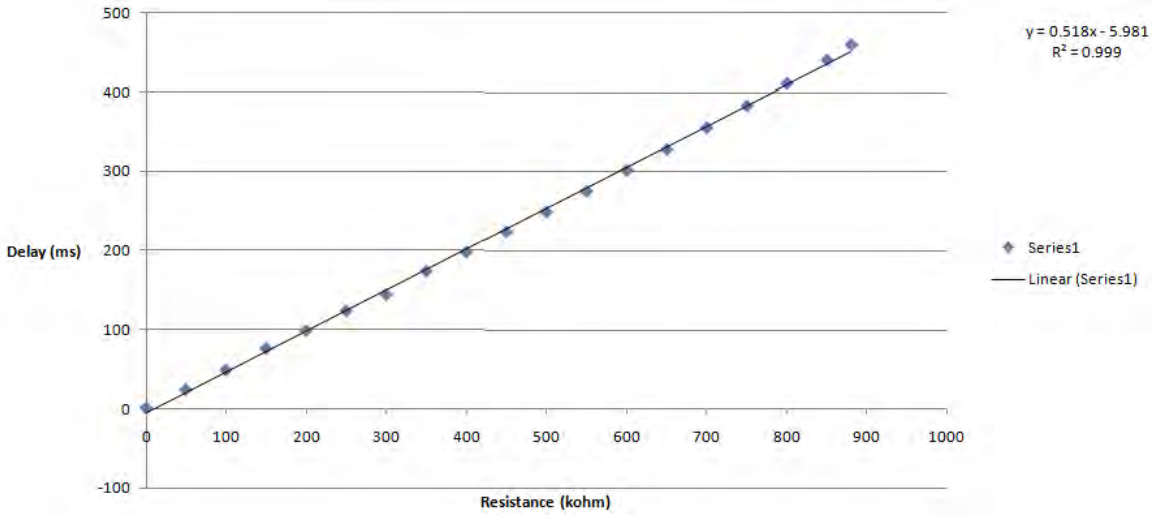

- Short the Blue near A and A25 to fire the circuit. At the moment, there is a button hooked up to a separate breadboard that can be pushed to perform this task.

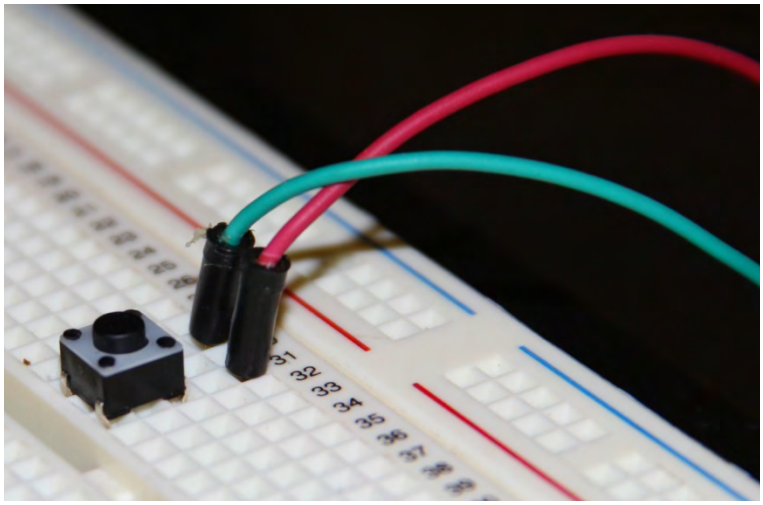

- One flash will fire immediately, the other one will fire after the delay based on the dashpot values.

Using the Camera:

- If you've never use a DSLR, read the manual a bit, especially the parts about changing aperture values, shutter speed, and ISO. In short:
    - Larger aperture value = smaller opening in the aperture => less light entering the system. We want this to be as high as possible without losing detail. Trial and error will be necessary.
    - Shutter speed value = the amount in seconds that the shutter is open. For our purposes, we want this to be about 1 second or so.
    - ISO value = gain in the sensor. The smaller, the better (100 is the smallest = least amount of digital noise).
- The images can be stored either in an SD card (currently the camera doesn't have one) or directly onto a computer using a USB cable and the EOS utility (found on the CD, install it, connect and turn on the camera, and then look for remote shooting).
- The idea is to have the camera set and zoomed perpendicular to (and as close as possible to) the plane of light coming from the flashes. The camera also needs to be focused to the plane of light. The easiest way to do this is to insert a relatively thin object in the test area so that it exists in the plane of the light (press the test button on the flash to get an idea of where that is). Then do a manual focus on that object, and leave the lens in manual focus mode.

- Now, take a photo (i.e. hit the button on the camera or the software). This will open the shutter for 1 second (or whatever the value of the shutter speed is). In that time, hit the touch button to fire the flashes, each flash will act as the opening of the shutter. If the camera is looking at a properly lighted and seeded flow system, it will capture two images, one on the green channel and one on the red channel.

Analyzing the Images:

- The images are analyzed using a python script. Ideally, the green flash will produce a pure green image of the seeding particles and the red flash a pure red image. This isn't entirely the case (read the "Issues and Recommendations" section). The code separates out the image by splitting the RGB channels. The green image is always okay, but the red image has a light image of the green in it (because the green flash overexposes and turns the particles white). One solution to this is to subtract the green (or blue) from the red, which is what the code currently does.

How to run the code:

- The code is in the "NEUP_Image_Splitter" folder and is in a file called "splitter.py" This is a python file and needs Python 2.4 (find at http://www.python.org/) as well as the Python Image Library for Python 2.4 (find at http://www.pythonware.com/products/pil/). Once both are installed, the file can be simply "double clicked" and run.
- When the script runs, a small window appears with one button (called GetFileNames). Clicking this opens a file browser, where you can select the image to be analyzed. Once analyzed, the two resulting images (green channel and red channel) will be saved in the "Out" folder inside the "NEUP_Image_Splitter" folder.
- These images can now be analyzed using PIV Lab.
- The picture below walks the reader through the "important" part of the code. This part is where the processing happens, the rest is declaration of dependencies and GUI stuff. The code isn't well documented but is fairly self explanatory.

```
def processFName(filename = ""):

    name = filename

    im = PIL.Image.open(name)

    im.convert("RGB")
    im = im.crop([1000,1000,4000,2500])
    [im1, im2, im3] = im.split()
                                    This function splits the image into RGB
    imd = list(im1.getdata())
    img = list(im3.getdata())
    imx = []
    for i in range(len(imd)):
        imx.append(imd[i] - img[i])

    im1.putdata(imx)
This is where the blue is subtracted from the red

    im1.save("Outs\\"+filename[(len(filename)-8):(len(filer
    im2.save("Outs\\"+filename[(len(filename)-8):(len(filer
    im3.save("Outs\\"+filename[(len(filename)-8):(len(filer
     This is where the images are saved (I'm saving the blue as well).
    print "done"
```

How to use PIV Lab:

- The first step is to have a working copy of Matlab. Then, download and unzip PIV Lab (http://pivlab.blogspot.com/). There is a *.m file in the PIV Lab folder, run it.
- The idea is to load the two images that were spat out by the image splitter, and analyze them using PIV Lab.
- The first step is to start a new sessions.
- Now you can load the two images into PIV Lab, and set the PIV settings.
    - The ones I care about the most are Window size and the number next to it. The window size describes the size of the grid (i.e. the distance between adjacent vectors). The second number defines the search area around the window for analysis (50% works in general). I usually turn the 2nd and 3rd pass options off (this uses interpolation to increase the number of vectors in the end result).
- Click the Analyze button (in the analyze menu). Note that you will need to click "Analyze This Frame" on the right afterwards to start the actual analysis.
- When the analysis is completed, the vector field will be shown.

Issues and Recommendations:

- The system doesn't work yet in a repeatable fashion, but has been shown to be working on sound principles (find proof of concept images in the "Proof of Concept (water is settling)" folder). The biggest issues I've run into are the following:
    - Getting a consistent plane of light is currently problematic. For PIV to work correctly, you need a thin but illuminating plane of light. At the moment we're doing this by collimating the flashes through a small slit. This works well enough for a small system by putting the flashes on either side at some distance (some trial and error required). The planes coming to either side need to overlap as much as possible. With Glenn's system, this caused a problem, as it could only be illuminated from one side. I was able to find no configuration in which two flashes would produce coplanar and/or sufficiently overlapping planes of light. Some optics work may be needed here (prisms could be the answer).
    - The green flash is overexposing the images and making them more white (causing noise in the red image, since white = green + blue + red). This is likely a function of the purity/darkness of the filter. I would recommend trying darker green glass, and also dark blue glass.
    - The red images are blurry compared to the green ones (which are rather crisp, and crisp = good). I'm unsure of why this is happening.
    - Reflections and blown highlights can be problematic. Remember to wipe the front and back of the system being photographed so that the images are not polluted by any stray marks. Blown highlights are a different issue and exist in regular PIV systems as well.
- If this project is going to continue, the following might help:
    - Optics: When I started this project, I thought a slit would produce a good enough plane, and it does (ish). At the very least, some research into optics that allow two different flashes to output the same amount of light, from the same point of origin, in the same direction, is necessary. As mentioned before, this may be possible using right angle prisms. If possible, some work into plane producing optics may also be beneficial. Information on these can be found in any good PIV book.
    - Better flashes: The flashes we have are relatively inexpensive but very good for regular photography. For PIV though, a "faster" flash would be better. By faster, I mean one that produces more light in less exposure time. The 500 ns flash

(http://prismscience.com/spot.php) is one possibility, which is on for only 500 ns when fired, compared to 6 ms in regular flashes.

- Better timer: this system will work well for slow flows, but for faster flows, a faster flash as well as a better timing system would be needed. The HiViz timing circuit is built for above-casual photography needs, and provides a least delay of about 0.2 ms. Coupled with the 500 ns flash this might be able to give much better results, but a timer like the Time Machine (http://www.bmumford.com/photo/camctlr.html) may ultimately be the better choice.

Appendix D-1

Measurement of Gap Spacing in the Flow Visualization Apparatus

Average channel gap width measurement

The average channel gap width was measured by,
1. Temporarily gluing and clamping with springs a plate on the bottom of the channel.
2. Filling to the top of the vertically oriented channel a carefully measured quantity of water. First, 250mml of water was poured from a 250ml graduated beaker, then 100ml of water from a 100ml graduated beaker, then a quantity from the 100ml graduated beaker that would just fill the channel to the top.
3. The measurement was repeated three times after initially filling and draining the channel in order to fill any small holes, such as the 0.040" pressure tap holes, or gaps.

The three measurements are,
392 ml
396 ml
398 ml

The average is 395 ml +/- 3 ml

The average gap calculated from this average is 0.137 in. +/- 0.002

This assumes that the channel width is 6.00 in. and the channel length is 28.50 in. and that there are eight bevels with dimensions 0.6275 in. by 0.327 in. The machining tolerance is approximately +/- 0.001 in.

Appendix D-2

Pressure measurement apparatus as located at the ISU Pocatello lab and test procedure.

The apparatus has been relocated from the now decommissioned ISU Skyline lab in Idaho Falls to the ISU Pocatello lab. A test procedure for operating the apparatus and photographs of the apparatus in its new home are shown.

Procedure for Use of Flow Visualization and Pressure Drop Systems

1) Make sure system is level, adjust as needed.
2) Measure water temperature
3) Determine desired flow rate using excel tab "Flow Rate for Re" entering the water temperature and desired Re.
4) Align valves for startup: Recirc- fully open
   Large tank fill – gate is open, ball is closed
   Vent – open (top of tank with hose, not shown in pictures)
   Control – closed (tank outlet on bottom)
5) Make sure open tank is full ~1" from top (if not, fill using faucet near bathroom)
6) Plug in pump making sure to keep electrical ends and switch off the floor and out of the water.
7) Turn on pump, water should be exiting from the recirc line only
8) Open ball valve on fill line
9) Adjust gate valves (fill and recirc) so that the SS tank fills, should fill until water begins flowing through overfill drain. Add water as needed to keep open tank full.
10) Continue adjusting valves until water just begins to run through the overfill drain (horizontal inlet).
11) Open control valve and adjust until flow rate shown by rotometer is near desired value, adjust gate valves(recirc and fill) as needed to keep water level constant. Easiest option is to maintain a small but continuous flow through the tank overflow drain.
12) Measure water temperature, record, if different than initial value wait until two similar values are measured and then record.
13) Using a bucket and stop watch measure the flow rate, record, repeat (3+) to confirm value.
14) Perform measurements.
15) When done quickly open the recirc valve and close the control valve and ball valve on fill line. Turn off pump.

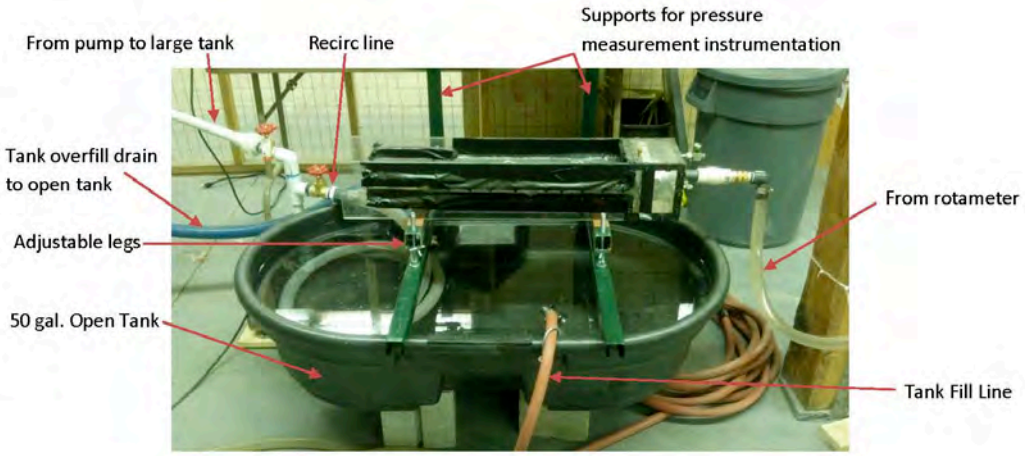

Figure 1: Open Tank

Figure 2: Rotameter location

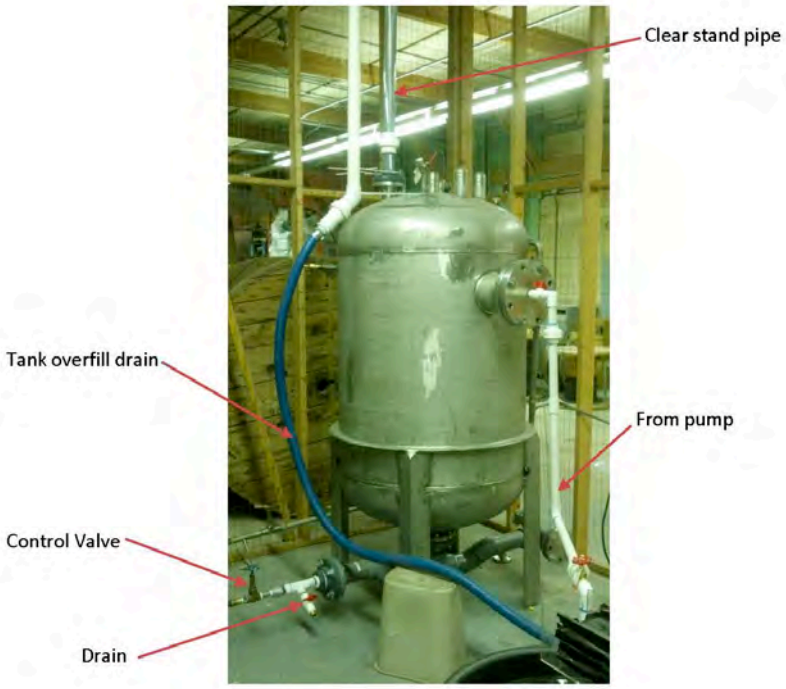

Figure 3: Large Tank

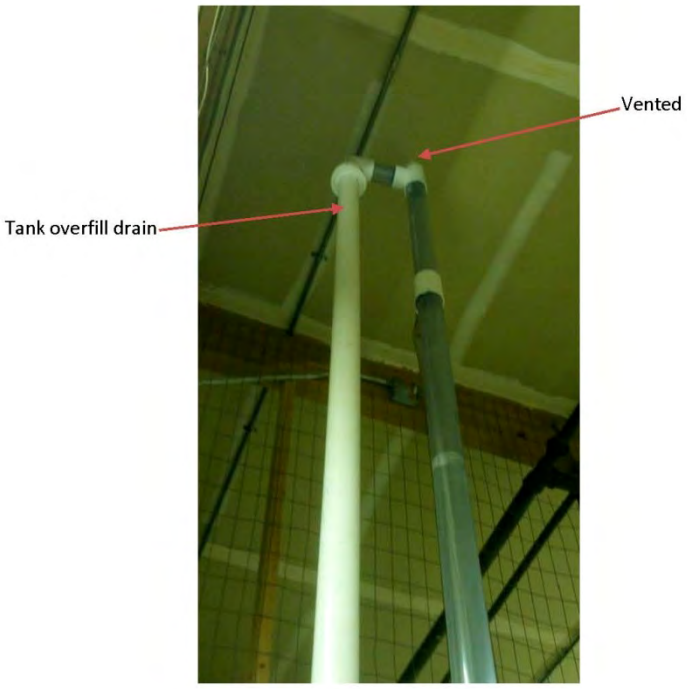

Figure 4: Top of Stand Pipe

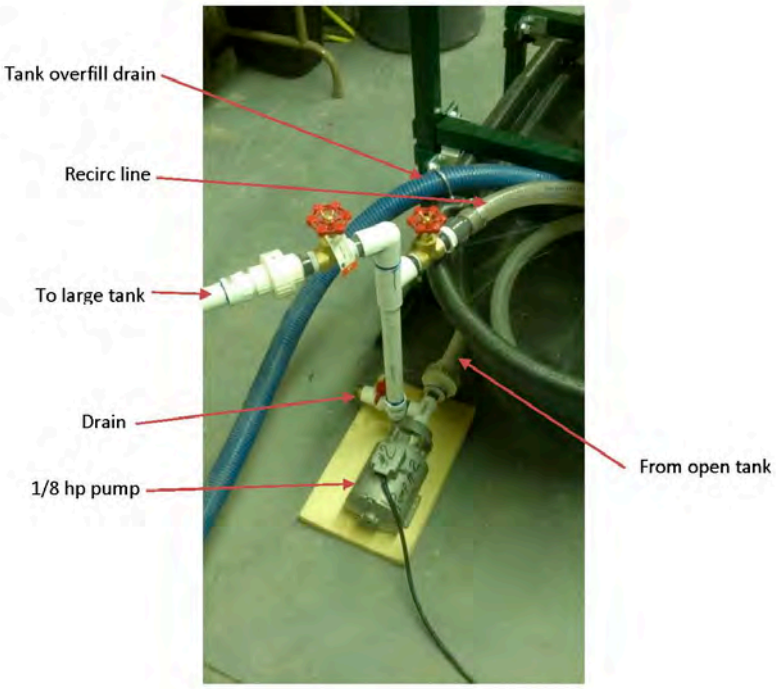
Tank overfill drain
Recirc line
To large tank
Drain
1/8 hp pump
From open tank

Appendix E

Plenum Flow Report:

INVESTIGATION OF PLENUM FLOW BEHAVIOR
WITH DIFFERENT ENTRANCE AND EXIT GEOMETRIES

Appendix G

Minutes of the November 30, 2011 NEUP Team QA Meeting

Minutes of ISU's NEUP (Distorted Heat Transfer) Team Meeting

Date: 30 November 2011

Begin: 1:00 pm

Location: LEL 233 Conference Room

Attending: Izzi Silver, Logan Tew, Jose Martinez, Jari Safi, and Brian Williams

Results of the QA (quality assurance) *roundtable* discussion. This discussion was a direct result of the DoE QA Assist visit that occurred at ISU during the week of November 14th.

1. Calibration:
    a. Use an Excel spreadsheet to document/track all instrumentation's calibration
        i. Include information such as:
            1. Manufacturer
            2. Model/style
            3. Serial and/or any identifying numbers
            4. Type and/or purpose (i.e., pressure transducer, thermocouple, multi-meter, etc.)
            5. Calibration source (i.e., NIST, manufacturer, in-house, calibration lab, etc.)
            6. Last calibration date
            7. Next calibration due date
        ii. Spreadsheet may then be sorted by the next calibration due date to determine those instruments needing a calibration update
            1. The frequency of calibration will be determined by the calibration data on each particular instrument – some may need calibration at each use, others might have calibrations that are valid for a year
            2. The frequency at which the calibration report will be created is TBD – might be monthly, bi-annually, or annually
        iii. A control document can be created to specify our calibration procedure
            1. This might be a good task for one of the undergraduate students
    b. Use access control to the lab to maintain the calibration status of all instruments
        i. Only allow those involved with the project to have access to the lab
            1. Control who has a key
        ii. Convert the "bolted-in double wire doors" into hinged doors with a lock

2. Data backup and/or copies:
    a. For digital items (i.e., electronic files, computers, etc.):
        i. Nomenclature for file names is very important
            1. We will need a document/plan so that everyone follows this nomenclature process
            2. Include a description of what the file is, for example, the filename could start with the term PROCEDURE, CALIBRATION, TEST, DATA, ANALYSIS, DESIGN etc., or some shortened version, corresponding to what action is contained within the file
            3. Always include a date on the file, for example, in the form 11-30-11
                a. This will allow for the retention of all document revisions
        ii. The backup frequency of electronic files needs to be determined

1. Daily, weekly, etc.

iii. The backup technique and/or approach also need to be determined. Possibilities suggested include:
    1. Google Docs
    2. Drop Box
        a. A master project Drop Box account could contain subaccounts/folders for the various team members
        b. The Drop Box files could be periodically backed up to a local hard drive system
    3. Our own server and/or "cloud"
    4. RAID-type backup system

b. Paper documents:
    i. Periodically (frequency TBD) scan lab notebooks or other paper documents
    ii. Connect scanner directly to the electronic document backup system (still TBD and discussed above) and follow the same protocol for file names

c. We can create a control document/procedure that outlines the process we will follow for ensuring the backup of our information

3. Training:
    a. Use a training log to track all instances of training
        i. For example, we have used a log to track the training/compliance of the safety procedures employed at the Skyline Lab in Idaho Falls
    b. Employ video pod casts as a training tool for instructing new users of equipment, instrumentation, operating/testing procedures, etc.
    c. Use written documents that are essentially checklists for guidance while using equipment, instrumentation, etc.
        i. Similarly to the flushing/checkout procedure document that we used at the IF Skyline Lab during the weekly operation of the HSIS demonstration station

4. Be sure to document (i.e., write down in your lab notebook) all calculations, analysis, etc., so that there is a record of what was done
    a. Stop using throw away scratch paper to do calculations
    b. Electronic versions of this can be used for peer review and inclusion in reports

Meeting adjourned at 1:55 pm